Linköping studies in science and technology
Thesis. No. 1608

Modeling and Optimization for Critical Vehicle Maneuvers

Kristoffer Lundahl

Linköping University
INSTITUTE OF TECHNOLOGY

Department of Electrical Engineering
Linköping University, SE-581 33 Linköping, Sweden

Linköping 2013

Linköping studies in science and technology
Thesis. No. 1608

This is a Swedish Licentiate's Thesis.
Swedish postgraduate education leads to a Doctor's degree and/or a Licentiate's degree.
A Doctor's degree comprises 240 ECTS credits (4 years of full-time studies).
A Licentiate's degree comprises 120 ECTS credits,
of which at least 60 ECTS credits constitute a Licentiate's thesis.

Kristoffer Lundahl
kristoffer.lundahl@liu.se
www.vehicular.isy.liu.se
Division of Vehicular Systems
Department of Electrical Engineering
Linköping University
SE-581 33 Linköping, Sweden

Lundahl, Kristoffer
Modeling and Optimization for Critical Vehicle Maneuvers
ISBN 978-91-7519-561-2
ISSN 0280-7971
LIU-TEK-LIC-2013:42

Typeset with LaTeX 2ε
Printed by LiU-Tryck, Linköping, Sweden 2013

"On a given day, a given circumstance, you think you have a limit. And you then go for this limit and you touch this limit, and you think, 'Okay, this is the limit'. And so you touch this limit, something happens and you suddenly can go a little bit further."

— Ayrton Senna

Abstract

As development in sensor technology, situation awareness systems, and computational hardware for vehicle systems progress, an opportunity for more advanced and sophisticated vehicle safety-systems arises. With the increased level of available information—such as position on the road, road curvature and knowledge about surrounding obstacles—future systems could be seen utilizing more advanced controls, exploiting at-the-limit behavior of the vehicle. Having this in mind, optimization methods have emerged as a powerful tool for offline vehicle-performance evaluation, providing inspiration to new control strategies, and by direct implementation in on-board systems. This will, however, require a careful choice of modeling and objectives, since the solution to the optimization problem will rely on this.

With emphasis on vehicle modeling for optimization-based maneuvering applications, a vehicle-dynamics testbed has been developed. Using this vehicle in a series of experiments, most extensively in a double lane-change maneuver, verified the functionality and capability of the equipment. Further, a comparative study was performed, considering vehicle models based on the single-track model, extended with, *e.g.*, tire-force saturation, tire-force lag and roll dynamics. The ability to predict vehicle behavior was evaluated against measurement data from the vehicle testbed.

A platform for solving vehicle-maneuvering optimization-problems has been developed, with state-of-the-art optimization tools, such as JModelica.org and Ipopt. This platform is utilized for studies concerning the influence different vehicle-model configurations have on the solution to critical maneuvering problems. In particular, different tire modeling approaches, as well as vehicle-chassis models of various complexity, are investigated. Also, the influence different road-surface conditions—*e.g.*, asphalt, snow and ice—have on the solution to time-optimal maneuvers is studied.

The results show that even for less complex models—such as a single-track model with a Magic Formula based tire-model—accurate predictions can be obtained when compared to measurement data. The general observation regarding vehicle modeling for the time-critical maneuvers is similar; even the least complex models can be seen to capture certain characteristics analogous to those of higher complexity.

Analyzing the results from the optimization problems, it is seen that the overall dynamics, such as resultant forces and yaw moment, obtained for different model configurations, correlates very well. For different road surfaces, the solutions will of course differ due to the various levels of tire-forces being possible to realize. However, remarkably similar vehicle paths are obtained, regardless of surface. These are valuable observations, since they imply that models of less complexity could be utilized in future on-board optimization-algorithms, to generate, *e.g.*, yaw moment and vehicle paths. In combination with additional information from enhanced situation-awareness systems, this enables more advanced safety-systems to be considered for future vehicles.

Acknowledgments

This work has been carried out at the Division of Vehicular Systems at the Department of Electrical Engineering, Linköping University.

First and foremost I would like to thank my supervisor Lars Nielsen for deceiving me into believing PhD studies are all fun and games, as well as for his support and enthusiasm. Jan Åslund is acknowledged for his role as co-supervisor and involvement in this work, which is much appreciated.

Karl Berntorp and Björn Olofsson, Lund University, are acknowledged for the cooperative work on optimal vehicle maneuvers, within the ELLIIT consortium.

Everyone at the Vehicular Systems division are thanked, for providing a pleasant and competent work environment.

Finally, my parents deserves to be acknowledged for nurturing my research interest at an early stage in life, by providing vehicular lab equipment, in the shape of toy cars. Lots of toy cars.

Kristoffer Lundahl

Linköping, June 2013

Contents

Chapter 1

Introduction

With an ever growing vehicle-transportation fleet, demands on vehicle and traffic safety increase, both from a consumer point-of-view, Koppel et al. (2008), as well as in shape of more stringent legislation requirements. Passive safety has seen a lot of refinements over the last decades, such as seat belts and structural deformation zones. Also active safety systems have experienced a vast improvement and a more extensive area of application recently. However, considering the vision of a partially, or even fully, autonomous vehicle fleet, still only a fraction of the potential for active safety systems is utilized today. Though, even if the technology was present, issues arise from public and political acceptance, legal responsibilities and integration with the current vehicle fleet. Advanced driver assistant systems therefore arise as a natural technological step in vehicle safety. The general purpose of these systems is to assist the driver in critical situations, thus, preventing accidents or minimizing injuries. Examples of such systems are Anti-lock Braking System (AntiBlockierSystem), ABS, and Electronic Stability Control, ESC, which have emerged as standard equipment in modern vehicles.

When considering future advanced driver assistant systems in general, the underlying subsystems could roughly be categorized into the following areas; *situation awareness*, *driver interaction* and *vehicle control actions*. In *situation awareness* systems the surrounding environment of the vehicle is considered, using various combinations of, *e.g.*, camera and radar sensors, satellite-based positioning systems, road-map databases, as well as vehicle-to-vehicle and vehicle-to-roadside communication, Faezipour et al. (2012). For *driver interactions*, two different approaches could be considered to span the majority of the area; interpreting the driver intentions solely through driver input actions, or completely neglect these and determine the most beneficial actions based on the vehicle and surrounding circumstances. The former is preferable when little to none of the situation awareness information is accessible, *e.g.*, the less complex variants

of ESC only use steering-wheel angle and forward velocity as a references for stabilizing the vehicle, see, *e.g.*, Van Zanten (2002). The latter is on the other hand valuable for situations where the driver commands are not trustworthy or when irrational driver behavior is expected, as for post-impact collision systems, such as in Yang et al. (2012). However, for most applications, some kind of intermediate variant is probably what to expect. When it comes to *vehicle control actions*, two elements of importance are covered; when to intervene and how to control the vehicle. To some extent, it is preferable to intervene as late as possible, to prevent undesired assistance. This, in turn, requires an accurate estimation and prediction of the vehicle motion, as well as knowledge about surrounding objects and road characteristics.

With the advancements in situation awareness systems, more advanced and sophisticated vehicle control systems will be possible, where knowledge about position on the road, road curvature, and sudden obstacles can be utilized for the control strategies. Also, more complex control algorithms and enhanced vehicle modeling may be enabled by the progress in computational-hardware development. This opens for more advanced control systems, utilizing at-the-limit modes and expanding the envelope of vehicle control. Voser et al. (2010) suggest that maneuvering inspired by race and rally car drivers could be exploited in future systems, and presents a drifting controller for a rear-wheel driven vehicle. Similarly, a handbrake drifting controller is developed in Velenis (2011). In these studies a rather simple vehicle model is used, namely, the single-track model, as for example described in Ellis (1994). It has seen an extensive use in vehicle-control applications, primarily due to its simple structure, while still capturing some of the essential dynamics. However, for applications where feedback is limited or more comprehensive predictions are necessary, a revised approach to the vehicle modeling might be necessary.

Although chassis modeling is an important and nontrivial part in vehicle dynamics applications, modeling of the tire-to-ground contact-patch is an even more intricate area, having an immense effect on the overall vehicle dynamics. Adding to the complexity is the constantly varying characteristics for different road surfaces, tire and road temperatures, tire wear, *etc.*, while variations in chassis characteristics often are limited to changes in mass related properties. For example, Carlson and Gerdes (2005) show that for a single tire, the longitudinal stiffness can vary between 20–100 %. In Svendenius et al. (2009) and Braghin et al. (2006) two separate tire models are validated for different road conditions, showing a radical variance for several of the tire characteristics. Another tire-model related issue, arising for at-the-limit modeling and control, is combined slip conditions. This is when longitudinal and lateral forces are employed simultaneously, for example, braking while cornering. Usually the *friction-ellipse* model is used for these applications, due to its simple structure. However, for large slip it becomes fallacious. In Pacejka (2006) an alternative approach using *weighting functions* is presented, that can be considered valid for a larger span, but, it also brings an increased model complexity and an

expanded set of model parameters.

The use of optimization technologies as a tool in the development of vehicle dynamics applications has been proven to be beneficial in several aspects. The optimization algorithms could be implemented and utilized in the on-board control systems, while solutions to optimization problems obtained offline could be of great value in itself, as it can provide insight to certain phenomenas or used as inspiration for control strategies, as stated in Sharp and Peng (2011). Optimization tools can also be an asset in the evaluation process, providing valuable understanding of the performance potential for different system configurations, or choice of model parameters. Several studies have been performed for this purpose, *e.g.*, in Sundström et al. (2010) safety-critical situations for a maximum entry-speed formulation are studied, and in Yang et al. (2012) a minimum lateral-deviation problem is considered. Similar tools have also seen an extensive use in more performance oriented applications, often with a minimum-time objective. Casanova et al. (2000) evaluate vehicle performance, based on maneuvering time, for various vehicle parameters, and in Kelly and Sharp (2010) a method for minimizing lap time of a race car is presented.

Even though optimization methods can be considered a powerful tool, the solution to an optimization problem will always rely on the problem formulation, *i.e.*, the choice of optimization objectives and model configurations. Thus, model validity plays an even more crucial role, compared to in simulation, where a congruent model only is necessary in the areas of intended operation. In optimization, however, it becomes imperative to ensure that inconsistencies or invalid model behavior are not within reach for the solver, to prevent the solution from utilizing these shortcomings.

1.1 Contributions

Here follows a brief summary of the main contributions in Paper A–D.

Paper A

In Paper A a vehicle dynamics testbed is developed, based on a Volkswagen Golf 2008 equipped with an optical slip-angle sensor, an optical roll/pitch measurement system, accelerometers, *etc.* Different variants of the single-track model are then parametrized and evaluated towards measurement data from the vehicle testbed. The study demonstrates the potential of utilizing the vehicle testbed in vehicle-dynamics analysis of aggressive and rapid nature. It can also be concluded that low-complexity models, such as the ones studied here, can predict vehicle behavior for the most essential variables.

Paper B

A platform for solving optimization problems in vehicle maneuvering is developed, based on modern high-level optimization tools and existing vehicle models, also utilized in Paper C and D. A minimum-time optimization problem is formulated for a hairpin-turn maneuver, and solved using a single-track model coupled to different tire-modeling approaches. The results indicate that even a few-state vehicle model can replicate advanced maneuvering—often associated with experienced rally drivers—in optimal-maneuvering applications, and can give valuable information for the development of improved vehicle safety systems.

Paper C

Using the optimization methodology presented in Paper B, a comparative analysis is performed considering different vehicle models in time-critical optimal maneuvering problems. Five different chassis models are treated, ranging from a single-track model to a double-track model with roll and pitch dynamics including load transfer. A minimum-time optimization problem is then applied to two maneuvers; a 90°-turn and a double lane-change scenario. The main findings suggest that variables potentially important for safety systems, such as yaw rate, slip angle, and vehicle path, are qualitatively the same for all models. Thus, less complex models could be sufficient for future on-board optimization-based safety systems.

Paper D

In Paper D the influence of different road-surface conditions in critical vehicle maneuvering is studied. Tire models representing asphalt, snow, and ice, are composed based on published experimental data. The minimum-time optimization problem is then applied to a hairpin turn, and solved for each surface. The obtained results show fundamental differences in the control strategies. However, the geometric path throughout the maneuver are remarkably similar for the different road-conditions.

1.2 Publications

A list of relevant publications by the author follows below.

The conference paper *Investigating Vehicle Model Detail for Close to Limit Maneuvers Aiming at Optimal Control*, Kristoffer Lundahl, Jan Åslund, and Lars Nielsen, presents a shorter and more preliminary work of the posterior study *Vehicle Dynamics Platform, Experiments, and Modeling Aiming at Critical Maneuver Handling*, Kristoffer Lundahl, Jan Åslund, and Lars Nielsen, published as an internal technical report at the Department of Electrical Engineering, Linköping University.

Conference Papers

- Kristoffer Lundahl, Jan Åslund, and Lars Nielsen. Investigating Vehicle Model Detail for Close to Limit Maneuvers Aiming at Optimal Control. In *the 22nd International Symposium on Dynamics of Vehicles on Roads and Tracks (IAVSD)*. Manchester, United Kingdom, 2011.

- Karl Berntorp, Björn Olofsson, Kristoffer Lundahl, Bo Bernhardsson, and Lars Nielsen. Models and Methodology for Optimal Vehicle Maneuvers Applied to a Hairpin Turn. In *the 2013 American Control Conference (ACC)*. Washington D.C., USA, 2013. **(Paper B)**

- Kristoffer Lundahl, Karl Berntorp, Björn Olofsson, Jan Åslund, and Lars Nielsen. Studying the Influence of Roll and Pitch Dynamics in Optimal Road-Vehicle Maneuvers. In *the 23nd International Symposium on Dynamics of Vehicles on Roads and Tracks (IAVSD)*. Qingdao, China, 2013. **(Paper C)**

- Björn Olofsson, Kristoffer Lundahl, Karl Berntorp, and Lars Nielsen. An Investigation of Optimal Vehicle Maneuvers for Different Road Conditions. In *the 7th IFAC Symposium on Advances in Automotive Control (AAC)*. Tokyo, Japan, 2013. **(Paper D)**

Technical Reports

- Kristoffer Lundahl, Jan Åslund, and Lars Nielsen. Vehicle Dynamics Platform, Experiments, and Modeling Aiming at Critical Maneuver Handling. *Technical Report LiTH-ISY-R-3064*. Department of Electrical Engineering, Linköpings Universitet, SE-581 83 Linköping, Sweden, 2013. **(Paper A)**

References

F Braghin, F Cheli, and E Sabbioni. Environmental effects on Pacejka's scaling factors. *Vehicle System Dynamics*, 44(7):547–568, 2006.

C.R. Carlson and J.C. Gerdes. Consistent nonlinear estimation of longitudinal tire stiffness and effective radius. *IEEE Trans. Control Syst. Technol.*, 13(6): 1010–1020, Nov. 2005.

D. Casanova, R.S. Sharp, and P. Symonds. Minimum time manoeuvring: The significance of yaw inertia. *Vehicle System Dynamics*, 34(2):77–115, 2000.

John Ronaine Ellis. *Vehicle Handling Dynamics.* Mechanical Engineering Publications, London, United Kingdom, 1994.

Miad Faezipour, Mehrdad Nourani, Adnan Saeed, and Sateesh Addepalli. Progress and challenges in intelligent vehicle area networks. *Commun. ACM*, 55(2):90–100, February 2012.

D. P. Kelly and R. S. Sharp. Time-optimal control of the race car: a numerical method to emulate the ideal driver. *Vehicle System Dynamics*, 48(12):1461–1474, 2010.

Sjaanie Koppel, Judith Charlton, Brian Fildes, and Michael Fitzharris. How important is vehicle safety in the new vehicle purchase process? *Accident Analysis & Prevention*, 40(3):994 – 1004, 2008.

Hans B. Pacejka. *Tire and Vehicle Dynamics.* Butterworth-Heinemann, Oxford, United Kingdom, second edition, 2006.

R. S. Sharp and Huei Peng. Vehicle dynamics applications of optimal control theory. *Vehicle System Dynamics*, 49(7):1073–1111, 2011.

Peter Sundström, Mats Jonasson, Johan Andreasson, Annika Stensson Trigell, and Bengt Jacobsson. Path and control optimisation for over-actuated vehicles in two safety-critical maneuvers. In *10th Int. Symp. on Advanced Vehicle Control (AVEC)*, Loughborough, United Kingdom, 2010.

J Svendenius, M Gäfvert, F Bruzelius, and J Hultén. Experimental validation of the brush tire model 5. *Tire Science and Technology*, 37(2):122–137, 2009.

Anton T Van Zanten. Evolution of electronic control systems for improving the vehicle dynamic behavior. In *Proceedings of the 6th International Symposium on Advanced Vehicle Control*, pages 1–9, 2002.

Efstathios Velenis. FWD vehicle drifting control: The handbrake-cornering technique. In *IEEE Conf. on Decision and Control (CDC)*, pages 3258–3263, Orlando, FL, 2011.

Christoph Voser, Rami Y Hindiyeh, and J Christian Gerdes. Analysis and control of high sideslip manoeuvres. *Vehicle System Dynamics*, 48(S1):317–336, 2010.

Derong Yang, T.J. Gordon, B. Jacobson, and M. Jonasson. Quasi-linear optimal path controller applied to post impact vehicle dynamics. *Intelligent Transportation Systems, IEEE Transactions on*, 13(4):1586–1598, 2012.

Publications

Paper A

Vehicle Dynamics Platform, Experiments, and Modeling Aiming at Critical Maneuver Handling*

A

*Published as *Technical Report LiTH-ISY-R-3064*, Department of Electrical Engineering, Linköping University, Linköping, Sweden, 2013.

Vehicle Dynamics Platform, Experiments, and Modeling Aiming at Critical Maneuver Handling

Kristoffer Lundahl, Jan Åslund, and Lars Nielsen

Vehicular Systems, Department of Electrical Engineering, Linköping University, SE-581 83 Linköping, Sweden

Abstract

For future advanced active safety systems, in road-vehicle applications, there will arise possibilities for enhanced vehicle control systems, due to refinements in, *e.g.*, situation awareness systems. To fully utilize this, more extensive knowledge is required regarding the characteristics and dynamics of vehicle models employed in these systems. Motivated by this, an evaluative study for the lateral dynamics is performed, considering vehicle models of more simple structure. For this purpose, a platform for vehicle dynamics studies has been developed. Experimental data, gathered with this testbed, is then used for model parametrization, succeeded by evaluation for an evasive maneuver. The considered model configurations are based on the single-track model, with different additional attributes, such as tire-force saturation, tire-force lag, and roll dynamics. The results indicate that even a basic model, such as the single-track with tire-force saturation, can describe the lateral dynamics surprisingly well for this critical maneuver.

1 Introduction

The increasing level of sensory instrumentation and control actuators in modern vehicles, along with higher demands on traffic safety, enables and motivates more advanced safety systems for future vehicles. To exploit these opportunities in the most beneficial way, extensive knowledge in terms of vehicle handling and dynamics will be essential. Also, perhaps even more important, is insight into the vehicle characteristics certain modeling approaches are able to capture in critical situations, and the extent of their appropriateness for on-board applications.

Inspired to investigate questions raised for the above topics, a platform for vehicle-dynamics studies has been developed. This testbed, shown in Figure 1, is based on a standard car equipped with vehicle-dynamics sensor-instrumentation for highly dynamic maneuvering. Experimental data from this testbed is here used in an evaluative study, primarily considering modeling and validation of the lateral dynamics. A similar study, with more preliminary results, was presented in Lundahl et al. (2011).

The intention of this study is to give a brief insight to the potential of established, simple structured, vehicle models, in terms of their ability to describe essential vehicle states and variables. With emphasis on the lateral dynamics, the considered models are based on the single-track model, extended with different additional characteristics, such as tire-force saturation, tire-force lag, and roll dynamics. To find parameters for these models, a number of experiments have been conducted, with the above mentioned vehicle testbed. Each of the model configurations was parametrized, followed by an evaluative comparison for a double lane-change maneuver.

Figure 1: The vehicle-dynamics testbed for studying critical maneuver handling.

2 Experimental Equipment

With the intention to offer a precise evaluation instrument for vehicle dynamics studies and applications, a vehicle testbed has been developed. The platform is based on a Volkswagen Golf V, 2008, equipped with a set of state-of-the-art sensors, measuring, *e.g.*, slip angle, roll and pitch angles, accelerations, and angular rates. In addition, information from the internal sensors are accessible over the vehicle CAN bus. This CAN access has been made possible through collaboration with Nira Dynamics AB, supporting with hardware and software interfaces to the vehicle. The additional sensors mainly consist of four different systems; an IMU, a GPS, a slip-angle sensor, and a roll/pitch measurement system. A measurement PC is used for sampling these systems, as well as for the data stream from the vehicle CAN bus. In Figure 2 a simplified scheme over the system is shown.

A more detailed description of the measurement systems and individual sensors follows below. Table 1 specifies measurement range, accuracy, and sampling frequency for the variables of most relevance.

Slip-Angle Sensor

The slip angle sensor is a Corrsys-Datron Correvit S-350. It uses optical instrumentation to measure speed and direction, with algorithms taking advantage of the irregularities in the road-surface micro-structure. The sensor is mounted in the front of the vehicle, and outputs measures for the longitudinal and lateral velocities of this position. However, arbitrary points can be described, *e.g.*, the

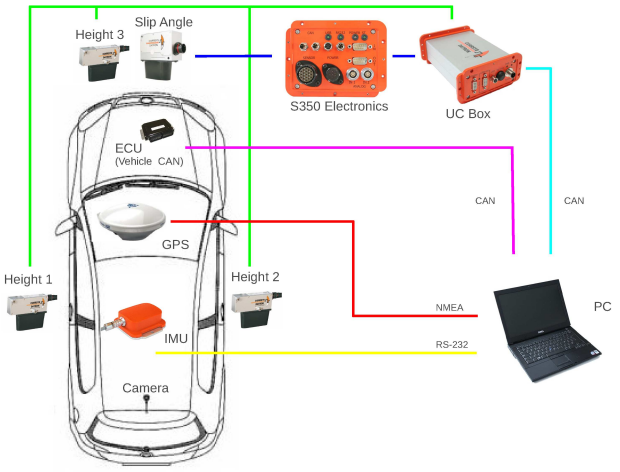

Figure 2: A schematic sketch over the measurement system.

Table 1: Technical specifications for the additional sensors.

Variable	Range	Accuracy	Frequency
Corrsys-Datron Correvit S-350			
Long. velocity, v_x	0.5–250 km/h	0.1 %	250 Hz
Lateral velocity, v_y		0.1 %	250 Hz
Slip angle, β	±40 deg	0.1 deg	250 Hz
Corrsys-Datron HF-500C			
Height	125–625 mm	0.2 %	250 Hz
Roll angle, ϕ	±15 deg	0.08 deg	250 Hz
Pitch angle, θ	±11 deg	0.06 deg	250 Hz
Xsens MTi			
Accelerations a_x, a_y, a_z	±17 m/s^2	0.02 m/s^2	100 Hz
Angular rates $\dot{\phi}, \dot{\theta}, \dot{\psi}$	±300 deg/s	0.3 deg/s	100 Hz
u-blox AEK-4P			
Position (GPS)		2.5 m	4 Hz

vehicle center of gravity, using these signals in combination with yaw-rate data. For further technical specifications see Cor (2009b).

Roll and Pitch Angle Measurement System

The system for roll and pitch angle measurement mainly consists of three height sensors, Corrsys-Datron HF-500C, mounted around the vehicle, and thereby mapping the plane of the vehicle body relative the ground. The sensors emit a visible laser at the road surface, and determine the height from the reflected light beam. The accuracies of the measured roll and pitch angles are linearly correlated to the relative placement of the sensors, assuming chassis deflections are neglected. For further technical specifications see Cor (2009a).

IMU — Accelerometer and Gyroscope

The *inertial measurement unit*, IMU, is an Xsens MTi, measuring accelerations and angular rates in three dimensions. Additionally, it has a built in magnetometer for possible yaw angle measurements, however, the responsiveness of this is a bit too slow for rapid vehicle dynamics studies. For further technical specifications see Xse (2009).

GPS

For vehicle positioning a GPS module of u-blox AEK-4P type is used. For more specific information see u-b (2005).

Internal Sensors

On the vehicle CAN bus several sensors, with relevance for vehicle dynamics applications, are accessible at a sampling rate of 10 Hz. Many of these are redundant due to the additional sensors, and of worse quality in terms of accuracy and noise. However, signals for steering wheel angle and wheel angular velocities are of great importance since no additional equipment has been added to sample these, or equivalent variables.

Test Track

Through a collaborative effort with Linköpings Motorsällskap, LMS, permission has been given to access their race and test track, Linköpings Motorstadion. Figure 3 illustrates a double lane-change maneuver at this facility.

3 Vehicle Modeling

The vehicle models that will be evaluated are of a simple structure, *e.g.*, neglecting load transfer and individual wheel-dynamics. The model configurations use the single-track model as a basis, to describe the lateral dynamics of the vehicle, coupled to tire models of different complexity. Additionally, an extended

Figure 3: A double lane-change maneuver at Linköpings Motorstadion.

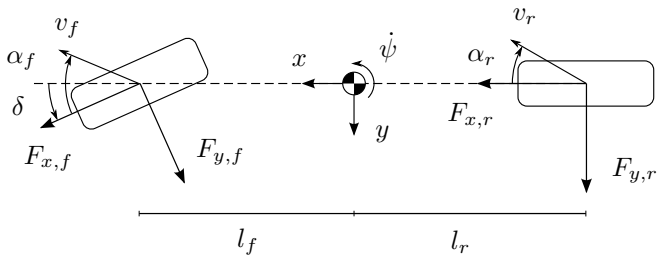

Figure 4: The single-track model.

version of the single-track model is considered, where roll dynamics has been added. The number of considered model configurations adds up to a total of four.

Single-Track Model

The single-track model is a simplified planar model describing the chassis dynamics, with left and right wheels lumped into a single front and a single rear wheel, see, *e.g.*, Wong (2008). The model is illustrated in Figure 4, and has its dynamics described by

$$m(\dot{v}_y + v_x\dot{\psi}) = F_{y,f}\cos(\delta) + F_{y,r} + F_{x,f}\sin(\delta), \tag{1}$$

$$I_{zz}\ddot{\psi} = l_f F_{y,f}\cos(\delta) - l_r F_{y,r} + l_f F_{x,f}\sin(\delta), \tag{2}$$

where m represents the total vehicle mass, I_{zz} the yaw inertia, l_f, l_r the distances from front and rear wheel axles to the center of gravity (CoG), δ the steer angle for the front wheels, v_x, v_y the longitudinal and lateral velocity at the CoG, $\dot{\psi}$ the yaw rate, and F_x, F_y longitudinal and lateral tire forces for the front and rear wheels. Since this study is focused on the lateral dynamics, no longitudinal excitations will be considered, hence, $F_{x,f} = 0$.

Single Track with Roll Dynamics

An extended variant of the above single-track model is also considered, where the roll angle, ϕ, has been added as an additional degree of freedom, *i.e.*, the rotational motion about the x-axis, as depicted in Figure 5. Thus, the motion dynamics follows from

$$m(\dot{v}_y + v_x\dot{\psi}) - m_s h\ddot{\phi} = F_{y,f}\cos(\delta) + F_{y,r} + F_{x,f}\sin(\delta), \tag{3}$$

$$I_{zz}\ddot{\psi} = l_f F_{y,f}\cos(\delta) - l_r F_{y,r} + l_f F_{x,f}\sin(\delta), \tag{4}$$

$$I_{xx}\ddot{\phi} + D_\phi\dot{\phi} + K_\phi\phi = m_s h a_y. \tag{5}$$

Here m_s is the sprung mass of the vehicle body, I_{xx} the roll inertia, h the distance between CoG and the roll center, K_ϕ the roll stiffness, and D_ϕ the roll

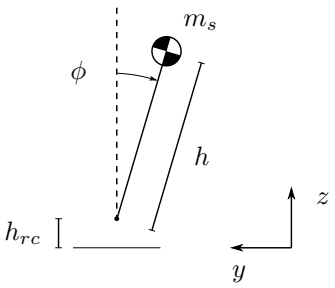

Figure 5: Illustration of the roll dynamics.

damping. The lateral acceleration a_y is described by the following relation,

$$a_y = \dot{v}_y + v_x\dot{\psi}.$$

Note that the variables v_x, v_y, and a_y, in this model, describe the motions of the roll center, rather than the CoG (which is moving from side to side, relative the remaining chassis dynamics).

3.1 Tire Modeling

For the tire modeling, three different models of various complexity are considered; a linear model, a nonlinear model, and a nonlinear model capturing tire-force lag. The slip angle, α, is defined as

$$\alpha_f = \delta - \arctan\left(\frac{v_y + l_f\dot{\psi}}{v_x}\right), \tag{6}$$

$$\alpha_r = -\arctan\left(\frac{v_y - l_r\dot{\psi}}{v_x}\right), \tag{7}$$

for the front and rear axles, following the definitions in Pacejka (2006).

Linear Tire-Model

The *linear tire-model* assumes a linear relation between the tire force and slip angle, described by

$$F_{y,i} = C_{\alpha,i}\alpha_i, \quad i = f, r, \tag{8}$$

where $C_{\alpha,f}, C_{\alpha,r}$ are the cornering stiffness for the front and rear axles.

Magic Formula

To represent the nonlinear force–slip tire characteristics, the *Magic Formula* tire model, Pacejka (2006), has been considered. The model is described by

$$F_{y,i} = \mu_{y,i}F_{z,i}\sin(C_{y,i}\arctan(B_{y,i}\alpha_i - E_{y,i}(B_{y,i}\alpha_i - \arctan B_{y,i}\alpha_i))), \tag{9}$$

with $i = f, r$. Here μ_y represent the lateral friction-coefficient and $C_{y,i}$, $E_{y,i}$ are model parameters, while $B_{y,i}$ can be calculated from

$$B_{y,i} = \frac{C_{\alpha,i}}{C_{y,i}\mu_{y,i}F_{z,i}}.$$

The normal loads, $F_{z,f}$ and $F_{z,r}$, are here considered static, since no load transfer is included in the chassis model. Hence, they are given by

$$F_{z,f} = mg\frac{l_r}{l}, \quad F_{z,r} = mg\frac{l_f}{l}, \tag{10}$$

where g is the gravity constant and l the wheel base according to $l = l_f + l_r$.

Relaxation Length

Due to compliences in the tire structure, a reduced response appears for the lateral tire-forces. This force lag can be described by a *relaxation length*, σ, introducing a time-delay for the slip angles, Pacejka (2006). The delayed slip angle, denoted α^*, is described by

$$\dot{\alpha}_i^* \frac{\sigma}{v_{x,i}} + \alpha_i^* = \alpha_i, \quad i = f, r. \tag{11}$$

This slip angle is then used in the tire-force equation, thereby forming a delayed tire-force response. The relaxation-length model will here only be used together with the Magic Formula tire-model, where F_y is described, analogous to (9), as

$$F_{y,i} = \mu_{y,i}F_{z,i}\sin(C_{y,i}\arctan(B_{y,i}\alpha_i^* - E_{y,i}(B_{y,i}\alpha_i^* - \arctan B_{y,i}\alpha_i^*))), \tag{12}$$

with $i = f, r$.

3.2 Model Configurations

The four different model configurations, composed of the above submodels, are the following:

- Single-track model, (1)–(2), with the linear tire model, (8).
- Single-track model, (1)–(2), with the Magic Formula tire model, (9).
- Single-track model, (1)–(2), with the Magic Formula tire model and relaxation length, (11)–(12).
- Single-track model with roll dynamics, (3)–(5), and the Magic Formula tire model, (9).

These models are summarized in Table 2, where also the corresponding model notations are stated.

Table 2: Notations for the considered model configurations.

Model	Notation
Single-track with linear tire-model	ST-L
Single-track with Magic Formula	ST-MF
Single-track with Magic Formula and relaxation length	ST-MF-RL
Single-track with roll dynamics and Magic Formula	ST-Roll-MF

4 Test Scenarios

Three different test scenarios, for parametrization and validation purposes, have been considered. The tests were held at Linköpings Motorstadion, using the vehicle testbed presented in Section 2.

The *slalom test* consists of seven lined up cones, separated by 17 m. The vehicle is driven through the course, in a slalom pattern, at constant speed.

The *double lane-change maneuver* is a standardized test, often used for vehicle stability evaluations, ISO 3888-2:2011 (2011). An overview sketch is shown in Figure 6.

An additional test, here referred to as the *rock'n'roll test*, is carried out for the vehicle at stand-still. The sprung body is pushed from the side, or *rocked* back and forth, initiating in a vibrating motion in the *roll* direction. Hence the name; the vehicle is *rocked* and then *rolls*. The sequence of interest is when the vehicle body is left to roll-vibrate freely, with no external forces being applied.

The experiments above have been conducted at two separate occasions, under slightly different weather conditions. The vehicle parameters, such as inertia and mass properties, are considered equal for both occasions, however, the tire parameters are not. Therefore, when referring to the measurement data, two separate batches are considered; *measurement batch 1* and *measurement batch 2*. The first batch consists of 26 different double lane-change maneuvers with different entry speeds. The second batch includes seven slalom runs, two double lane-change maneuvers, and the rock'n'roll test for two different load cases (normal load-condition and with a 75 kg roof load).

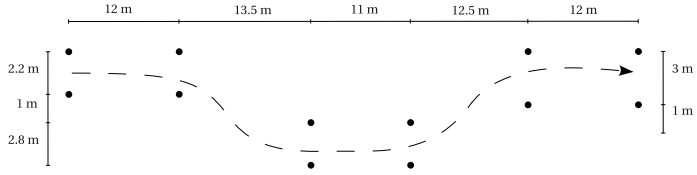

Figure 6: A sketch over the double lane-change maneuver.

5 Model Parameter Estimation

The parametrization, for the models in Section 3, has been carried out with established estimation methods, on data sets gathered with the vehicle testbed presented in Section 2.

5.1 Estimation Method

A *prediction-error identification method* (PEM), Ljung (1999), has been used for the parameter estimations. Consider a system represented by

$$\dot{x}(t,\theta) = f(x(t),u(t);\theta), \tag{13}$$
$$y(t,\theta) = h(x(t,\theta),u(t);\theta) + e(t), \tag{14}$$

with x being the state vector, u the input, y the system output (*i.e.*, the measurements), e the measurement noise and θ the parameter set. A prediction for the output of this system, $\hat{y}$, can then be formulated according to

$$\dot{\hat{x}}(t,\theta) = f(\hat{x}(t,\theta),u(t);\theta), \tag{15}$$
$$\hat{y}(t,\theta) = h(\hat{x}(t,\theta),u(t);\theta), \tag{16}$$

where $\hat{x}$ represent the estimated state vector. A cost function, V, based on the predictive error, ε, is then defined as

$$\varepsilon(t,\theta) = y(t,\theta) - \hat{y}(t,\theta), \tag{17}$$
$$V(\theta) = \frac{1}{N}\sum_{t_0}^{t_N} \varepsilon(t,\theta)^T W \varepsilon(t,\theta), \tag{18}$$

for the measurement set of N samples. The weighting matrix W is a diagonal matrix which enables the user to weight the different error predictions against each other, based on noise, relative magnitude, or confidence to a specific sensor. The estimated parameter set, $\hat{\theta}$, is then found by minimizing the cost function,

$$\hat{\theta} = \arg\min_{\theta} V(\theta). \tag{19}$$

To perform this estimation procedure, the Matlab toolbox *System Identification Toolbox*, The MathWorks, Inc. (2013), has been utilized.

5.2 Vehicle Parameters

The vehicle parameters that need to be determined, are the ones used in (1)–(2) and (3)–(5), being m, l_f, l_r, and I_{zz}, if temporarily neglecting parameters for the roll dyanmics (they will be treated below). The total vehicle mass, m, and CoG-to-wheel-axis distances, l_f and l_r, have been determined in a more straightforward fashion, not utilizing the above estimation routine, with a vehicle scale and manual tape-measuring. To determine the yaw inertia, I_{zz}, data

from five different slalom runs and two double lane-change runs were used, belonging to measurement batch 2. The estimation method was then employed to determine I_{zz} and the complete set of tire parameters for the ST-MF model (using ST-MF-RL or ST-Roll-MF instead, results in equivalent values for I_{zz}). Since, the validation procedure will consider measurement batch 1, and the tire parameters found here only are valid for measurement batch 2, these are discarded.

Roll Dynamics Parameters

To determine the parameters corresponding to the roll dynamics, data from the stand-still rock'n'roll test was used. In (5), five parameters appear; I_{xx}, D_ϕ, K_ϕ, m_s, and h, but only three lumped parameters can be distinguished from this equation;

$$\frac{D_\phi}{I_{xx}}, \quad \frac{K_\phi}{I_{xx}}, \quad \text{and} \quad \frac{m_s h}{I_{xx}}.$$

However, in (3) $m_s h$ appears apart from I_{xx}. Thus, as a minimum, the following four parameters need to be determined;

$$I_{xx}, \quad D_\phi, \quad K_\phi, \quad \text{and} \quad m_s h.$$

For this purpose, two different load cases of the rock'n'roll test was used; no additional loading and a 75 kg roof-load. The roof load was here treated as a point mass, $m_{aux} = 75$ kg, located $h_{aux} = 1.60$ m above ground, thus, contributing with an additional roll inertia of $I_{aux} = m_{aux}(h_{aux} - h_{rc})^2$.

If the vehicle is considered to vibrate freely about the roll axis, which is the case for the rock'n'roll tests, this implies no external forces are present, *i.e.* $a_y = 0$. Thus, (5) can therefore be rewritten as

$$I_{xx}\ddot{\phi} + D_\phi\dot{\phi} + K_\phi\phi = 0,$$

for the normal load-case and

$$(I_{xx} + I_{aux})\ddot{\phi} + D_\phi\dot{\phi} + K_\phi\phi = 0,$$

for the load case with a roof load. Applying the estimation method on these two equations, with data from the rock'n'roll tests, the lumped parameters in Table 3 can be determined. These four parameters forms an overdetermined system for the unknown parameters, I_{xx}, D_ϕ, and K_ϕ, which is solved with the least square method.

The remaining roll parameters, *i.e.*, the lumped parameter $m_s h$ and the roll-center height h_{rc}, was subsequently estimated simultaneously with the tire parameters, from the double lane-change tests. Here the relation

$$a_y = a_{y,imu} + (h_{imu} - h_{rc})\ddot{\phi},$$

Table 3: Estimated lumped roll-dynamics parameters.

Load case	Notation	Value	Std. dev.
No load	D_ϕ/I_{xx}	7.255	0.045
	K_ϕ/I_{xx}	173.2	0.57
Roof load	$D_\phi/(I_{xx}+I_{aux})$	5.617	0.029
	$K_\phi/(I_{xx}+I_{aux})$	138.5	0.32

was utilized to determine h_{rc}, where a_y represent the lateral acceleration at the roll center, while $a_{y,imu}$ is the lateral acceleration the IMU sensor sees, *i.e.*, at a distance $h_{imu} = 0.40$ m from the ground.

In Table 4 all the determined vehicle parameters are specified, with corresponding standard deviations for I_{zz}, $m_s h$, and h_{rc}. The low magnitude of these standard deviations, in relation to the parameter values, indicates a confident estimate for these parameters. Standard deviations are not specified for m, l_f, and l_r since no estimation method has been involved to acquire them, and neither for I_{xx}, D_ϕ, and K_ϕ because they are simply least-square values from the parameters in Table 3. For all the parameters in Table 4, reasonable values are obtained when considering physical dimensions. Except for the lumped parameter $m_s h$. The sprung mass m_s is only a subset of the total mass m, thus, $m_s < m$. However, for this condition to hold, the CoG-to-roll-center height needs to be $h > 0.57$ m. This implies a CoG height of $h > 0.74$ m, which by physical means, seems a bit high. This indicates that the lumped parameter $m_s h$ is capturing characteristics beside the physical quantities m_s and h, or that it compensates for poor parametrization of, *e.g.*, the roll inertia or roll stiffness/damping.

Table 4: Vehicle parameters.

Notation	Value	Unit	Std. dev.
m	1415	kg	-
l_f	1.03	m	-
l_r	1.55	m	-
I_{zz}	2581	kgm^2	13.5
I_{xx}	616	kgm^2	-
D_ϕ	4390	Nms/rad	-
K_ϕ	106600	Nm/rad	-
$m_s h$	807	kgm	0.67
h_{rc}	0.165	m	0.0046

5.3 Tire Parameters

The tire parameters were determined from 23 different double lane-change runs, sampled in measurement batch 1, leaving three tests from this batch for validation purpose (see the following section). The tire parameters were estimated for ST-MF, ST-MF-RL, and ST-Roll-MF separately, and is summarized in Table 5 with corresponding standard deviations. For ST-L, the cornering stiffness, $C_{\alpha,f}$ and $C_{\alpha,r}$—being the only tire parameters for this model—were taken from the estimated ST-MF parameter-set. In Figure 7 the force–slip characteristics is shown for the different estimated parameter-sets. Here the cornering stiffness seems less stiff for ST-MF, compared to ST-MF-RL and ST-Roll-MF, which is congruent with the specified values for C_α in Table 5. Since ST-MF does not incorporate any kind of response delay, such as relaxation length in ST-MF-RL or the roll dynamics in ST-Roll-MF, it compensates for this with a more compliant force model. Also, the cornering stiffness for the front wheels is lower, compared the rear-wheel cornering-stiffness, for all models. This should be a combined effect of different normal loads, F_z, on the wheel axes, as well as more compliance in front suspension and steering. For the rear wheel force–slip curves in Figure 7, considerable deviations between the models can be seen for slip angles $\alpha > 0.07$ rad. This is a result of a limited number of data samples in this region, which is also indicated by the high standard deviations for C_y and E_y, suggesting these are unreliable parameter values. The characteristics seen in this region is therefore purely an extrapolated effect of the parametrization at lower slip angles. However, this will only be an issue if the vehicle models are subjected to maneuvers provoking very large slip angles.

Table 5: Estimated tire parameters.

	ST-MF		ST-MF-RL		ST-Roll-MF	
Notation	Value	Std. dev.	Value	Std. dev.	Value	Std. dev.
$C_{\alpha,f}$	103600	701	114600	648	128200	881
$C_{\alpha,r}$	120000	1288	138400	1923	162300	991
$\mu_{y,f}$	1.20	0.079	1.12	0.019	1.07	0.062
$\mu_{y,r}$	0.85	0.002	0.91	0.011	0.86	0.001
$C_{y,f}$	1.15	0.86	0.809	0.026	1.13	0.78
$C_{y,r}$	1.46	0.055	0.924	0.031	1.82	0.13
$E_{y,f}$	0.41	2.18	-0.73	0.073	0.354	1.51
$E_{y,r}$	-1.55	0.19	-4.47	0.28	-0.029	0.22
σ	-	-	0.571	0.0066	-	-

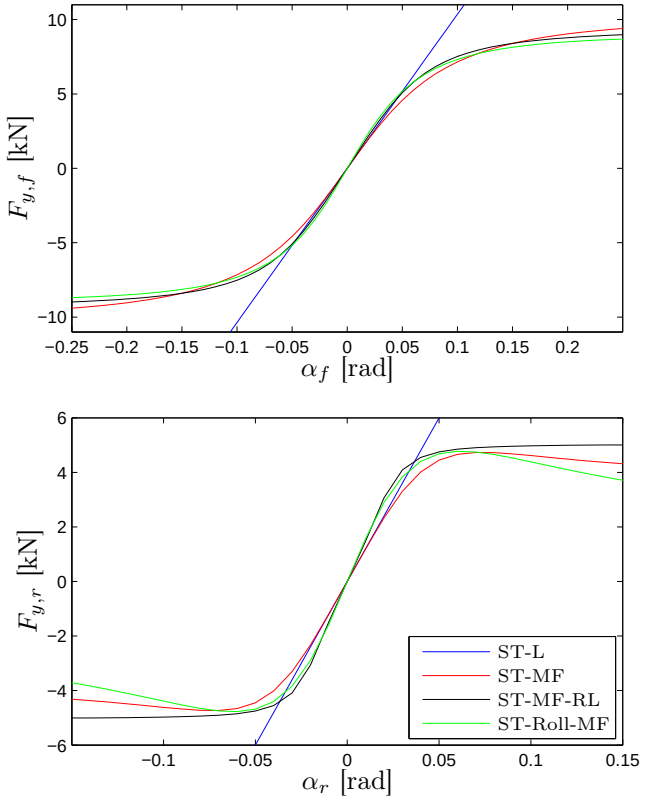

Figure 7: Tire forces vs slip angles, for the different models.

6 Model Validation and Analysis

As a basis for the model validation, data from three double lane-change tests, belonging to measurement batch 1, were used. These tests were employed with different initial speeds, thus, triggering various levels of dynamics. The tests are denoted Test 1, Test 2, and Test 3, corresponding to the results shown in Figure 8, 9 and 10. In these figures, measurement data for yaw rate $\dot{\psi}$, lateral acceleration a_y, front slip-angle α_f, and rear slip-angle α_r are displayed along with simulated data for the models in Section 3, with the parameter sets from Section 5. In Figure 11–13 the measured roll angle is compared to the simulated for ST-Roll-MF. The simulation results are acquired with an ODE solver, using steer-wheel angle δ and longitudinal velocity v_x from the measurement data as input signals. Table 6 specifies the initial velocity v_{init} and maximum values for steering-wheel angle δ_{sw}, steering-wheel-angle rate-of-change $\dot{\delta}_{sw}$, yaw rate $\dot{\psi}$, lateral acceleration a_y, slip angle α, and slip-angle rate-of-change $\dot{\alpha}$, corresponding to measurement data for Test 1–3. Notice that

δ_{sw} here denotes the angle the driver is turning the steering wheel, unlike δ, which denotes the steer angle of the front wheels. The values in Table 6 give a representative overview for the tests, indicating the nature of each test run. The fundamental differences between these runs are the different entry speeds, which propagates to affect the overall behavior. A higher entry speed requires more rapid maneuvering, in terms of $\dot{\delta}_{sw}$, resulting in higher values for $\dot{\psi}$, a_y, α, and $\dot{\alpha}$.

In Figure 8, showing results for Test 1, the different models produce very consistent behavior, with good agreement to the experimental data. This is natural since the maneuvering mainly is making use of the linear region of the tire models, which is indicated by the measured maximum slip-angle values, $\alpha_{f,max}$ and $\alpha_{r,max}$, in Table 6. Although this test would be considered as quite a hefty maneuver compared to normal driving, for example in terms of $a_{y,max}$ and $\dot{\delta}_{sw,max}$, it is still not enough to trigger notable effects from relaxation length or roll dynamics.

For Test 2, in Figure 9, larger tire forces are required to handle the more rapid dynamics. Hence, slip angles outside of the linear region are utilized, see Figure 7. The ST-L model therefore becomes less valid for these parts of the maneuver, being most obvious for $\dot{\psi}$ and a_y around $t = 2.7$ s. For the other three models, only minor differences appear.

In Test 3, more distinct differences appear for the different models, see Figure 10. This is simply a consequence of the faster and more aggressive level of dynamics, *e.g.*, in terms of $a_{y,max}$, $\dot{\alpha}_{f,max}$, and $\dot{\alpha}_{r,max}$, that comes with the higher entry speed. The differences are most pronounced towards the end of the maneuver, while for the first half they all show remarkably similar behavior, following the measurement well. For the second half, ST-L is off by quite a margin. Both ST-MF and ST-MF-RL follow the measurement data by similar means, although, ST-MF-RL seems to be able to capture the most rapid characteristics slightly more accurate. ST-Roll-MF, on the other hand, shows quite erroneous behavior for the last half second of the maneuver, where the rear slip-angle encounters a large overshoot at $t = 3.5$ s, subsequently affecting other variables. This overshoot-tendency can also be seen at $t = 2.8$ s. The reason for this behavior, is mainly due to the tire-model parametrization. In Figure 7, $F_{y,r}$ for ST-Roll-MF decays fast for $\alpha_r > 0.07$ rad, compared to the other models. Thus, for rear slip-angles of this magnitude, ST-Roll-MF is unable to produce large enough $F_{y,r}$, resulting in an increasing α_r.

Considering the roll angle behavior in Test 1 and 2, as well as the first part of Test 3, see Figure 11–13, ST-Roll-MF captures the overall roll-angle dynamics very well. Except around some of the peak values, which might be an indication of erroneous roll-parameters or nonlinear characteristics in the roll dynamics, that could contribute to false simulation behavior or tire-model parametrization (such as the fast decay of $F_{y,r}$, discussed above).

Table 6: Initial velocity and maximum values, for a few selected variables, corresponding to the measurement data for Test 1–3. Note that δ_{sw} refers to the steering wheel angle.

Variable	Test 1	Test 2	Test 3	Unit
v_{init}	38.3	51.4	62.4	km/h
$\delta_{sw,max}$	154	147	157	deg
$\dot{\delta}_{sw,max}$	615	742	1013	deg/s
$\dot{\psi}_{max}$	0.535	0.586	0.710	rad/s
$a_{y,max}$	5.78	7.96	9.23	m/s^2
$\alpha_{f,max}$	0.062	0.097	0.124	rad
$\alpha_{r,max}$	0.034	0.060	0.102	rad
$\dot{\alpha}_{f,max}$	0.386	0.551	0.814	rad/s
$\dot{\alpha}_{r,max}$	0.239	0.400	0.690	rad/s

7 Conclusions

A vehicle dynamics testbed has been developed, for the purpose of studying road-vehicle behavior and characteristics in aggressive and rapid maneuvers. A parametrization procedure is subsequently presented, determining individual vehicle and tire parameters for different model configurations, from measurement data gathered with the vehicle testbed. The treated models capture various dynamic properties, such as tire-force saturation, tire-force lag, and roll dynamics. Data for a double lane-change maneuver has then been used for validating and analyzing the dynamic characteristics of these models with their corresponding parameter sets.

The study shows that for an evasive maneuver, a simple model—such as the single-track with a tire model capturing the tire-force saturation—can predict the lateral dynamics well, even for very quick and rapid maneuvering. Additional complexity could be added, *e.g.*, by introducing tire-force lag, but the gain in accuracy is minor. This is promising for further studies on the subject, indicating that less complex vehicle-models might be accurate enough for certain critical-maneuvering applications. However, for more convincing conclusions to be established, additional thorough investigations will be needed, *e.g.*, considering combined lateral and longitudinal dynamics.

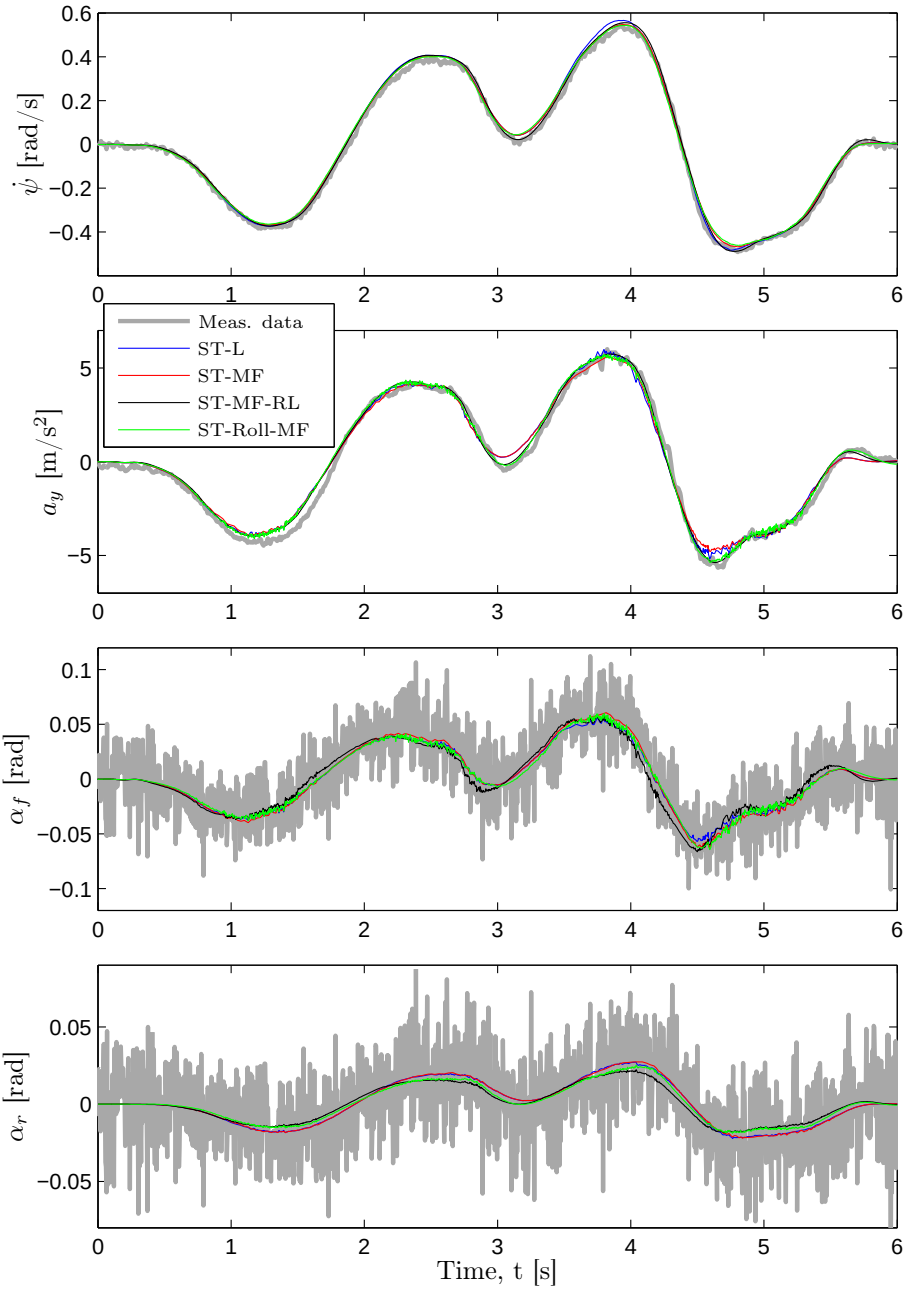

Figure 8: Measurement data compared to simulations of ST-L, ST-MF, ST-MF-RL, and ST-Roll-MF for Test 1, *i.e.* a double lane-change maneuver with initial velocity of $v_{init} = 38$ km/h.

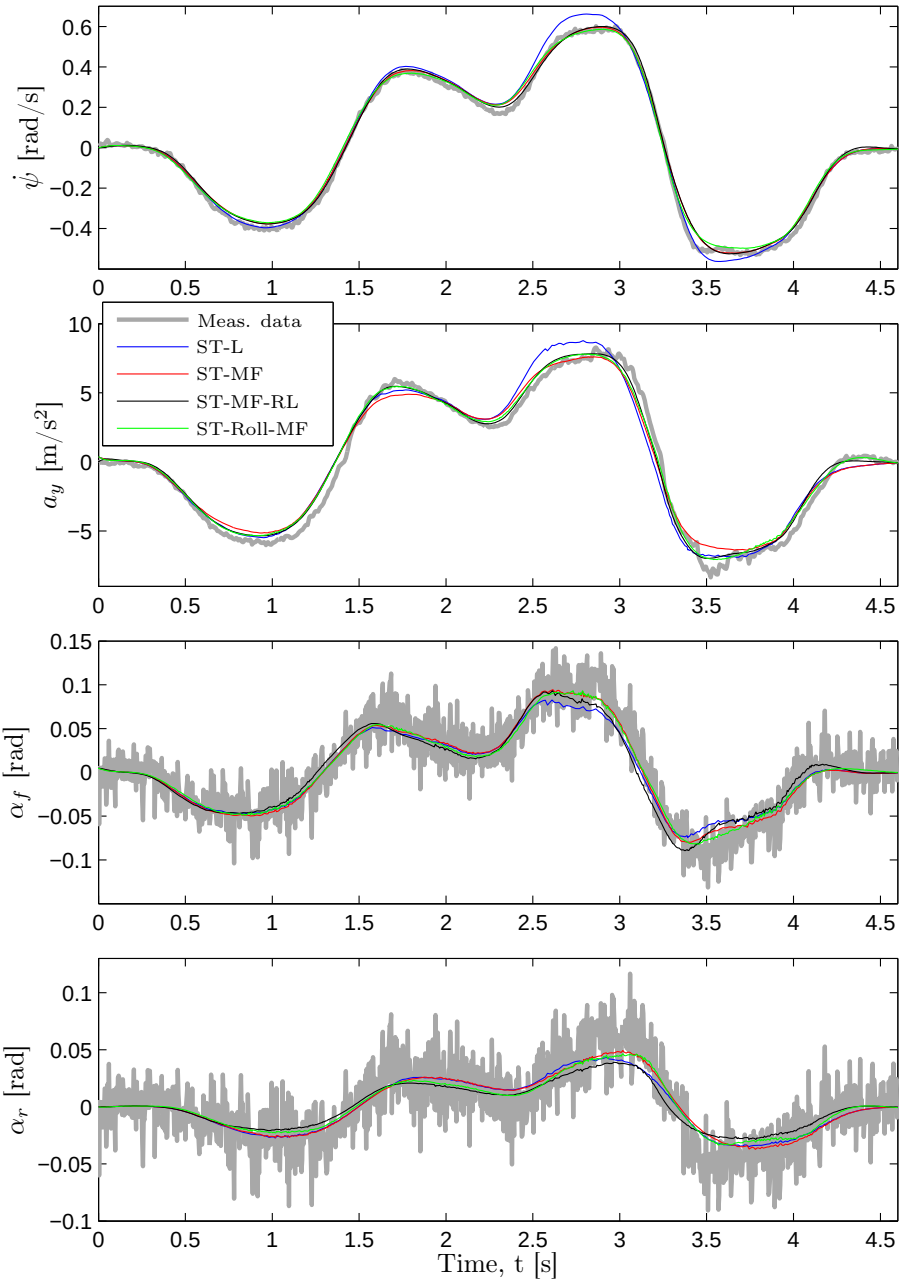

Figure 9: Measurement data compared to simulations of ST-L, ST-MF, ST-MF-RL, and ST-Roll-MF for Test 2, *i.e.* a double lane-change maneuver with initial velocity of $v_{init} = 51$ km/h.

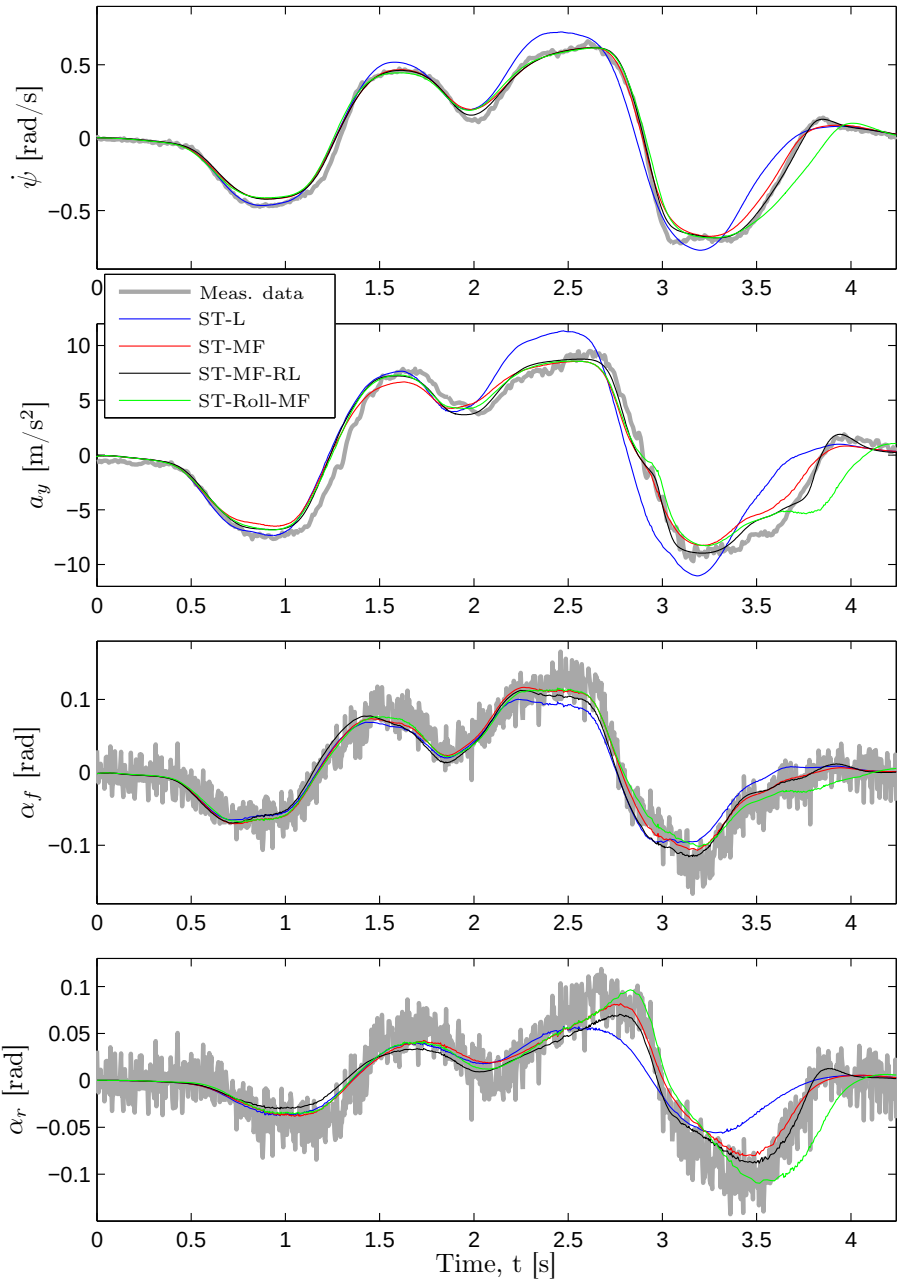

Figure 10: Measurement data compared to simulations of ST-L, ST-MF, ST-MF-RL, and ST-Roll-MF for Test 3, *i.e.* a double lane-change maneuver with initial velocity of $v_{init} = 62$ km/h.

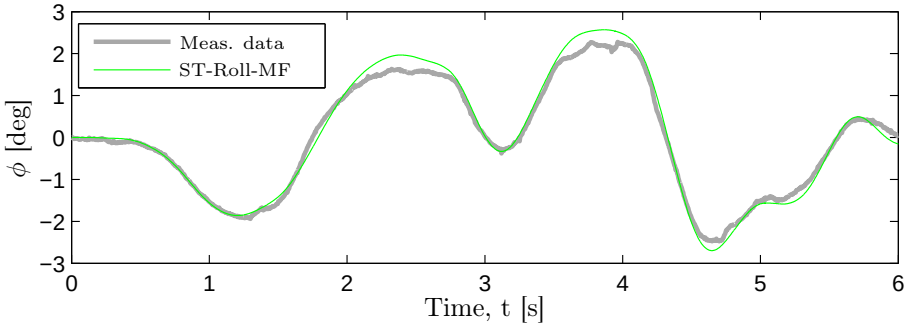

Figure 11: Roll-angle measurement compared to simulation with ST-Roll-MF, for Test 1.

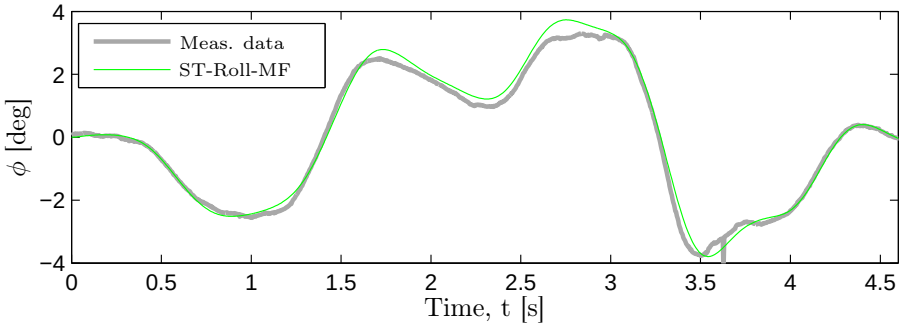

Figure 12: Roll-angle measurement compared to simulation with ST-Roll-MF, for Test 2.

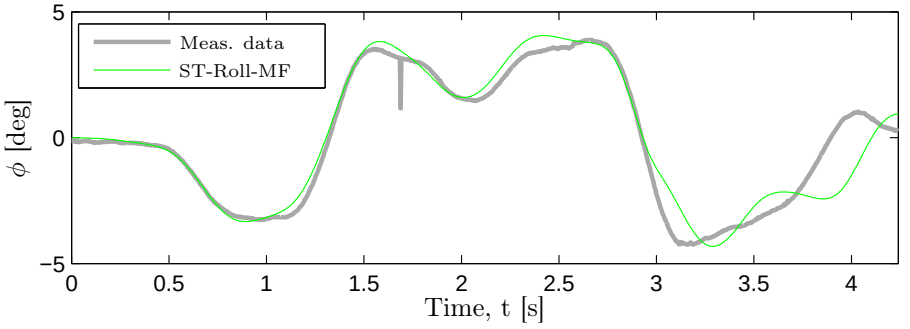

Figure 13: Roll-angle measurement compared to simulation with ST-Roll-MF, for Test 3.

References

HF Sensors, HF-250C/HF-500C/HF-750C, Optical Laser Height Sensor with CORREVIT SF Housing Profile for Non-contact Distance Measurement, User Manual Volume I. Corrsys-Datron Sensorsysteme GmbH, 2009a.

CORREVIT S-350 Aqua, Non-contact 2-axis Optical Sensor for Slip Free Measurement of Longitudinal and Transversal Dynamics, User Manual Volume I. Corrsys-Datron Sensorsysteme GmbH, 2009b.

ISO 3888-2:2011. *Passenger cars — Test track for a severe lane-change manoeuvre — Part 2: Obstacle avoidance.* International Organization for Standardization, Geneva, Switzerland, 2011.

Lennart Ljung. *System Identification: Theory for the User, 2/e.* Prentice Hall, second edition, 1999.

Kristoffer Lundahl, Jan Åslund, and Lars Nielsen. Investigating vehicle model detail for close to limit maneuvers aiming at optimal control. In *22nd Int. Symp. on Dynamics of Vehicles on Roads and Tracks (IAVSD)*, Manchester, United Kingdom, 2011.

Hans B. Pacejka. *Tire and Vehicle Dynamics.* Butterworth-Heinemann, Oxford, United Kingdom, second edition, 2006.

The MathWorks, Inc. MATLAB: System Identification Toolbox, 2013. URL `http://www.mathworks.se/products/sysid/`.

AEK-4P, AEK-4H, GPS and SuperSense Evaluation Kits, ANTARIS 4 Positioning Engine. u-blox AG, 2005.

J.Y. Wong. *Theory of Ground Vehicles.* John Wiley & Sons, INC, Ottawa, Canada, fourth edition, 2008.

MTi and MTx User Manual and Technical Documentation. Xsens Technologies B.V., 2009.

Paper B

Models and Methodology for Optimal Vehicle Maneuvers Applied to a Hairpin Turn*

B

*In *the 2013 American Control Conference*, Washington D.C., USA, 2013.

Models and Methodology for Optimal Vehicle Maneuvers Applied to a Hairpin Turn

Karl Berntorp[a], Björn Olofsson[a], Kristoffer Lundahl[b],
Bo Bernhardsson[a], and Lars Nielsen[b]

[a] *Department of Automatic Control,*
Lund University, SE–221 00 Lund, Sweden

[b] *Vehicular Systems, Department of Electrical Engineering,*
Linköping University, SE-581 83 Linköping, Sweden

Abstract

There is currently a strongly growing interest in obtaining optimal control solutions for vehicle maneuvers, both in order to understand optimal vehicle behavior and to devise improved safety systems, either by direct deployment of the solutions or by including mimicked driving techniques of professional drivers. However, it is nontrivial to find the right mix of models, formulations, and optimization tools to get useful results for the above purposes. Here, a platform is developed based on a state-of-the-art optimization tool together with adoption of existing vehicle models, where especially the tire models are in focus. A minimum-time formulation is chosen to the purpose of gaining insight in at-the-limit maneuvers, with the overall aim of possibly finding improved principles for future active safety systems. We present optimal maneuvers for different tire models with a common vehicle motion model, and the results are analyzed and discussed. Our main result is that a few-state single-track model combined with different tire models is able to replicate the behavior of experienced drivers. Further, we show that the different tire models give quantitatively different behavior in the optimal control of the vehicle in the maneuver.

1 Introduction

Optimization of vehicle trajectories can be motivated from different perspectives. One objective is to develop improved active safety systems for standard customer cars. The Electronic Stability Program (ESP) systems, see Isermann (2006) and Liebemann et al. (2005), of today are still behind the maneuvering performance achievable by professional race car drivers in critical situations, but the vision for improvement is there, see Funke et al. (2012). A recent survey on optimal control in automotive applications Sharp and Peng (2011) points out:

> Most often, the optimal control itself will be interesting mainly insofar as it enables the discovery of the best possible system performance. Occasionally, the optimal control will provide a basis for the design and operation of practical systems.

Further, the survey points out that finding the right balance between models, correct formulations, and optimization methods is nontrivial, and that the state-of-the-art today is hampered by long simulation runs. The goal in this paper, regarding methodology, is to develop and investigate a platform for useful solutions to these problems.

It is a common observation that the criterion of time-optimality in aggressive vehicle maneuvers, combined with input and state constraints, often results in control signals using the extremal cases of the input and state regions. It is

Figure 1: An example of a hairpin turn. Photo courtesy of RallySportLive.

therefore crucial how, *e.g.*, the tires are modeled outside their normal range of operation.

The interaction between tire and road is complex, and different tires have different characteristics. Even when only considering the longitudinal stiffness, the experimental values differ considerably between tires, and the variability can typically be 20–100 %, see Carlson and Gerdes (2005). Further, in addition to the differences in stiffness—*i.e.*, the slope of the longitudinal force-slip curve—there are also differences between the characteristic shape of the curve at the maximum force, where the peak can be more or less accentuated. This is illustrated for Pacejka's Magic Formula and the HSRI model in Carlson and Gerdes (2005). The complete tire model capturing both longitudinal and lateral forces can thus be expected to have large variability both in shape, parameters, and parameter irregularity.

The control oriented goal of this paper is to find a formulation that gives insight into improved safety systems; *e.g.*, future ESP systems performing closer to what the most experienced drivers can do. To that end we study a time-optimal maneuver in a hairpin turn, an interesting situation testing the limits of maneuverability of a car in a certain situation. In Lundahl et al. (2011) we reported that simplified vehicle models identified from experimental data managed to replicate the behavior of real vehicles. However, this was based on less aggressive driving situations, and not using optimization. Previous work in the subject of optimal control of vehicles in certain time-critical situations such as T-bone collisions and cornering can be found in, *e.g.*, Chakraborty et al. (2011); Velenis and Tsiotras (2005); Velenis (2011). In Anderson et al. (2010, 2012), methods for constraint-based trajectory planning for optimal maneuvers are presented. Further, the papers Sundström et al. (2010); Andreasson (2009) discuss optimal control of over-actuated vehicles, where similar optimization tools as those used in the present paper are utilized.

This paper is outlined as follows: The problem description and overall aim of the paper are discussed in Sec. 2. Vehicle and tire modeling and the specific models investigated in this study are presented in Sec. 3, followed by the formulation and solution of the studied time-optimal maneuvering problem in Sec. 4. Optimization results and a subsequent discussion of the obtained results are provided in Sec. 5. Finally, conclusions and aspects on future work are given in Sec. 6.

2 Problem Description

The goal of the work presented in this paper is twofold. The first goal is to find the time-optimal vehicle trajectory when maneuvering through a hairpin turn, see Figure 1 for an example, with the vehicle being subject to various constraints.

Another aim of the study is to explore whether different vehicle models yield fundamentally different solutions, not only in the cost function but also

in the internal behavior of the vehicle. Hence, a part of the work is devoted to investigating how the models differ. We consider differential-algebraic models of the form

$$\begin{aligned} \dot{x}(t) &= G(x(t), y(t), u(t)), \\ 0 &= h(x(t), y(t), u(t)), \end{aligned}$$

where $G(x(t), y(t), u(t))$ and $h(x(t), y(t), u(t))$ are twice continuously differentiable nonlinear functions of the vehicle differential variables x, algebraic variables y, and control inputs u. The models used are based on the same vehicle model, but differ in the tire modeling aspects.

The motivation for the twofold goal is that, to the best of our knowledge, most model comparisons in literature are based on simulation rather than optimization. Since time-optimal optimization problems tend to push the vehicle more to the extremes than simulations do, it is plausible that different conclusions about model behavior can be made from such an analysis.

3 Modeling

The vehicle dynamics modeling in this section incorporates the vehicle motion modeling and the tire force modeling, with emphasis on the latter. Further, calibration of the tire models is discussed and a subsequent investigation of the qualitative behavior of the models studied is presented.

3.1 Vehicle Modeling

As a basis for the vehicle dynamics model, a two-dimensional single-track model, with two translational and one rotational degrees-of-freedom, was used, see Figure 2. The motion equations are expressed by, see Schindler (2007); Ellis (1994),

$$\dot{v}_x - v_y\dot{\psi} = \frac{1}{m}(F_{x,f}\cos(\delta) + F_{x,r} - F_{y,f}\sin(\delta)), \tag{1}$$

$$\dot{v}_y + v_x\dot{\psi} = \frac{1}{m}(F_{y,f}\cos(\delta) + F_{y,r} + F_{x,f}\sin(\delta)), \tag{2}$$

$$I_z\ddot{\psi} = l_f F_{y,f}\cos(\delta) - l_r F_{y,r} + l_f F_{x,f}\sin(\delta), \tag{3}$$

where m is the vehicle mass, I_z is the vehicle inertia, $\dot{\psi}$ is the yaw rate, δ is the steering wheel angle, $v_{x,y}$ are the longitudinal and lateral velocities, $l_{f,r}$ are the distances from center-of-gravity to the front and rear wheel base, and $F_{x,y}$ are the longitudinal and lateral forces acting on the front and rear wheels. The slip

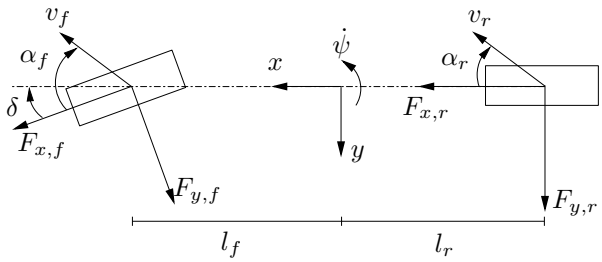

Figure 2: The single-track model considered in this paper.

angles, $\alpha_{f,r}$, and slip ratios, $\kappa_{f,r}$, are described by

$$\alpha_f = \delta - \arctan\left(\frac{v_y + l_f\dot{\psi}}{v_x}\right), \tag{4}$$

$$\alpha_r = -\arctan\left(\frac{v_y - l_r\dot{\psi}}{v_x}\right), \tag{5}$$

$$\kappa_f = \frac{R_e\omega_f - v_{x,f}}{v_{x,f}}, \tag{6}$$

$$\kappa_r = \frac{R_e\omega_r - v_{x,r}}{v_{x,r}}, \tag{7}$$

$$v_{x,f} = v_x\cos(\delta) + (v_y + l_f\dot{\psi})\sin(\delta), \tag{8}$$

$$v_{x,r} = v_x, \tag{9}$$

where R_e is the effective wheel radius and $\omega_{f,r}$ are the front and rear wheel angular velocities. The wheel dynamics, necessary for slip ratio computation, is given by

$$T_i - I_w\dot{\omega}_i - F_{x,i}R_w = 0\ , \quad i = f, r. \tag{10}$$

Here, T_i is the driving/braking torque, I_w is the wheel inertia, and R_w is the loaded wheel radius. The numerical values for the vehicle model parameters used in this study are provided in Table 1.

3.2 Tire Modeling

When developing a platform for investigation of optimal maneuvers, it is of interest to be able to handle and compare different tires, and thus to cope with different tire models. We have considered two different model categories for tire modeling, whose characteristics are described next.

The nominal tire forces—*i.e.*, the forces under pure slip conditions—are

Table 1: Vehicle model parameters used in (1)–(10).

Notation	Value	Unit
l_f	1.3	m
l_r	1.5	m
m	2100	kg
I_z	3900	kgm^2
R_e	0.3	m
R_w	0.3	m
I_w	4.0	kgm^2
g	9.82	ms^{-2}

computed with the Magic Formula model Pacejka (2006), given by

$$F_{x0,i} = \mu_x F_{z,i} \sin(C_{x,i} \arctan(B_{x,i}\kappa_i)), \tag{11}$$

$$F_{y0,i} = \mu_y F_{z,i} \sin(C_{y,i} \arctan(B_{y,i}\alpha_i)), \tag{12}$$

$$F_{z,i} = mg(l - l_i)/l, \ i = f, r. \tag{13}$$

In (11)–(13), μ_x and μ_y are the friction coefficients, B and C are model parameters, $l = l_f + l_r$, and g is the constant of gravity .

Under combined slip conditions—*i.e.*, both κ and α are nonzero—the longitudinal and lateral tire forces will depend on both slip quantities. How this coupling is described can have immense effect on the vehicle dynamics. In an optimal maneuver, the solution will use the best combination of longitudinal and lateral force, and these forces are, of course, coupled via the physics of the tire. In order to compare different models, plotting of the resulting tire force is illustrative, *c.f.* Figures 3–6, to visualize the interaction between longitudinal and lateral force.

Even though detailed experiments, like the ones in Carlson and Gerdes (2005) for longitudinal stiffness, are lacking for the complete longitudinal-lateral tire interaction, there is a vast plethora of characteristics, see Isermann (2006), Pacejka (2006), Kiencke and Nielsen (2005), and Rajamani (2006). We have chosen two different tire models for our study, described below.

Friction Ellipse

A common way to model combined slip is to use the friction ellipse, described by

$$F_{y,i} = F_{y0,i}\sqrt{1 - \left(\frac{F_{x0,i}}{\mu_x F_{z,i}}\right)^2}, \tag{14}$$

where F_x is used as an input variable. However, we have opted for using the driving/braking torques as input, see (10), since this is a quantity that can be controlled in a physical setup of a vehicle.

Weighting Functions

Another approach described in Pacejka (2006) is to scale the nominal forces, (11)–(12), with weighting functions, $G_{x\alpha,i}$ and $G_{y\kappa,i}$, which depend on α and κ. The relations in the x-direction are

$$B_{x\alpha,i} = B_{x1,i}\cos(\arctan(B_{x2,i}\kappa_i)), \tag{15}$$
$$G_{x\alpha,i} = \cos(C_{x\alpha,i}\arctan(B_{x\alpha,i}\alpha_i)), \tag{16}$$
$$F_{x,i} = F_{x0,i}G_{x\alpha,i}. \tag{17}$$

The corresponding relations in the y-direction are given by

$$B_{y\kappa,i} = B_{y1,i}\cos(\arctan(B_{y2,i}(\alpha_i - B_{y3,i}))), \tag{18}$$
$$G_{y\kappa,i} = \cos(C_{y\kappa,i}\arctan(B_{y\kappa,i}\kappa_i)), \tag{19}$$
$$F_{y,i} = F_{y0,i}G_{y\kappa,i}. \tag{20}$$

3.3 Calibrating Tire Models for Comparison

When comparing an optimal maneuver based on two different tire models, it is not obvious how to calibrate the models to get comparable solutions. For example, in Figure 3 and Figure 6 we show two different types of tire models. In order to equalize these models in comparative studies, one way would be to have the same average resultant force, whereas another way would be to equalize the longitudinal stiffness. In this study, the same parameters have been used for the nominal lateral force; *i.e.*, the lateral force characteristics are the same for all models when considering pure lateral slip.

3.4 Qualitative Behavior of Tire Models

In Figures 3–6 it is shown how the resulting force, defined by

$$F_{\text{res}} = \sqrt{F_{x,i}^2 + F_{y,i}^2},\ i = f, r,$$

for the above tire models varies over slip angle and slip ratio with the parameters presented in Table 2. Studying Figures 3–6 gives a basis for discussion of the behavior of the tire models in an optimal maneuver.

Figure 3 displays the friction ellipse model, and Figure 4 shows the weighting functions model for an isotropic parametrization. These are both considered isotropic in the sense that they have the same properties in the lateral and longitudinal directions. The most obvious difference in these figures can be seen for large slip angles, where an increase in the slip ratio will increase the resulting force for the friction ellipse model and, on the contrary, decrease it for the model based on weighting functions.

In contrast, considering the nonisotropic models, Figures 5 and 6, different force characteristics are obtained in the longitudinal and lateral directions. The

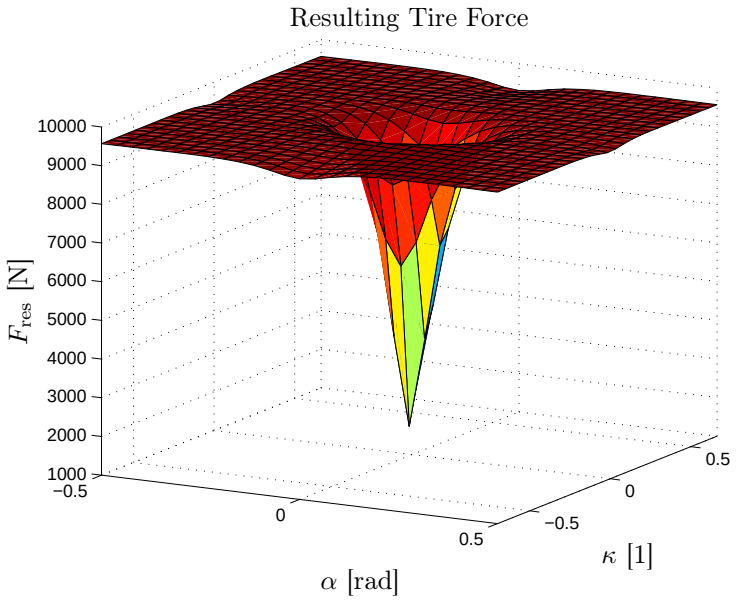

Figure 3: Resultant tire force F_{res} for a friction ellipse model parametrized to give isotropic behavior.

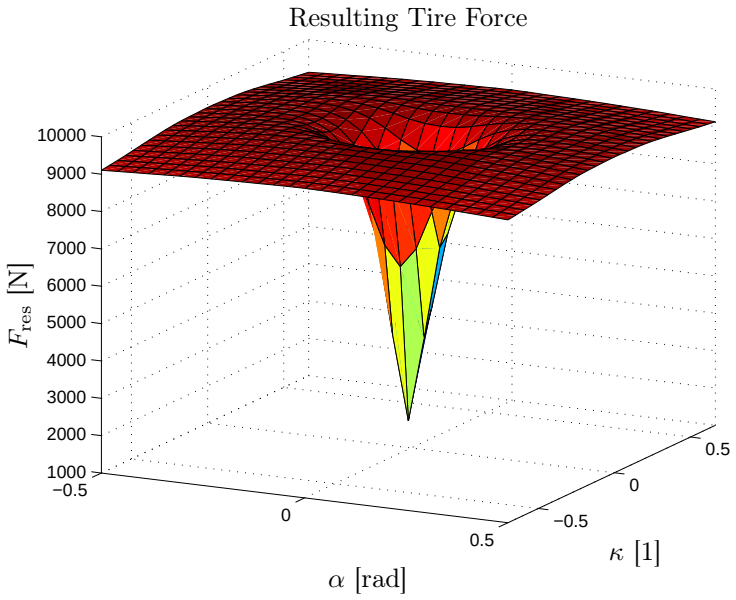

Figure 4: Resultant tire force F_{res} for a weighting functions model parametrized to give isotropic behavior.

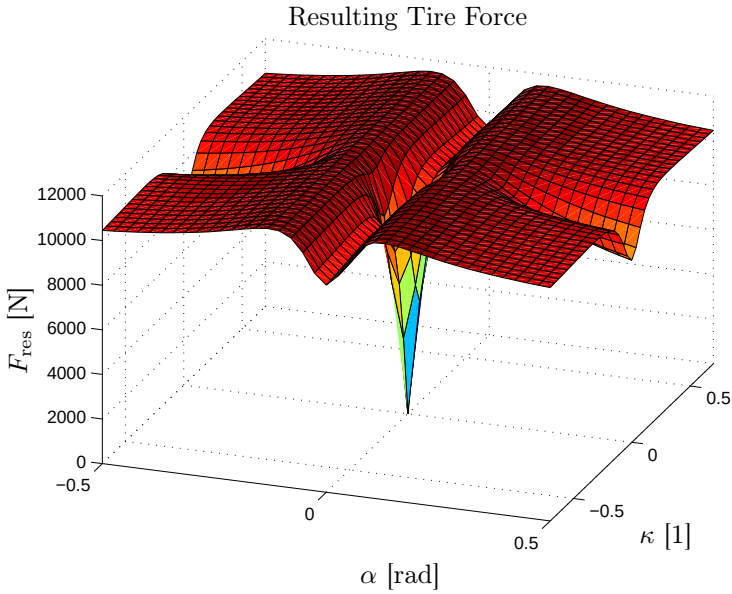

Figure 5: Resultant tire force F_{res} with a friction ellipse model with experimental parameters from Pacejka (2006) ($\mu_x = 1.2,\ \mu_y = 1.0$).

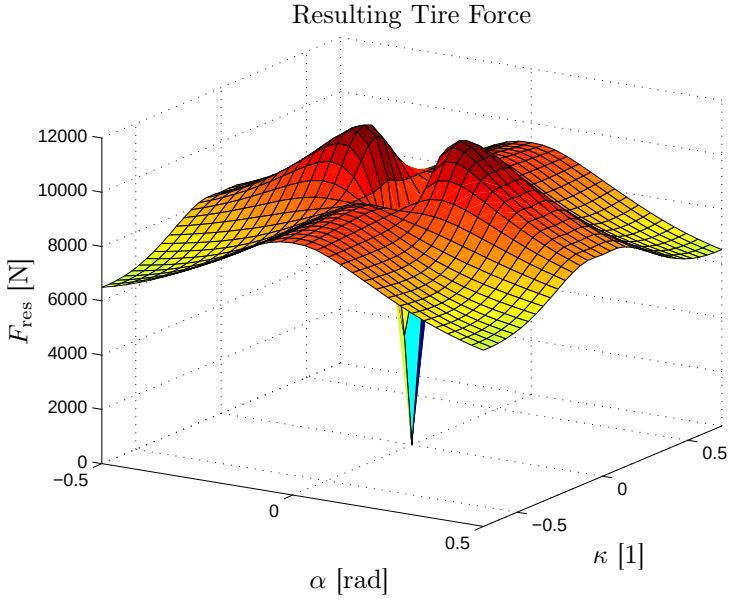

Figure 6: Resultant tire force F_{res} for a weighting functions model with the same friction coefficients as in Figure 5.

Table 2: Tire model parameters for friction ellipse with isotropic behavior (FE-Iso), nonisotropic behavior (FE-Noniso), and weighting functions with isotropic behavior (WF-Iso), nonisotropic behavior (WF-Noniso).

Parameter	FE-Iso	FE-Noniso	WF-Iso	WF-Noniso
μ_x	1.0	1.2	1.0	1.2
μ_y	1.0	1.0	1.0	1.0
$C_{\alpha,f}$	1.09e5	1.09e5	1.09e5	1.09e5
$C_{\alpha,r}$	1.02e5	1.02e5	1.02e5	1.02e5
$C_{\kappa,f}$	1.09e5	2.38e5	1.09e5	2.38e5
$C_{\kappa,r}$	1.02e5	2.06e5	1.02e5	2.06e5
C_x	1.3	1.7	1.3	1.7
C_y	1.3	1.3	1.3	1.3
$B_{x1,f}$	-	-	8.55	11.23
$B_{x2,f}$	-	-	8.33	10.80
$C_{x\alpha,f}$	-	-	1.03	1.14
$B_{y1,f}$	-	-	8.63	6.37
$B_{y2,f}$	-	-	8.35	2.64
$B_{y3,f}$	-	-	0	0
$C_{y\kappa,f}$	-	-	1.03	1.03
$B_{x1,r}$	-	-	9.28	11.71
$B_{x2,r}$	-	-	9.04	11.61
$C_{xa,r}$	-	-	1.03	1.14
$B_{y1,r}$	-	-	9.38	5.88
$B_{y2,r}$	-	-	9.08	2.98
$B_{y3,r}$	-	-	0	0
$C_{y\kappa,r}$	-	-	1.02	1.08

model based on the weighting functions is parametrized according to the Pacejka model in Pacejka (2006), thus representing a realistic tire behavior. The friction ellipse model also uses the Pacejka parameters in Pacejka (2006) for the nominal tire forces. Hence, both of the nonisotropic models will exhibit equivalent tire characteristics for pure slip conditions. Further, the characteristic peaks in F_{res}—not visible in the isotropic models—influence the behavior of the tire force model significantly.

4 Optimization

Based on the dynamics described in the previous section, the time-optimal maneuver for the hairpin turn is to be determined. This is expressed as an optimization problem, and, considering the physical setup of the problem, it is clear that an optimal solution exists. The resulting optimization problem is more challenging than thought at first sight, since the time-optimality implies that

the tire friction model operates on the boundary of its validity. Also, solving dynamic optimization problems where the final time is free, is more demanding than a problem with fixed end time. Further, we have found that numerical issues easily arise and that the optimization does not converge without proper initialization. In order to make the convergence more robust from a numerical point of view, scaling of the optimization variables is essential.

4.1 Formulation of Optimization Problem

Consider the time horizon $t \in [0, t_f]$, where t_f is the free final time to be determined as part of the solution procedure. Express the vehicle dynamics (1)–(3) and (10) as $\dot{x}(t) = G(x, y, u)$, where x are the differential variables and y are the algebraic variables. The wheel driving/braking torques $T = \begin{pmatrix} T_f & T_r \end{pmatrix}$ and the steering angle δ are considered as the input variables, $u = \begin{pmatrix} T & \delta \end{pmatrix}^{\mathrm{T}}$. Further, express (4)–(9), (11)–(13), and (14) or (15)–(20), depending on the friction model considered, as $0 = h(x, y, u)$. The dynamic optimization problem to be solved can then be stated as follows:

$$\begin{aligned}
\text{minimize} \quad & t_f && (21)\\
\text{subject to} \quad & T_{i,\min} \le T_i \le T_{i,\max}, \ i = f, r && (22)\\
& |\delta| \le \delta_{\max}, \quad |\dot{\delta}| \le \dot{\delta}_{\max} && (23)\\
& |F_{x,i}| \le F_{x,i,\max}, \ i = f, r && (24)\\
& |F_{y,i}| \le F_{y,i,\max}, \ i = f, r && (25)\\
& \left(\frac{X_p}{R_1^i}\right)^6 + \left(\frac{Y_p}{R_2^i}\right)^6 \ge 1 && (26)\\
& \left(\frac{X_p}{R_1^o}\right)^6 + \left(\frac{Y_p}{R_2^o}\right)^6 \le 1 && (27)\\
& x(0) = x_0, \quad y(0) = y_0 && (28)\\
& x(t_f) = x_{t_f}, \quad y(t_f) = y_{t_f} && (29)\\
& \dot{x}(t) = G(x, y, u), \quad 0 = h(x, y, u), && (30)
\end{aligned}$$

where (x_0, y_0) are the initial conditions for the differential/algebraic variables, (x_{t_f}, y_{t_f}) are the desired values at the final time $t = t_f$, and (X_p, Y_p) is the position of the center-of-gravity of the vehicle. Note that the path constraint is formulated using super-ellipses and the shape of the path is determined by the radii R_1^i, R_2^i, R_1^o, and R_2^o.

4.2 Solution of Optimization Problem

Because of the complex nature of the nonlinear and nonconvex optimization problem in (21)–(30), analytical solutions are intractable. Instead, we utilize numerical methods based on simultaneous collocation Biegler et al. (2002). Direct collocation is used, where all state and input variables, originally described

in continuous time, are discretized prior to the optimization. This results in a discrete-time nonlinear program (NLP). The collocation procedure transforms the original infinite-dimensional problem to a finite-dimensional problem with a large, however finite, number of optimization variables, on which numerical optimization methods are applied.

4.3 Implementation and Solution

The vehicle and tire dynamics are implemented using the modeling language Modelica Modelica Association (2012). Utilizing Optimica Åkesson (2008), which is an extension of Modelica for high-level description of optimization problems based on Modelica models, the implementation of the vehicle and tire dynamics described in Sec. 3 and the optimal control problem is straightforward.

The collocation procedure and solution of the optimization problem are performed using the open-source software platform JModelica.org Åkesson et al. (2010); JModelica.org (2012). In JModelica.org, orthogonal collocation is implemented, where Lagrange polynomials are used for representation of the state profiles in each element and the location of the collocation points are chosen as the corresponding Radau points. The resulting NLP is solved internally using the numerical solver Ipopt Wächter and Biegler (2006), which is a solver based on interior-point methods opted for large, but sparse, optimization problems.

4.4 Initialization Procedure

Robust convergence to a solution of the NLP in Ipopt relies on proper initialization. Two approaches are available to this purpose: Simulation of an initial guess using driver models and division of the problem into smaller subproblems, respectively. In this paper, the latter approach is utilized. Consequently, the hairpin turn problem is solved in four steps, see Figure 7. The results from the solution of each subproblem is used for initialization of the subsequent problem. Hence, the final optimal maneuver is determined stepwise.

5 Results

For the evaluations we set the maximum allowed wheel angle, δ, and wheel-angle change rate, $\dot{\delta}$, to 30 deg and 60 deg/s, respectively, which are reasonable parameters, both seen from physical and driver limitations. Also, constraints on the driving/braking torques and tire forces were introduced:

$$T_f \leq 0, \tag{31}$$

$$T_f \geq -\mu_x F_{z,f} R_w, \tag{32}$$

$$|T_r| \leq \mu_x F_{z,r} R_w, \tag{33}$$

$$|F_{x,i}| \leq \mu_x F_{z,i}, \ i = f, r, \tag{34}$$

$$|F_{y,i}| \leq \mu_y F_{z,i}, \ i = f, r. \tag{35}$$

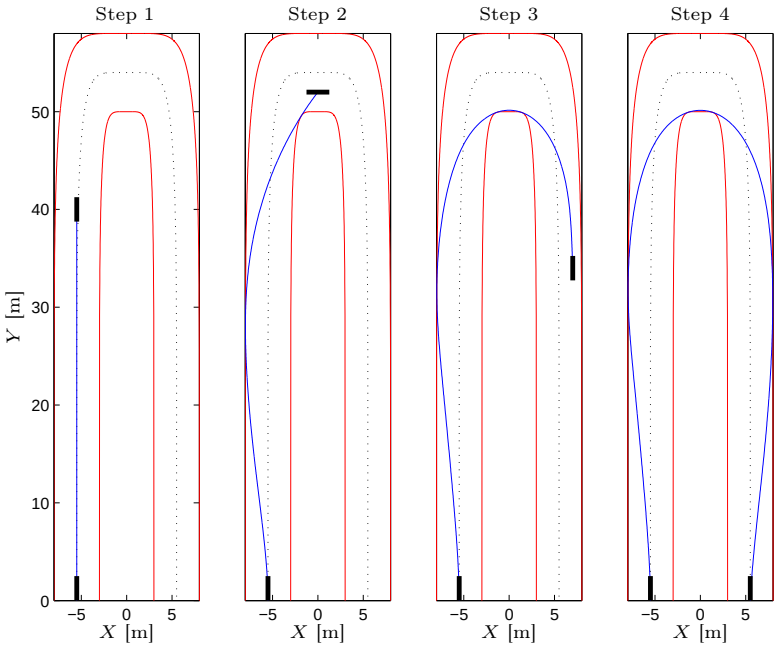

Figure 7: Initialization procedure for solving the time-optimal hairpin turn maneuver problem. The whole problem is solved by stepwise solving four successive problems. The black rectangles in the figure indicate the position and direction of the vehicle at the initial and final state in each problem.

We let the road be 5 m wide. Further, the start, (X_p^0, Y_p^0), and final vehicle position, $(X_p^{t_f}, Y_p^{t_f})$, were set to be in the middle of the road. The initial velocity was $v_0 = 25$ km/h. Figures 8–11 show the vehicle trajectory together with the most relevant states for all four models. Note that the vehicle is rear-wheel driven. All models have similarities: The vehicle starts with giving full engine torque while turning to allow for wider curve taking. When entering the curve the vehicle starts to break with both wheels, which it does approximately until reaching the half-way point. Furthermore, all models give rise to vehicle slip. The trajectory plots show that the slip—*i.e.*, the angle between the velocity vector and the longitudinal direction of the vehicle—is significant, exceeding 30 deg in the most critical parts of the maneuver. The maneuvering achieving this behavior is very similar to drifting techniques, where the rear wheel driving/braking torque is used to control the rear lateral tire force. The front wheels are only controlled with the steering angle, utilizing counter steering if necessary. Also, the qualitative slip behavior is congruent with the driving behavior often seen when rally drivers perform similar maneuvers, indicating that the obtained optimization results manage to replicate behavior utilized in reality.

Furthermore, it also shows that even a few-state single-track model using the friction ellipse for tire modeling manages to capture fundamental and relevant behavior, even for minimum-time optimization problems.

For the four parameter sets in Table 2, the final time values are for the respective column: $t_f \approx 8.82$, $t_f \approx 8.42$, $t_f \approx 8.80$, and $t_f \approx 8.44$. Hence, the objective function, t_f, deviates approximately 0.4 s when comparing all four model configurations. Comparing the isotropic and nonisotropic models, the deviation in final time between the friction ellipse model and the weighting functions model is less than 0.02 s.

5.1 Comparison of Isotropic Models

Studying the obtained results closer, we see that Figures 8 and 9 only have minor differences, if any. This should, of course, come as no surprise since the two models are parametrized to be isotropic, *c.f.* Figures 3–4. This is a verification that the optimization tool is able to handle both of these models, and also that two completely different model categories, parametrized to achieve equivalent resultant force characteristics, give similar results for the optimal maneuver. Figures 12 and 13 show the force trajectories as functions of α and κ, corresponding to Figures 8 and 9. By inspection we note that the α and κ trajectories, and consequently the resulting tire force trajectory, vary more for the rear wheels, which is caused by the vehicle being rear-wheel driven. Further, when comparing the force curves for the rear wheel it is clear that the friction ellipse model seems to penalize combined slip more throughout the turn. This can be explained by that the lateral tire force decreases faster with increasing slip ratio for the friction ellipse than for the weighting functions model. For example, when the longitudinal force approaches its maximum value, the lateral force tends to zero. For the corresponding slip ratio, the weighting functions model predicts a larger lateral force than the friction ellipse model does.

5.2 Comparison of Nonisotropic Models

When investigating Figures 10 and 11 we see that there are fundamental differences. First, the maximum steering angle, δ, in Figure 11 is twice as large as δ in Figure 10. Second, the maximum yaw rate is larger for the weighting functions model, see Figure 11, but the yaw rate when in the turn (between $t \approx 3.5$–4.5 s) is smaller. Third, the weighting functions model seldom uses the rear wheel for braking. Rather, it maximizes the braking force on the front wheel instead of distributing the braking force to both wheels. We believe that this behavior stems from that the weighting functions model provide, in addition to the low-slip solution, a large-slip alternative—*i.e.*, does not penalize combined slip—for a given resulting force. The force trajectories in Figures 14 and 15 verify this claim. These observations indicate that this behavior is model dependent rather than parameter dependent.

Another interesting behavior can be seen when studying the slip ratios, κ. For the weighting functions model, a large peak occurs when increasing the yaw rate at $t \approx 2.3$ s. At this stage, when trying to turn quickly, it is desired to have a small lateral force at the rear, which, in the weighting functions model, can be achieved by increasing the slip ratio as much as possible. In the isotropic weighting functions model, this tendency can also be seen. However, since the force decrease in the longitudinal direction is comparatively small, only a modest peak in the slip ratio appears. Studying the friction ellipse model instead, no such peak in slip ratio can be seen. Also, the friction ellipse model as it is implemented here, will increase the lateral force if the slip ratio exceeds the maximum longitudinal force.

5.3 Comparing the Isotropic and Nonisotropic Models

When comparing the friction ellipse model for the two different parameter sets—*i.e.*, Figures 8 and 10—we note a couple of discrepancies. The peak of δ is more accentuated in Figure 10. Also, the longitudinal force, and thereby the longitudinal velocity, is larger in magnitude. This is attributed to the larger longitudinal friction coefficient, μ_x, see Table 2. This, in turn, is a result of the fitting procedure used, described in Sec. 3.3. The difference in steering angle can, most probably, also be deduced to this, since a larger velocity will demand more aggressive steering to counteract the larger forces. When comparing the force trajectories for the same models, Figures 12 and 14, we see that they are very similar.

The weighting functions have more pronounced differences: First, δ in Figure 9 hardly exceeds 0 rad. Moreover, the yaw rate is larger in Figure 11. Third, the forces differ significantly. Partly, the differences can be attributed to the difference in longitudinal friction coefficient. We believe that a contributor is the significant differences between the maxima and minima in Figure 15.

6 Conclusions and Future Work

This paper aimed at using vehicle and tire models frequently encountered in literature to give insight into improved safety systems. We presented a comparison of vehicle behavior for minimum-time optimization of a hairpin maneuver, where different tire models were used. We exploited a single-track model for vehicle modeling. Although the results differed in some respects, the qualitative behavior was similar for all models. We showed that even a few-state single-track model using the friction ellipse for tire modeling managed to capture fundamental and relevant behavior. This implies that for future optimization-based safety systems rather simple models may suffice. However, the friction ellipse model and weighting functions model showed some dissimilarities; *e.g.*, the braking behavior was different. This might have impact on model choice, especially considering safety systems such as yaw rate controllers where the

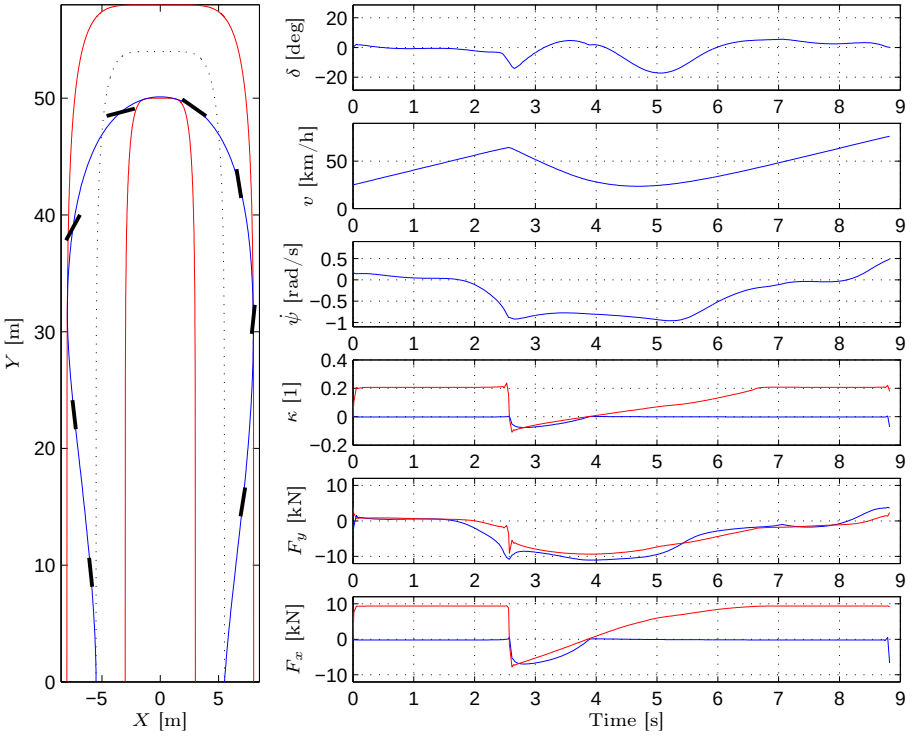

Figure 8: Optimization result for friction ellipse model with isotropic behavior with parameters as in column two in Table 2. In the κ, F_x, and F_y plots the blue curves visualize the front wheel and the red curves the rear wheel. The black rectangles in the XY-trajectory plot show the sideslip angle each second of the maneuver.

brakes typically are the actuators.

For the future we plan to do a similar investigation for different tires and surfaces, which provides insight into optimal control of maneuvers under different road conditions. Further, investigating optimal path tracking is a natural extension of the work presented in this paper; in this context other optimization criteria than time-optimality, such as deviation from the specified path or energy consumption, are of interest.

Acknowledgments

This work has been supported by ELLIIT, the Strategic Area for ICT research, funded by the Swedish Government.

K. Berntorp, B. Olofsson, and B. Bernhardsson are members of the LCCC Linnaeus Center at Lund University, supported by the Swedish Research Council.

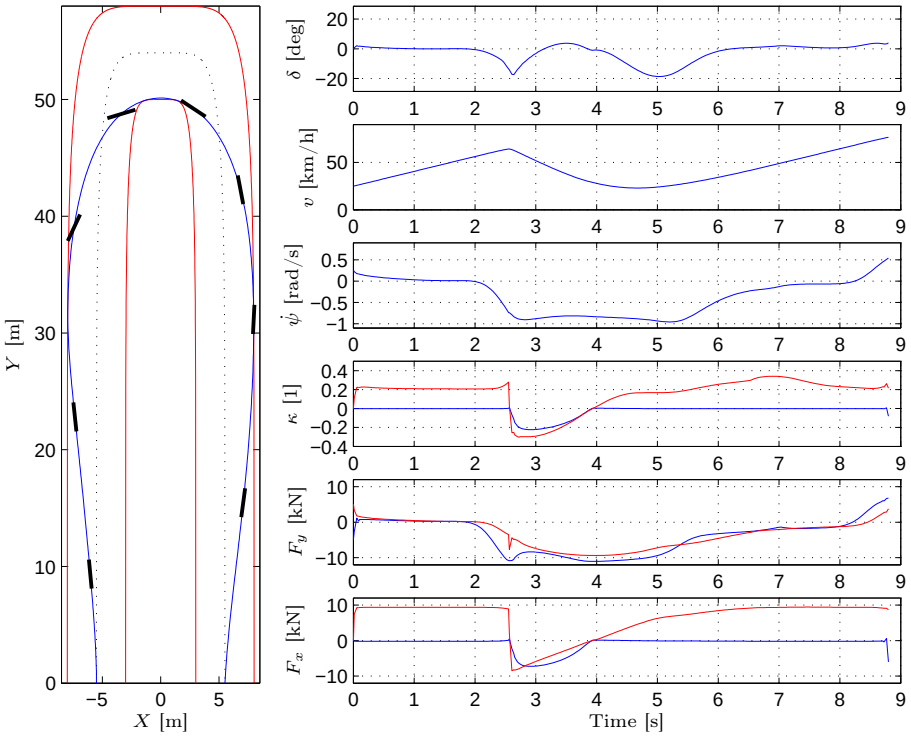

Figure 9: Optimization result for weighting functions model with isotropic behavior with parameters as in column four in Table 2. Same notation and colors as in Figure 8.

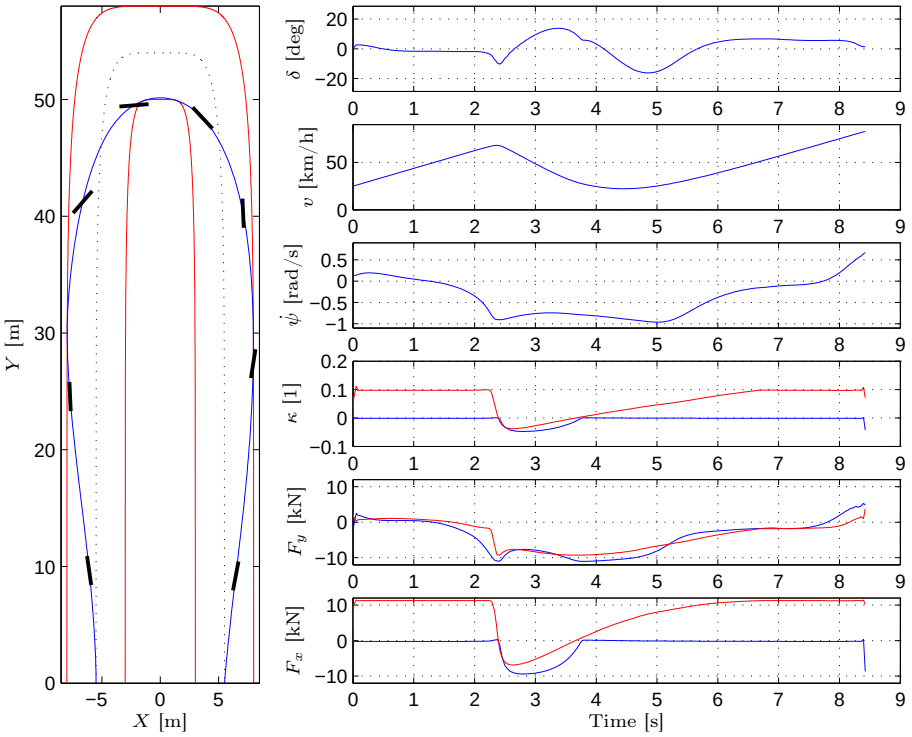

Figure 10: Optimization results for friction ellipse model with parameters as in column three in Table 2. Same notation and colors as in Figure 8.

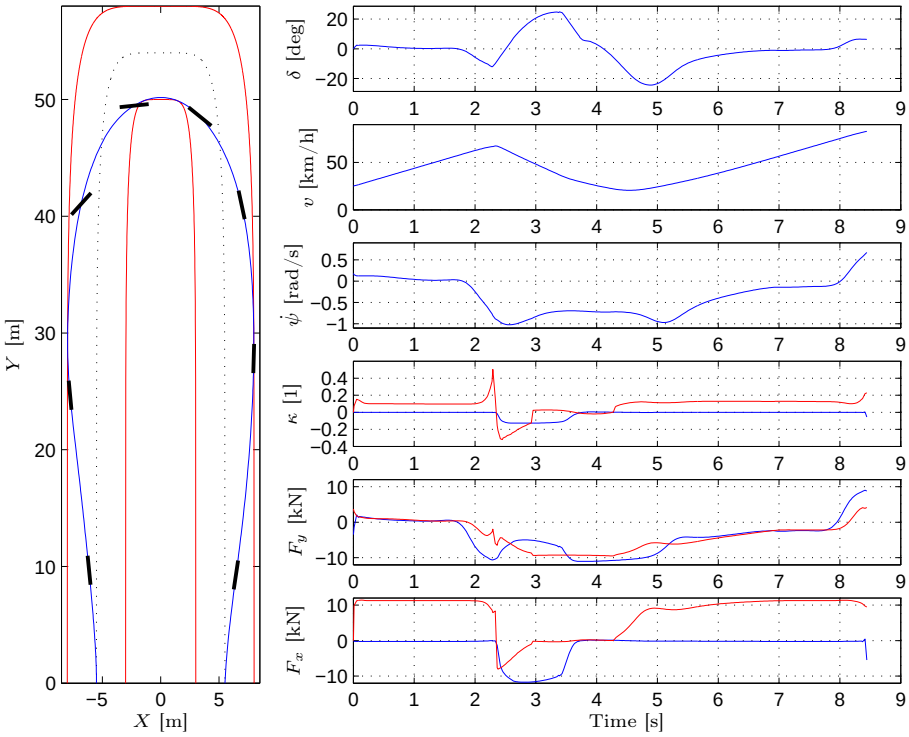

Figure 11: Optimization results for weighting functions model with parameters as in column five in Table 2. Same notation and colors as in Figure 8.

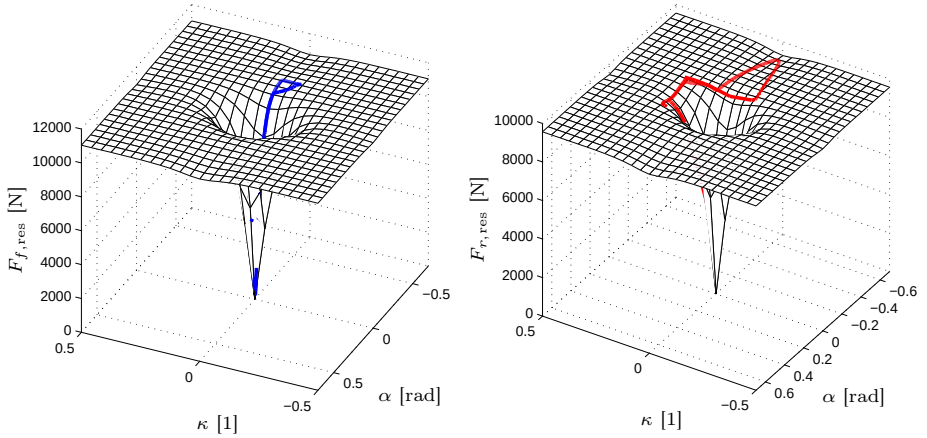

Figure 12: 3D plot of force curve for friction ellipse model with isotropic behavior corresponding to Figure 8. Blue (front wheel) and red curves (rear wheel) are the trajectories generated by optimization.

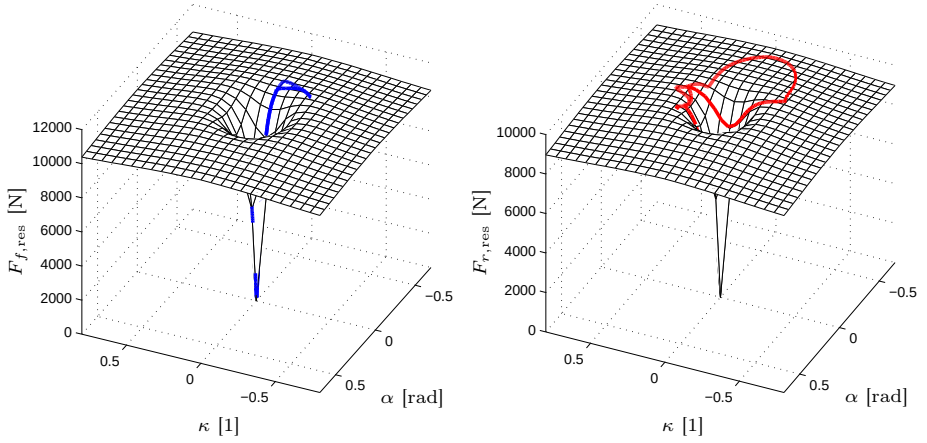

Figure 13: 3D plot of force curve for weighting functions model with isotropic parameters corresponding to Figure 9.

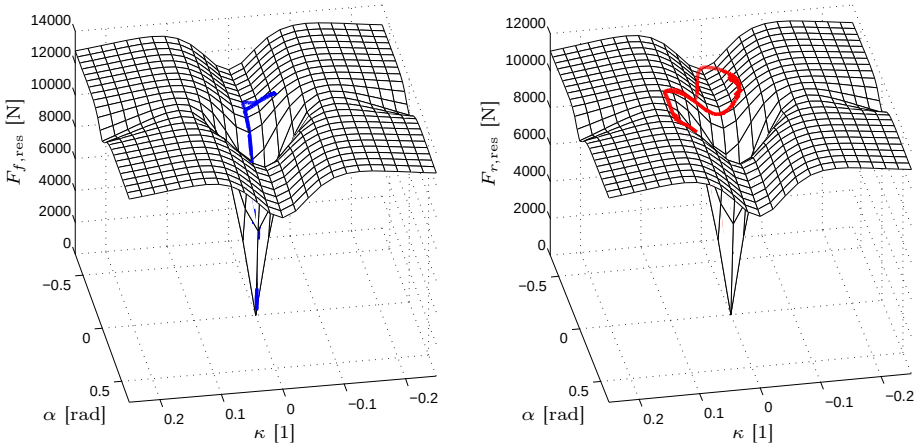

Figure 14: 3D plot of force curve for friction ellipse model with parameters corresponding to Figure 10.

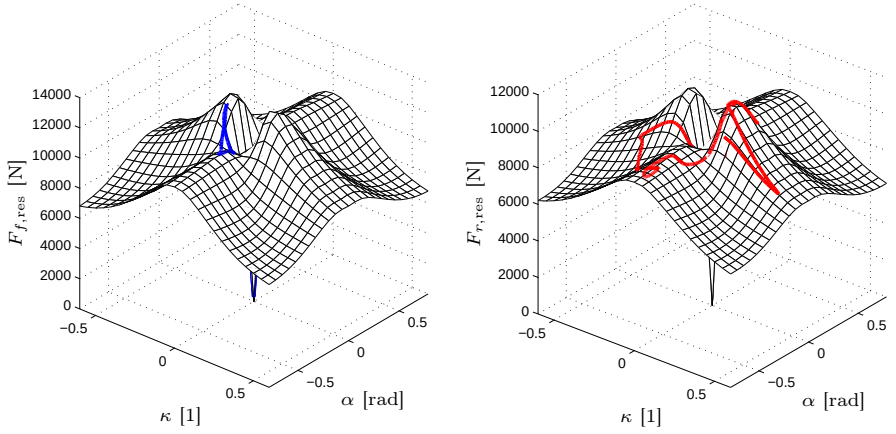

Figure 15: 3D plot of force curve for weighting functions model with parameters corresponding to Figure 11.

References

Johan Åkesson. Optimica—an extension of Modelica supporting dynamic optimization. In *6th Int. Modelica Conf. 2008*. Modelica Association, Mar. 2008.

Johan Åkesson, Karl-Erik Årzén, Magnus Gäfvert, Tove Bergdahl, and Hubertus Tummescheit. Modeling and optimization with Optimica and JModelica.org—Languages and tools for solving large-scale dynamic optimization problems. *Computers and Chemical Engineering*, Jan. 2010.

S.J Anderson, S.C. Peters, T.P. Pilutti, and K.D. Iagnemma. An optimal-control-based framework for trajectory planning, threat assessment, and semi-autonomous control of passenger vehicles in hazard avoidance scenarios. *Int. J. Vehicle Autonomous Systems*, 8(2/3/4):190–216, 2010.

S.J Anderson, S.B. Karumanchi, and K.D. Iagnemma. Constraint-based planning and control for safe, semi-autonomous operation of vehicles. In *IEEE Intelligent Vehicles Symp.*, pages 383–388, Alcalá de Henares, Spain, 2012.

J. Andreasson. Enhancing active safety by extending controllability — How much can be gained? In *IEEE Intelligent Vehicles Symp.*, pages 658–662, Xi'an, Shaanxi, China, June 2009.

Lorenz T Biegler, Arturo M Cervantes, and Andreas Wächter. Advances in simultaneous strategies for dynamic process optimization. *Chemical Engineering Science*, 57:575–593, 2002.

C.R. Carlson and J.C. Gerdes. Consistent nonlinear estimation of longitudinal tire stiffness and effective radius. *IEEE Trans. Control Syst. Technol.*, 13(6): 1010–1020, Nov. 2005.

Imon Chakraborty, Panagiotis Tsiotras, and Jianbo Lu. Vehicle posture control through aggressive maneuvering for mitigation of T-bone collisions. In *IEEE Conf. on Decision and Control (CDC)*, pages 3264–3269, Orlando, FL, 2011.

John Ronaine Ellis. *Vehicle Handling Dynamics*. Mechanical Engineering Publications, London, United Kingdom, 1994.

J. Funke, P. Theodosis, R. Hindiyeh, G. Stanek, K. Kritatakirana, C. Gerdes, D. Langer, M. Hernandez, B. Muller-Bessler, and B. Huhnke. Up to the limits: Autonomous Audi TTS. In *IEEE Intelligent Vehicles Symp.*, pages 541–547, Alcalá de Henares, Spain, June 2012.

Rolf Isermann. *Fahrdynamik-Regelung: Modellbildung, Fahrerassistenzsysteme, Mechatronik*. Vieweg-Verlag, Wiesbaden, Germany, 2006.

JModelica.org, 2012. URL: http://www.jmodelica.org.

U. Kiencke and L. Nielsen. *Automotive Control Systems—For Engine, Driveline and Vehicle*. Springer-Verlag, Berlin Heidelberg, second edition, 2005.

K. Liebemann, K. Meder, J. Schuh, and G. Nenninger. Safety and performance enhancement: The Bosch electronic stability control. Paper Number 05-0471m, Robert Bosch GmbH, 2005.

Kristoffer Lundahl, Jan Åslund, and Lars Nielsen. Investigating vehicle model detail for close to limit maneuvers aiming at optimal control. In *22nd Int. Symp. on Dynamics of Vehicles on Roads and Tracks (IAVSD)*, Manchester, United Kingdom, 2011.

Modelica Association, 2012. URL: http://www.modelica.org.

Hans B. Pacejka. *Tire and Vehicle Dynamics*. Butterworth-Heinemann, Oxford, United Kingdom, second edition, 2006.

R Rajamani. *Vehicle Dynamics and Control*. Springer-Verlag, Berlin Heidelberg, 2006.

E. Schindler. *Fahrdynamik: Grundlagen Des Lenkverhaltens Und Ihre Anwendung Für Fahrzeugregelsysteme*. Expert-Verlag, Renningen, Germany, 2007.

R. S. Sharp and Huei Peng. Vehicle dynamics applications of optimal control theory. *Vehicle System Dynamics*, 49(7):1073–1111, 2011.

Peter Sundström, Mats Jonasson, Johan Andreasson, Annika Stensson Trigell, and Bengt Jacobsson. Path and control optimisation for over-actuated vehicles in two safety-critical maneuvers. In *10th Int. Symp. on Advanced Vehicle Control (AVEC)*, Loughborough, United Kingdom, 2010.

E. Velenis and P. Tsiotras. Minimum time vs. maximum exit velocity path optimization during cornering. In *IEEE Int. Symp. on Industrial Electronics (ISIE)*, pages 355–360, Dubrovnik, Croatia, June 2005.

Efstathios Velenis. FWD vehicle drifting control: The handbrake-cornering technique. In *IEEE Conf. on Decision and Control (CDC)*, pages 3258–3263, Orlando, FL, 2011.

Andreas Wächter and Lorenz T Biegler. On the implementation of an interior-point filter line-search algorithm for large-scale nonlinear programming. *Mathematical Programming*, 106(1):25–57, 2006.

Paper C

Studying the Influence of Roll and Pitch Dynamics in Optimal Road-Vehicle Maneuvers*

C

*In *the 23rd International Symposium on Dynamics of Vehicles on Roads and Tracks*, Qingdao, China, 2013.

Studying the Influence of Roll and Pitch Dynamics in Optimal Road-Vehicle Maneuvers

Kristoffer Lundahl[a], Karl Berntorp[b], Björn Olofsson[b],
Jan Åslund[a], and Lars Nielsen[a]

[a] *Vehicular Systems, Department of Electrical Engineering, Linköping University, SE-581 83 Linköping, Sweden*

[b] *Department of Automatic Control, Lund University, SE–221 00 Lund, Sweden*

Abstract

A comparative analysis shows how vehicle motion models of different complexity, capturing various characteristics, influence the solution when used in time-critical optimal maneuvering problems. Vehicle models with combinations of roll and pitch dynamics as well as load transfer are considered, ranging from a single-track model to a double-track model with roll and pitch dynamics and load transfer. The optimal maneuvers in a 90°-turn and a double lane-change scenario are formulated as minimum-time optimization problems, and are solved using numerical optimization software. The results obtained with the different models show that variables potentially important for safety systems, such as the yaw rate, slip angle, and geometric path, are qualitatively the same. Moreover, the numeric differences are mostly within a few percent. The results also indicate that although input torques differ about 50–100 % for certain parts of the maneuver between the most and least complex model considered, the resulting vehicle motions obtained are similar, irrespective of the model. Our main conclusion is that this enables the use of low-order models when designing the onboard optimization-based safety systems of the future.

1 Introduction

With recent advancements in optimization technology and software, new approaches unfold for the development of active vehicle safety systems and driver assistance technologies, see, *e.g.*, Sharp and Peng (2011). The solution to an optimal control problem can give valuable insight into the performance capabilities of the system being investigated. Also, it can be used as an inspiration for new control strategies. The solution to the optimization problem will depend on the choice of model configurations and optimization objectives, investigated in Berntorp et al. (2013) and Olofsson et al. (2013). There, we developed an optimization methodology with special emphasis on tire modeling and uncertain road-surfaces, and this work continues the development towards more complex chassis models.

Motivated by the above, this study investigates the similarities and differences in the solutions obtained when several vehicle chassis models, capturing different dynamic properties such as roll and pitch dynamics with load transfer, are employed in optimal maneuvering problems. The aim is to perform a comparative study on how different vehicle motion models affect the optimal control solution in certain critical situations. The long-term goal of this work is real-time control. Hence, the models investigated are fairly simplistic compared to models usually employed for vehicle simulation purposes. For example, detailed suspension kinematics and gear dynamics have been neglected. One motivation for this is that the models are to be used together with dynamic optimization algorithms, requiring twice continuously differentiable functions in the model description. In addition, and perhaps more importantly, we are interested in investigating what characteristics of a maneuver that can be captured with this kind of models.

Optimal control of vehicles has been investigated previously in literature, see Sharp and Peng (2011); Kelly and Sharp (2010); Velenis and Tsiotras (2005); Chakraborty et al. (2011) for a few examples. Further, in Sundström et al. (2010); Andreasson (2009) an optimization problem for over-actuated vehicles is solved using the same software as used in this paper. A majority of the work in these references focus on a specific vehicle and tire model. Thus, to the best of our knowledge, no comprehensive approach to perform comparisons of different chassis models in an optimization scenario has been made, which motivates the study presented here.

The evaluation of the models is performed on two different maneuvering problems: A 90°-turn and a double lane-change situation, where the objective is to minimize the execution time of the maneuver. This formulation is one example of how to trigger a critical situation where the vehicle is performing at its very limit in terms of maneuvering.

2 Modeling

The emphasis in the vehicle modeling is on the chassis dynamics. Five different chassis models of various complexity are considered. The wheel dynamics and tire force modeling are the same in the five cases, where the former is expressed by a first-order rotational dynamic system. The tire forces are described by Pacejka's Magic Formula tire model in combination with weighting functions Pacejka (2006) for modeling combined longitudinal and lateral slip.

2.1 Chassis Models

The single-track model (ST), illustrated in Figure 1, is used as a basis model for the vehicle motion modeling. The left and right wheels on each axle are lumped together, and the model has two translational and one rotational degrees of freedom Kiencke and Nielsen (2005); Isermann (2006). The model dynamics are

$$\dot{v}_x - v_y\dot{\psi} = \frac{1}{m}(F_{x,f}\cos(\delta) + F_{x,r} - F_{y,f}\sin(\delta)), \tag{1}$$

$$\dot{v}_y + v_x\dot{\psi} = \frac{1}{m}(F_{y,f}\cos(\delta) + F_{y,r} + F_{x,f}\sin(\delta)), \tag{2}$$

$$I_{zz}\ddot{\psi} = l_f F_{y,f}\cos(\delta) - l_r F_{y,r} + l_f F_{x,f}\sin(\delta), \tag{3}$$

where m is the total vehicle mass, I_{zz} is the vehicle inertia about the z-axis, $\dot{\psi}$ is the yaw rate, δ is the steer angle, v_x, v_y are the longitudinal and lateral velocities at the center of gravity, l_f, l_r are the distances from the center of gravity to the front and rear wheel base, and F_x, F_y are the longitudinal and lateral tire forces acting at the front and rear wheels. The nominal normal force resting on the respective wheel is given by

$$F_{z0,f} = mg\frac{l_r}{l}, \quad F_{z0,r} = mg\frac{l_f}{l}, \tag{4}$$

where g is the constant of gravity and $l = l_f + l_r$.

Four extensions of the ST model are considered in this study:

- Single-track model with roll dynamics (ST-roll), where an additional degree of freedom about the x-axis is included.
- Single-track model with pitch dynamics (ST-pitch)—*i.e.*, an additional degree of freedom about the y-axis—and longitudinal load transfer.
- Double-track model with roll dynamics (DT-roll) and lateral load transfer.
- Double-track model with roll and pitch dynamics (DT-roll-pitch) and both longitudinal and lateral load transfer.

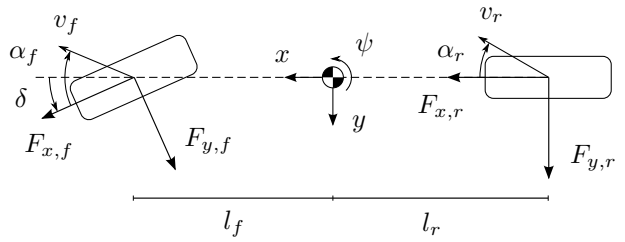

Figure 1: Basic single-track model.

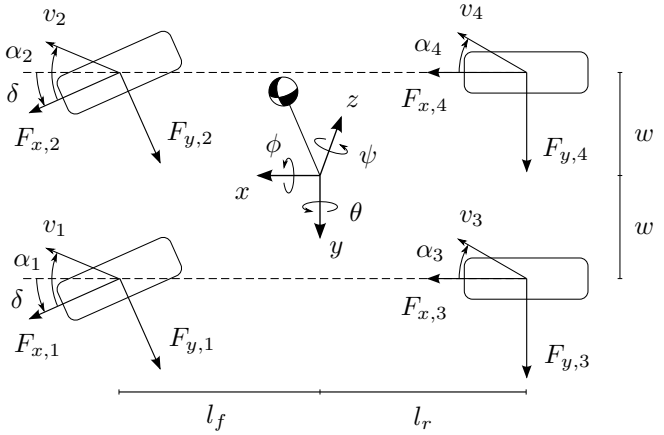

Figure 2: Double-track model with roll and pitch dynamics.

In the double-track models, each of the four wheels are modeled separately. In Figure 2, the DT-roll-pitch model is illustrated, with the roll angle ϕ and the pitch angle θ. The chassis rotational motion in the roll and pitch directions is characterized by the vehicle chassis inertias I_{xx} and I_{yy}, respectively. Further, in the derivation of the models it was assumed that the suspension system of the vehicle can be modeled with a spring-damper system. Consequently, the moment produced by the suspension system in the roll direction is given by

$$\tau_\phi = (K_{\phi,f} + K_{\phi,r})\phi + (D_{\phi,f} + D_{\phi,r})\dot{\phi}, \tag{5}$$

and correspondingly in the pitch direction according to

$$\tau_\theta = K_\theta \theta + D_\theta \dot{\theta}, \tag{6}$$

where K and D are model parameters for the stiffness and damping. For the derivation and complete dynamic equations for the DT-roll-pitch model, see Berntorp (2013). The dynamic equations for the longitudinal load transfer are given by

$$F_{z,f} l_f - F_{z,r} l_r = K_\theta \theta + D_\theta \dot{\theta}, \quad \sum_{i=f,r} F_{z,i} = mg, \tag{7}$$

for ST-pitch, where the time-dependent normal forces $F_{z,f}$ and $F_{z,r}$ have been introduced. The relation (7) is also valid for DT-roll-pitch with the substitution $F_{z,f} = F_{z,1} + F_{z,2}$ and $F_{z,r} = F_{z,3} + F_{z,4}$. The lateral load transfer is determined by the relations

$$-w(F_{z,1} - F_{z,2}) = K_{\phi,f}\phi + D_{\phi,f}\dot{\phi}, \tag{8}$$

$$-w(F_{z,3} - F_{z,4}) = K_{\phi,r}\phi + D_{\phi,r}\dot{\phi}, \tag{9}$$

where w is defined in Figure 2.

2.2 Wheel and Tire Dynamics

The wheel dynamics is formulated as a first-order system with the wheel angular velocity ω as the state and the driving and braking torques T on the wheels defined as inputs, according to

$$T_i - I_w \dot{\omega}_i - F_{x,i} R_w = 0, \ i = f, r \text{ or } 1, 2, 3, 4, \tag{10}$$

where I_w is the wheel inertia and R_w is the wheel radius. The longitudinal slip κ and the slip angle α are introduced following Pacejka (2006), and are given by

$$\kappa_i = \frac{R_w \omega_i - v_{x,i}}{v_{x,i}}, \tag{11}$$

$$\dot{\alpha}_i \frac{\sigma}{v_{x,i}} + \alpha_i = -\arctan\left(\frac{v_{y,i}}{v_{x,i}}\right), \quad i = f, r \text{ or } 1, 2, 3, 4, \tag{12}$$

where σ is the relaxation length and $v_{x,i}$, $v_{y,i}$ are the velocities resolved in the wheel frames. Note that Figures 1–2 depict the static slip angles, describing a purely geometric relation, in contrast to the dynamic slip angles in (12). The vehicle and wheel model parameters in (1)–(12) used in this study are specified in Table 1.

The tire forces are modeled by Pacejka's Magic Formula in combination with weighting functions Pacejka (2006) for modeling the combined longitudinal and lateral slip. The longitudinal and lateral tire forces, F_x and F_y, read

$$F_{x0,i} = \mu_x F_{z,i} \sin(C_{x,i} \arctan(B_{x,i}\kappa_i - E_{x,i}(B_{x,i}\kappa_i - \arctan B_{x,i}\kappa_i))), \quad (13)$$
$$B_{x\alpha,i} = B_{x1,i} \cos(\arctan(B_{x2,i}\kappa_i)), \quad (14)$$
$$G_{x\alpha,i} = \cos(C_{x\alpha,i} \arctan(B_{x\alpha,i}\alpha_i)), \quad (15)$$
$$F_{x,i} = F_{x0,i} G_{x\alpha,i}, \quad (16)$$
$$F_{y0,i} = \mu_y F_{z,i} \sin(C_{y,i} \arctan(B_{y,i}\alpha_i - E_{y,i}(B_{y,i}\alpha_i - \arctan B_{y,i}\alpha_i))), \quad (17)$$
$$B_{y\kappa,i} = B_{y1,i} \cos(\arctan(B_{y2,i}\alpha_i)), \quad (18)$$
$$G_{y\kappa,i} = \cos(C_{y\kappa,i} \arctan(B_{y\kappa,i}\kappa_i)), \quad (19)$$
$$F_{y,i} = F_{y0,i} G_{y\kappa,i}, \ i = f, r \text{ or } 1, 2, 3, 4, \quad (20)$$

where μ_x, μ_y are the longitudinal and lateral friction coefficients and B, C, E are model parameters. In Table 2 the tire model parameters in (13)–(20) used in this study are provided. The parameters have been derived from Pacejka (2006) and correspond to a tire on dry asphalt. Further, in Table 3 the state variables for the respective vehicle and wheel model configuration are summarized.

3 Optimization

The models presented in the previous section are formulated as differential-algebraic equation systems according to $\dot{x}(t) = G(x(t), y(t), u(t))$, where x is the state vector, y are the algebraic variables, and u is the input signal vector. The time-dependency of the variables will be implicit in the rest of the paper. The wheel driving and braking torques, $T = \begin{pmatrix} T_f & T_r \end{pmatrix}$, as well as the steer angle δ of the front wheels are considered as inputs. For simplicity we assume that the front wheels have the same steer angle in the double-track models. To allow an equitable comparison with the single-track models, the double-track models only have two wheel-torque inputs as well, which are equally distributed between the wheels at the respective axles, *i.e.*, $T_1 = T_2 = T_f/2$ and $T_3 = T_4 = T_r/2$, where T_1, T_2, T_3, and T_4 are the corresponding wheel torques for wheel 1–4. Further, the tire-force model is written as the equation system $h(x, y, u) = 0$. The chassis and tire dynamics are implemented using the modeling language Modelica Modelica Association (2012). The optimization problem is formulated over the time horizon $t \in [0, t_f]$. The objective of the optimization is to minimize the final time t_f of the maneuver. Accordingly, the dynamic optimization problem

Table 1: Vehicle and wheel parameters in (1)–(12).

Notation	Value	Unit
l_f	1.3	m
l_r	1.5	m
w	0.8	m
m	2 100	kg
I_{xx}	765	kgm^2
I_{yy}	3 477	kgm^2
I_{zz}	3 900	kgm^2
R_w	0.3	m
I_w	4.0	kgm^2
σ	0.3	m
g	9.82	ms^{-2}
h	0.5	m
$K_{\phi,f}, K_{\phi,r}$	89 000	Nm(rad)^{-1}
$D_{\phi,f}, D_{\phi,r}$	8 000	Nms(rad)^{-1}
K_θ	363 540	Nm(rad)^{-1}
D_θ	30 960	Nms(rad)^{-1}

Table 2: Tire model parameters in (13)–(20).

Notation	Front	Rear
μ_x	1.20	1.20
B_x	11.7	11.1
C_x	1.69	1.69
E_x	0.377	0.362
μ_y	0.935	0.961
B_y	8.86	9.30
C_y	1.19	1.19
E_y	-1.21	-1.11
$C_{x\alpha}$	1.09	1.09
B_{x1}	12.4	12.4
B_{x2}	-10.8	-10.8
$C_{y\kappa}$	1.08	1.08
B_{y1}	6.46	6.46
B_{y2}	4.20	4.20

to be solved can be written as:

$$\begin{aligned}
\text{minimize} \quad & t_f && (21)\\
\text{subject to} \quad & T_{i,\min} \le T_i \le T_{i,\max},\ i = f, r, && (22)\\
& |\delta| \le \delta_{\max}, \quad |\dot{\delta}| \le \dot{\delta}_{\max}, && (23)\\
& x(0) = x_0, \quad y(0) = y_0, && (24)\\
& x(t_f) = x_{t_f}, \quad y(t_f) = y_{t_f}, && (25)\\
& f(X_p, Y_p) \le 0, && (26)\\
& \dot{x} = G(x, y, u), \quad h(x, y, u) = 0, && (27)
\end{aligned}$$

where x_0, y_0 are the initial conditions for the differential states and algebraic variables, x_{t_f}, y_{t_f} are the desired values at the final time $t = t_f$, and (X_p, Y_p) is the position of the center-of-gravity of the vehicle. In practice, the initial and final conditions are only applied to a subset of the model variables. Further, $f(X_p, Y_p)$ is a mathematical description of the road constraint for the center-of-gravity of the vehicle for the respective maneuver. These constraints are formulated as super-ellipses with different radii and degrees in the XY-plane.

The continuous-time optimal control problem (21)–(27) for each model configuration and maneuver is solved utilizing the open-source software JModelica.org Åkesson et al. (2010), according to the method presented in Berntorp et al. (2013). In particular, the continuous-time optimization problem is discretized using direct collocation methods Biegler et al. (2002), and the resulting

Table 3: State variables for the different vehicle chassis model configurations, including wheel dynamics.

Model	Notation	States
Single-track	ST	$v_x, v_y, \dot{\psi}, \omega_f, \omega_r, \alpha_f, \alpha_r$
Single-track + roll dynamics	ST-roll	$v_x, v_y, \dot{\psi}, \dot{\phi}, \omega_f, \omega_r, \alpha_f, \alpha_r$
Single-track + pitch dynamics	ST-pitch	$v_x, v_y, \dot{\psi}, \dot{\theta}, \omega_f, \omega_r, \alpha_f, \alpha_r$
Double-track + roll dynamics	DT-roll	$v_x, v_y, \dot{\psi}, \dot{\phi}, \omega_1$–$\omega_4, \alpha_1$–$\alpha_4$
Double-track + roll and pitch	DT-roll-pitch	$v_x, v_y, \dot{\psi}, \dot{\phi}, \dot{\theta}, \omega_1$–$\omega_4, \alpha_1$–$\alpha_4$

discrete-time nonlinear optimization problem (NLP) is solved numerically using the interior-point solver Ipopt Wächter and Biegler (2006). The Jacobian and the Hessian related to the problem are required in the iterative numerical optimization procedure. Considering the complexity of the employed chassis and tire models, exact calculation of these quantities with automatic differentiation Griewank (2000) significantly reduces convergence times and increases numerical stability compared to the case with numerical approximations. For further details on the solution methodology, see Berntorp et al. (2013).

4 Results

The minimum-time optimization problem (21)–(27) was solved for the 90°-turn and the double lane-change maneuver. The solution of the problem was determined for each of the vehicle models presented in Section 2 The steer angle and steer rate-of-change were limited to $\delta_{\max} = 30$ deg and $\dot{\delta}_{\max} = 60$ deg/s, respectively, corresponding to reasonable driver limitations. The lower wheel torque limitations were set to $T_{f,\min} = T_{r,\min} = -\mu_{x,f} mg$. The upper wheel torque limits were set to $T_{f,\max} = 0$ and $T_{r,\max} = \mu_{x,r} F_{z0,r}$, which implies a rear-wheel driven vehicle. The choice of torque limitations originates from the fact that the maximum braking torque that can be applied on the wheels is significantly larger than the corresponding acceleration torque. Further, the driving torque limit was set to prevent excessive wheel spin equivalent to large slip ratios. This is motivated since the employed empirical tire models are based on tire force measurements that for experimental reasons are only possible to obtain for a limited area in the α-κ plane. In addition, the wheel velocities were limited to be nonnegative, since solutions with wheel backspin are not desired.

4.1 Optimal Maneuver in the 90°-Turn

In the turn maneuver, the vehicle start position was set to $(X_{p,0}, Y_{p,0}) = (37.5, 0)$ m, *i.e.*, in the lower right corner in Figure 3. The initial velocity was $v_0 = 70$ km/h and the vehicle was aligned with the road direction, $\psi_0 = \pi/2$.

The target vehicle position was set to $(X_{p,t_f}, Y_{p,t_f}) = (0, 37.5)$ m, where the vehicle heading was in the road direction, $\psi_{t_f} = \pi$. The computed optimal maneuvers for the different vehicle chassis models in the 90°-turn are presented in Figure 3. The variable v represents the absolute vehicle velocity and β is the body-slip angle, defined as

$$\beta = \arctan\left(\frac{v_y}{v_x}\right).$$

Figure 4 shows the sum of the longitudinal and lateral tire-forces resolved in the road-surface plane. Also visualized is the nominal yaw moment M_Z generated from the tire forces, *i.e.*, the moment about an axis orthogonal to the road. These quantities are visualized as function of the driven distance s for reasons of comparability. Figures 5–6 show the *Force-Slip (FS)-diagrams*—as first introduced in Berntorp et al. (2013)—for ST and DT-roll-pitch. Here the normalized resultant tire-force, defined as

$$F_{i,res} = \frac{\sqrt{F_{x,i}^2 + F_{y,i}^2}}{F_{z,i}}, \quad i = f, r \text{ or } 1, 2, 3, 4,$$

is visualized as a surface, varying over α and κ. On this surface the corresponding time-optimal solution is drawn, as well as projected underneath in the α-κ plane. In Table 4, the execution times for the maneuver for the respective model are specified. The execution times vary 4 % at most, which occurs between the ST-pitch and DT-roll models. However, no significant differences between the five chassis models considered in this study are observed.

Similarities Between the Solutions

The first observation when investigating the results in Figure 3 is that the solutions practically coincide for several variables, being ϕ, θ, $\dot{\psi}$, and β. This implies that variables often utilized in safety systems to indicate maneuvering instability are invariant to model complexity, at least for the models considered

Table 4: Time for executing the maneuver for each model configuration in the 90°-turn.

Model	Execution time
ST	4.2662 s
ST-roll	4.2677 s
ST-pitch	4.2041 s
DT-roll	4.3660 s
DT-roll-pitch	4.3371 s

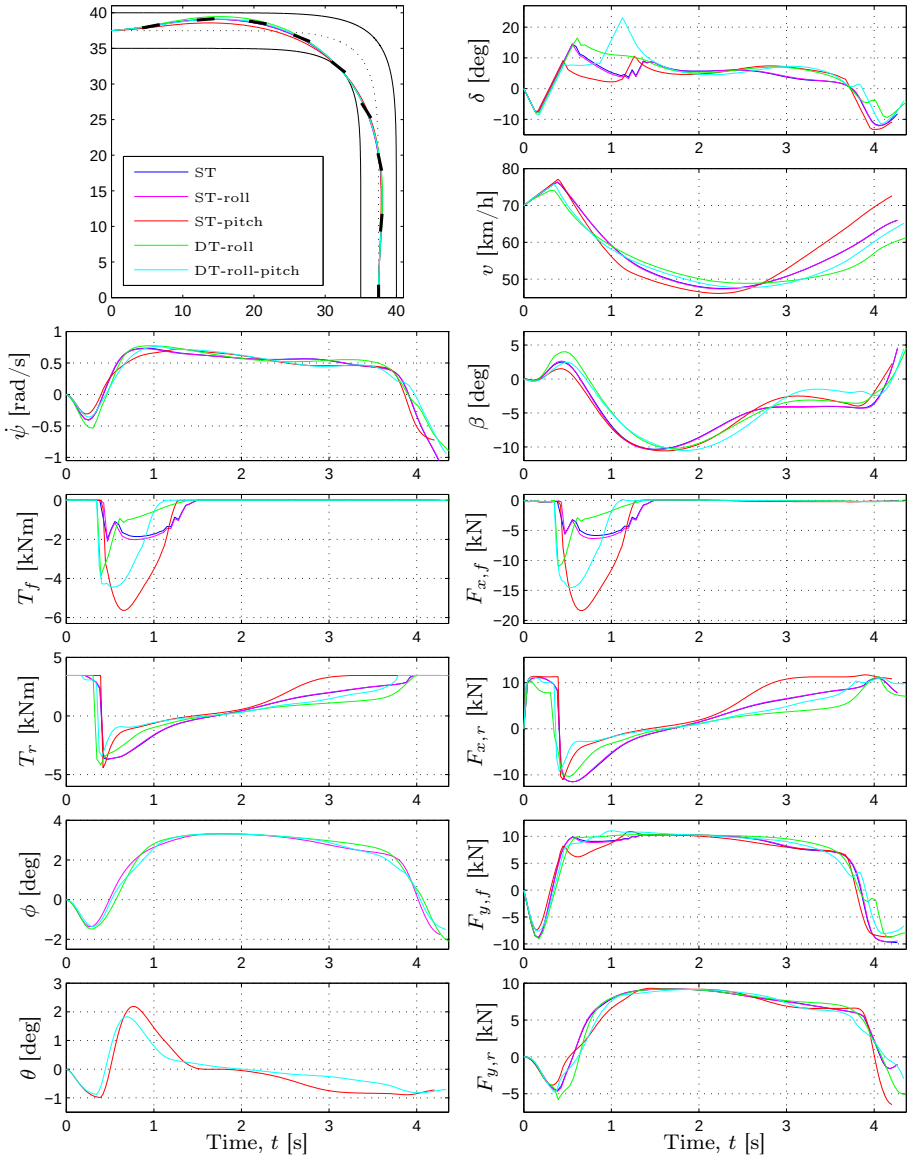

Figure 3: Time-optimal solutions obtained for the 90°-turn, for ST, ST-roll, ST-pitch, DT-roll, and DT-roll-pitch. The black bars in the upper left XY-plot represent the vehicle heading for the DT-roll-pitch solution every half second.

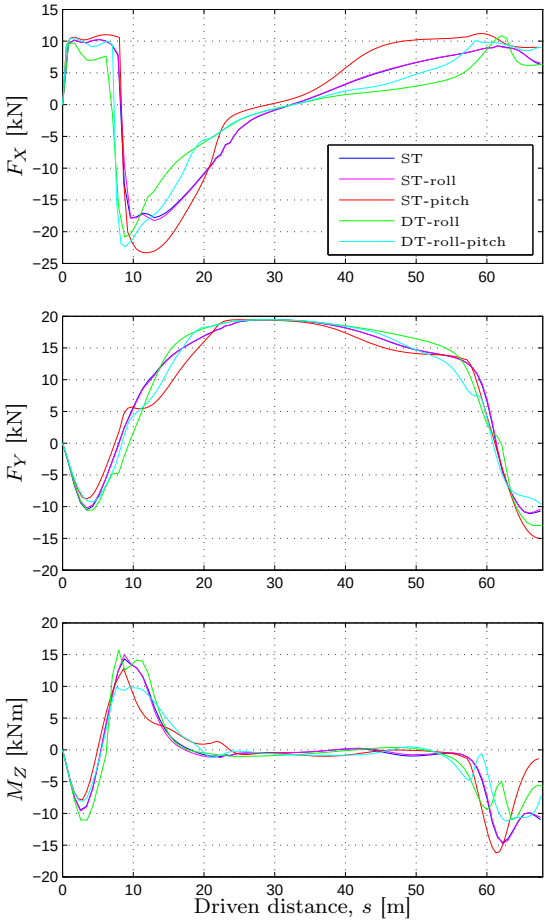

Figure 4: Longitudinal force F_X, lateral force F_Y, and yaw moment M_Z, developed by the tires, for the 90°-turn, illustrated as functions of the driven distance s. Note the similarities for F_Y and M_Z.

here. The geometric trajectories shown in the upper left plot of Figure 3 are also similar. The largest deviations of the geometric trajectories, which occur between ST-pitch and DT-roll during the exit phase, are approximately 15 % of the road width. However, the differences between ST and DT-roll-pitch are minor throughout the maneuver.

As seen in Figure 4, F_Y and M_Z are similar, with only minor quantitative differences between the models. This observation can also be deduced from the tire force plots in Figure 3 and is important considering that M_Z is used as a high-level input in several safety systems, such as in yaw-rate controllers and rollover-prevention systems. There are larger numeric discrepancies in F_X, at least during shorter periods of the maneuver. In a physical setup, however, model parameters such as the friction coefficients, vehicle mass, and tire parameters are uncertain. Thus, conservative bounds on the control variables might, for safety reasons, be necessary in on-board applications, consequently reducing the differences for the models even further.

Investigating the results further, Figure 3 shows that the different models result in characteristics that are similar in several aspects. Prior to turning into the corner, all solutions exhibit a slight rightward maneuvering while accelerating. This is followed by a braking phase, where both front and rear wheels are used. In the braking phase, initially a significant braking torque is applied, gradually reducing as the vehicle approaches the turn, see T_f and T_r in Figure 3. Unsurprisingly, larger lateral forces are generated in the turn. Half-way through the turn, at $t \approx 2$ s, all solutions generate an increasing driving torque, which accelerates the vehicle out of the turn. In the final stage, all solutions apply maximum driving torque.

Differences Between the Solutions

The most prominent differences between the solutions appear for the control inputs and variables closely coupled to the longitudinal dynamics, such as T_f, T_r, and v in Figure 3, and F_X in Figure 4. In the initial braking phase, starting at $t \approx 0.4$ s, the chassis for the ST-pitch and DT-roll-pitch models are subjected to a forward load transfer. This is utilized by applying a larger braking effort at the front wheels, see T_f in Figure 3. At the rear wheels, for the ST-pitch and DT-roll-pitch models, a large braking torque is initially applied. This torque is then rapidly reduced as the longitudinal load transfer results in less load on the rear wheels, see T_r around $t = 0.5$ s in Figure 3.

Comparing ST with DT-roll, and ST-pitch with DT-roll-pitch, the double-track models reduce front-wheel braking earlier. This is a consequence of T_f being equally distributed between the front wheels for the double-track models. Thus, when braking while cornering, the inner wheels will have less load and thus risk to lock up for large braking torques. Similarly, during the exit phase where lateral load-transfer still is present, a too large driving torque will spin out the inner rear-wheel. Therefore, a smaller driving torque is applied for the DT-roll and DT-roll-pitch models compared with ST, ST-roll, and ST-pitch.

In Figure 3, the steer angle varies between the models. At $t \approx 0.7$ s, a smaller δ is obtained for the ST-pitch and DT-roll-pitch models, since the sought lateral force $F_{y,f}$ for the current levels of front load and braking effort requires a different slip angle α_f. Also, for the ST-pitch model a strategy with more emphasis on braking is obtained, with the lateral force being slightly smaller. Hence, a lower δ is natural. Shortly after, sharp peaks are seen for the steer angle with the ST-pitch and DT-roll-pitch model around $t = 1.1$ s. Given the resulting forces developed at the front wheels at this time, resolved in the chassis frame, there exist two different strategies to achieve these: Either by utilizing front wheel braking together with a moderate steering angle, or by only applying a large steer angle and achieve the longitudinal contribution from $F_{y,f}\sin(\delta)$ solely. The latter seems to be what, to some extent, is utilized for ST-pitch and DT-roll-pitch, and the advantage could be a more beneficial contribution to the yaw moment. Additionally, for DT-roll-pitch, front-wheel braking could conflict with lock-up for the inner wheel, thus braking might be disfavored. However, the gain in final time of using either of the strategies seems to be minor.

The FS-diagrams in Figure 5–6 display slightly different slip characteristics for the two models. For ST, the solver chooses the slip quantities to reside closer to the coordinate axes, especially for the front wheel. The DT-roll-pitch model, having dynamically varying normal forces, exhibits different slip trajectories for the left and right wheels.

4.2 Optimal Maneuver in the Double Lane-Change

The geometric track-boundaries for the double lane-change maneuver are specified according to the standardized test ISO 3888-2 ISO 3888-2:2011 (2011), often used for vehicle stability evaluations. The vehicle starts at the left-hand side of the XY-plot in Figure 7, at $(X_{p,0}, Y_{p,0}) = (0, 1)$ m, with an initial velocity of $v_0 = 80$ km/h. Mid-way through, an obstacle forces the vehicle into an evasive maneuver. Finally, the vehicle rejoins the initial drive lane at the final position $(X_{p,t_f}, Y_{p,t_f}) = (61, 0.6)$ m. The initial and final vehicle heading angles are set to $\psi_0 = \psi_{t_f} = 0$. In Figure 7, the time-optimal solutions for the double lane-change maneuver are shown. In Figure 8, F_X, F_Y, and M_Z are shown as function of the driven distance s, similarly to Figure 4. In Figures 9 and 10 the FS-diagrams for the solutions obtained with the ST and DT-roll-pitch models are shown. The execution times for the different models in the double lane-change maneuver are specified in Table 5. As for the 90°-turn, the execution times are similar and differing at most by 4 %.

Similarities Between the Solutions

The global trajectories, shown in Figure 7, are almost inseparable. This is partially a consequence of the narrow path formed by the track boundaries. However, for several other variables strong resemblance is also obtained, as for example $\dot{\psi}$, β, $F_{y,f}$, and $F_{y,r}$ in Figure 7. The total lateral force F_Y, as well as

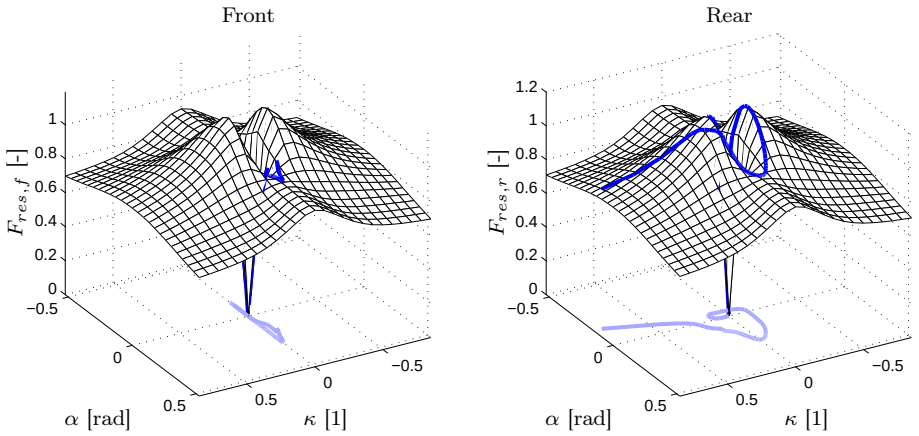

Figure 5: Resultant tire forces for ST in the 90°-turn.

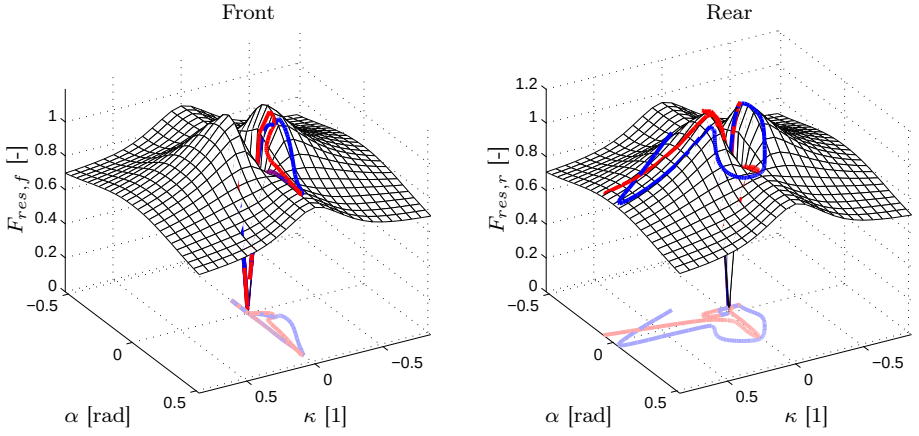

Figure 6: Resultant tire forces for DT-roll-pitch in the 90°-turn (blue–left wheel, red–right wheel).

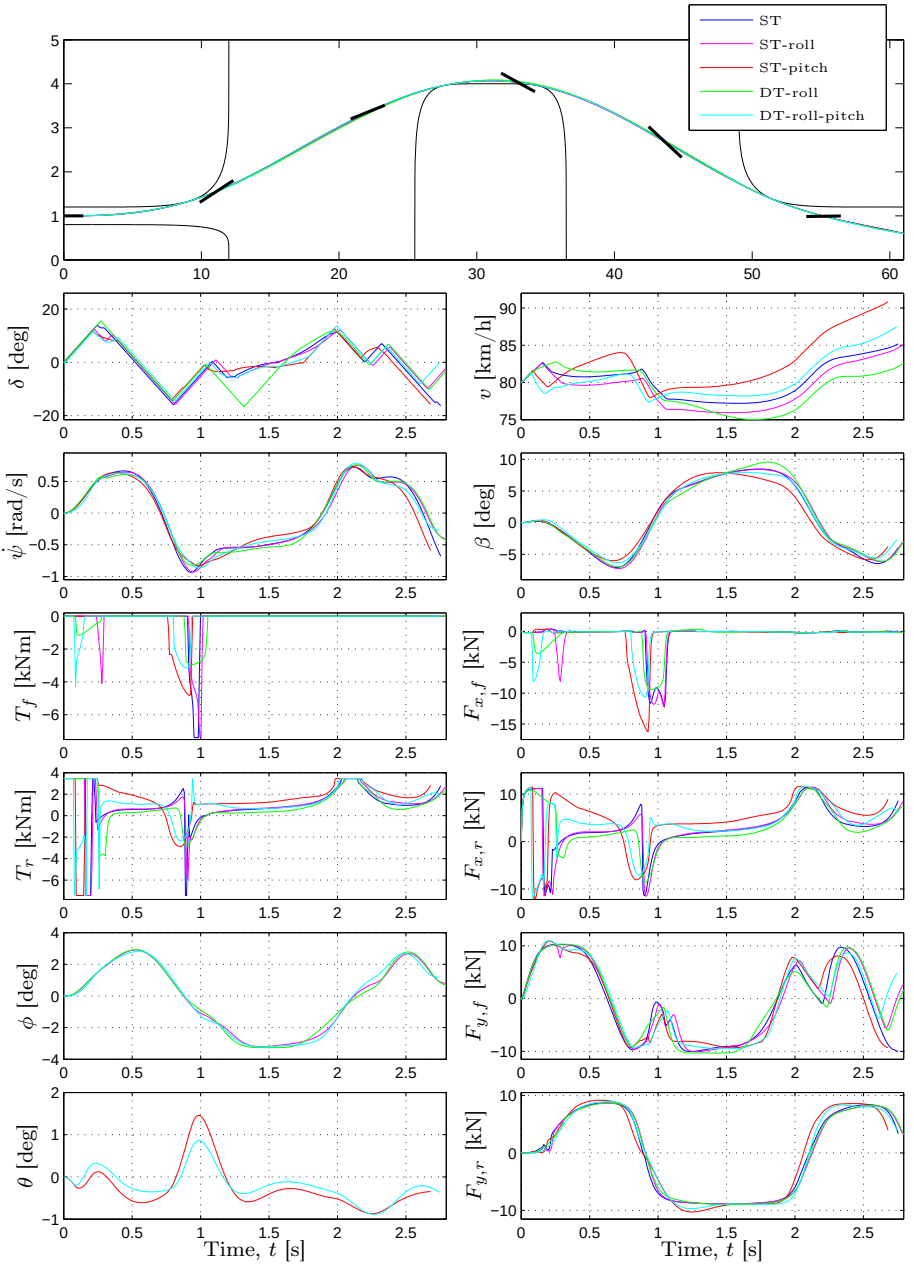

Figure 7: Time-optimal solutions for the double lane-change maneuver. Same models and color scheme as in Figure 3.

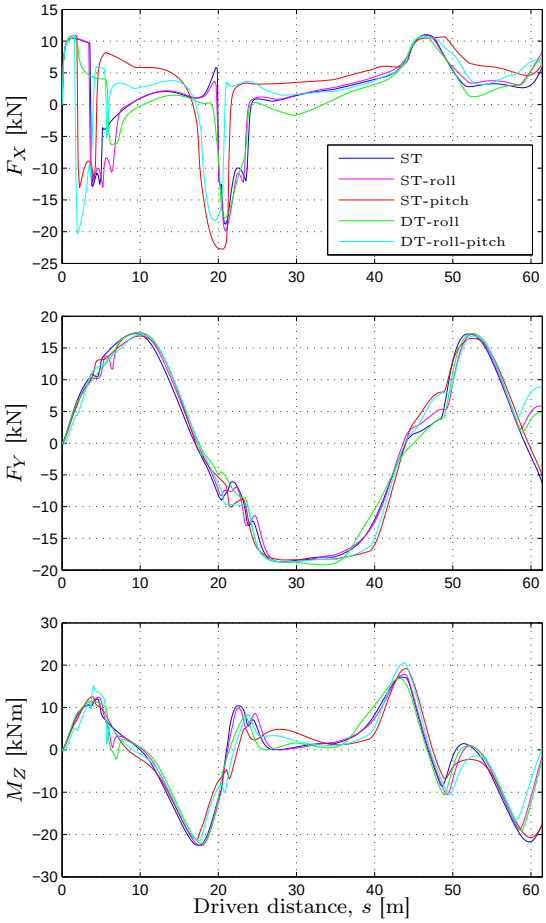

Figure 8: Longitudinal force F_X, lateral force F_Y, and yaw moment M_Z developed by the tires, for the double lane-change maneuver, illustrated as functions of the driven distance s. Note the similarities for F_Y and M_Z.

the yaw moment M_Z in Figure 8, show very similar behavior, almost coinciding for the main parts of the maneuver. Note the similarities in F_Y and M_Z even for considerable differences in F_X, for example around $s = 10$ m.

Analyzing the solutions more in-depth, all models result in full driving torque during the initial stage, followed by a short braking phase at the rear wheels, see T_r in Figure 7. Subsequently, various levels of driving torque are applied when approaching the obstacle, followed by a braking phase utilizing both front and rear wheel braking. For the second half of the maneuver, similar strategies can be seen for all models. A moderate driving torque is applied, interrupted by a smooth but significant increase at $t = 2$ s. At this stage the rear lateral force $F_{y,r}$ shifts from negative to positive, thus only using a portion of the available lateral tire-force, $\mu_{y,r}F_{z,r}$. Consequently, a longitudinal force can be employed without adversely affecting the lateral forces.

Differences Between the Solutions

As for the 90°-turn, differences between the solutions are most visible in the longitudinal dynamics. This is particularly noticeable for the wheel torques, T_f and T_r in Figure 7, differing both in magnitude and point of operation. In the initial braking phase, the braking effort is slowly reduced for ST, ST-roll, and DT-roll, *i.e.*, the models without pitch dynamics, and eventually a modest driving torque is applied, see T_r in Figure 7. The models with pitch dynamics (ST-pitch and DT-roll-pitch) instead result in a maneuvering that shortly regain a driving torque, which then slowly is reduced. In the pitch-dynamics models, the rearward load transfer is here utilized, enabling larger rear-wheel tire-forces because of the increased normal load on the rear wheels. Approaching the obstacle, the pitch-dynamics models show an earlier initiated braking phase, presumably because of their larger velocity. For the models without pitch dynamics, a driving torque at the rear wheels is shortly applied, followed by a very short rear-wheel braking around $t = 0.9$ s in Figure 7. The reason for this behavior is probably linked to the increased yaw rate, where a reduced rear-wheel lateral tire-force $F_{y,r}$ is desired. This can here be achieved by acquiring a large longitudinal slip.

Table 5: Time for executing the maneuver for each model configuration in the double lane-change situation.

Model	Execution time
ST	2.7540 s
ST-roll	2.7869 s
ST-pitch	2.6804 s
DT-roll	2.7939 s
DT-roll-pitch	2.7459 s

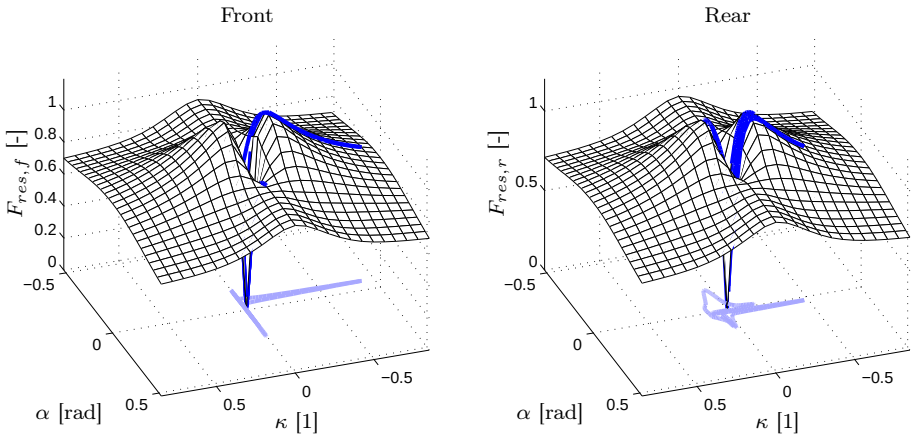

Figure 9: Resultant tire forces for ST in the double lane-change maneuver.

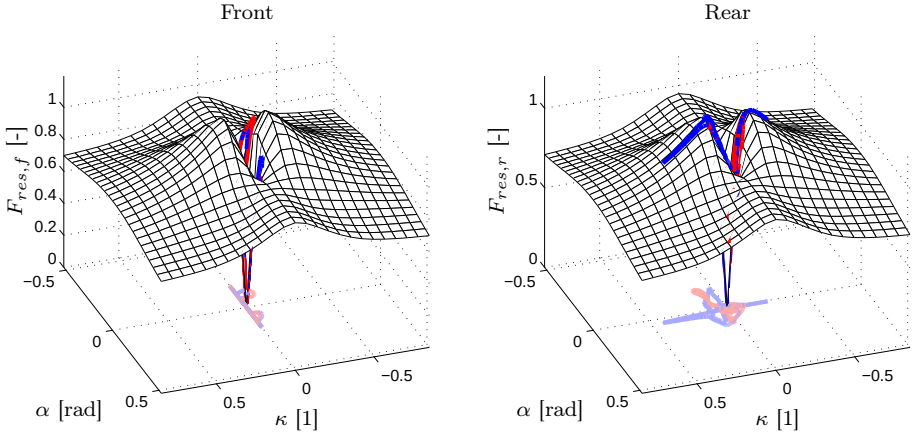

Figure 10: Resultant tire forces for DT-roll-pitch in the double lane-change (blue–left wheel, red–right wheel).

The steering angle δ in Figure 7 exhibits overall equivalent behavior throughout the maneuver for the different models, with the steer rate-of-change limit $\dot{\delta}_{max}$ being active during a majority of the maneuver. However, at $t = 1.3$ s a distinct peak appear for the DT-roll model solely. This seems—as was discussed for ST-pitch and DT-roll-pitch in the 90°-turn—to be a consequence of the existence of two different strategies resulting in equivalent optimization objective. Instead of braking the front wheel, for the DT-roll model a large steer angle can be observed which result in a braking component determined by $F_{y,f} \sin(\delta)$. By this strategy, combined with a double-track model, a large front lateral force can be realized, while simultaneously reducing the speed without the risk of wheel lock-up. For the DT-roll-pitch model this strategy is not applied, since reducing the speed at this point in time seems to be neither necessary nor desired, when analyzing T_f and T_r. For the single-track models, the risk of wheel lock-up is in this situation not imminent. Hence, the absence of the large steer-angle strategy.

Investigating the FS-diagrams for the solutions obtained with the ST and DT-roll-pitch models, displayed in Figures 9 and 10, the solutions exhibit a quite narrow area of operation in the α-κ plane. Also, combined slip is not utilized to the same extent as for the 90°-turn. Observing the slip trajectories closer, the rear wheels exhibit larger slip values than the front wheels, especially for the DT-roll-pitch model. This is coupled to the time-critical nature of the maneuver, which becomes even more significant for the DT-roll-pitch model with dynamic normal loads.

5 Conclusions

Five different vehicle motion models were considered, ranging from a single-track model to a double-track model with roll and pitch dynamics including load transfer. These models were investigated in a 90°-turn and a double lane-change maneuver, and the optimal control problems for finding the minimum-time solution in each case were solved.

The solution behavior for the different models is similar in several key aspects for both maneuvers, as observed in Figures 3 and 7. For example, variables often used in safety systems, such as the yaw rate, the slip angle, and the roll angle, only exhibit minor discrepancies. The input torques differ significantly during parts of the maneuver. However, the overall lateral forces and yaw moments generated by the tires—F_Y and M_Z in Figures 4 and 8—for the different models have similar characteristics, with only quantitative differences in between. The largest discrepancies occur in the longitudinal forces; in Figure 8 the largest difference in absolute value of the longitudinal force between ST and DT-roll-pitch is approximately 50 %. However, this major difference is only seen for a few samples and does not have much impact on the other variables. Moreover, considering an online implementation, torque and force bounds have to be set conservatively because of uncertainty in model parameters and disregarded

dynamics, which will suppress this difference.

All of these observations are important, since they imply that variables traditionally considered as high-level inputs in safety systems, such as M_Z, may be generated by optimization using models with low complexity, *e.g.*, the single-track model. These high-level inputs can then be utilized as inputs to a low-level optimizer, which benefit more from complex models for distributing the desired torque to the respective wheel. This fact, together with the increased amount of sensor data and computational power available in modern road vehicles, opens up for the use of simplistic models when designing the on-board optimization-based safety systems of tomorrow.

References

Johan Åkesson, Karl-Erik Årzén, Magnus Gäfvert, Tove Bergdahl, and Hubertus Tummescheit. Modeling and optimization with Optimica and JModelica.org—Languages and tools for solving large-scale dynamic optimization problems. *Computers and Chemical Engineering*, 34(11):1737–1749, November 2010.

J. Andreasson. Enhancing active safety by extending controllability — How much can be gained? In *IEEE Intelligent Vehicles Symp.*, pages 658–662, Xi'an, Shaanxi, China, June 2009.

Karl Berntorp. Derivation of a six degrees-of-freedom ground-vehicle model for automotive applications. Technical Report ISRN LUTFD2/TFRT--7627--SE, Department of Automatic Control, Lund University, Sweden, February 2013.

Karl Berntorp, Björn Olofsson, Kristoffer Lundahl, Bo Bernhardsson, and Lars Nielsen. Models and methodology for optimal vehicle maneuvers applied to a hairpin turn. In *Am. Control Conf. (ACC)*, Washington, DC, 2013. *Accepted*.

Lorenz T Biegler, Arturo M Cervantes, and Andreas Wächter. Advances in simultaneous strategies for dynamic process optimization. *Chemical Engineering Science*, 57:575–593, 2002.

Imon Chakraborty, Panagiotis Tsiotras, and Jianbo Lu. Vehicle posture control through aggressive maneuvering for mitigation of T-bone collisions. In *IEEE Conf. on Decision and Control (CDC)*, pages 3264–3269, Orlando, FL, 2011.

Andreas Griewank. Evaluating derivatives: Principles and techniques of algorithmic differentiation. *Frontiers in Applied Mathematics, SIAM*, 19, 2000.

Rolf Isermann. *Fahrdynamik-Regelung: Modellbildung, Fahrerassistenzsysteme, Mechatronik*. Vieweg-Verlag, Wiesbaden, Germany, 2006.

ISO 3888-2:2011. *Passenger cars — Test track for a severe lane-change manoeuvre — Part 2: Obstacle avoidance*. International Organization for Standardization, Geneva, Switzerland, 2011.

D. P. Kelly and R. S. Sharp. Time-optimal control of the race car: a numerical method to emulate the ideal driver. *Vehicle System Dynamics*, 48(12):1461–1474, 2010.

U. Kiencke and L. Nielsen. *Automotive Control Systems—For Engine, Driveline and Vehicle*. Springer-Verlag, Berlin Heidelberg, second edition, 2005.

Modelica Association, 2012. URL: http://www.modelica.org.

Björn Olofsson, Kristoffer Lundahl, Karl Berntorp, and Lars Nielsen. An investigation of optimal vehicle maneuvers for different road conditions. In *7th IFAC Symp. on Advances in Automotive Control (AAC)*, Tokyo, Japan, 2013. *Accepted*.

Hans B. Pacejka. *Tyre and Vehicle Dynamics*. Butterworth-Heinemann, Oxford, United Kingdom, second edition, 2006.

R. S. Sharp and Huei Peng. Vehicle dynamics applications of optimal control theory. *Vehicle System Dynamics*, 49(7):1073–1111, 2011.

Peter Sundström, Mats Jonasson, Johan Andreasson, Annika Stensson Trigell, and Bengt Jacobsson. Path and control optimisation for over-actuated vehicles in two safety-critical maneuvers. In *10th Int. Symp. on Advanced Vehicle Control (AVEC)*, Loughborough, United Kingdom, 2010.

E. Velenis and P. Tsiotras. Minimum time vs. maximum exit velocity path optimization during cornering. In *IEEE Int. Symp. on Industrial Electronics (ISIE)*, pages 355–360, Dubrovnik, Croatia, June 2005.

Andreas Wächter and Lorenz T Biegler. On the implementation of an interior-point filter line-search algorithm for large-scale nonlinear programming. *Mathematical Programming*, 106(1):25–57, 2006.

Paper D

An Investigation of Optimal Vehicle Maneuvers for Different Road Conditions*

D

*In *the 7th IFAC Symposium on Advances in Automotive Control*, Tokyo, Japan, 2013.

An Investigation of Optimal Vehicle Maneuvers for Different Road Conditions

Björn Olofsson[a], Kristoffer Lundahl[b], Karl Berntorp[a], and Lars Nielsen[b]

[a] *Department of Automatic Control, Lund University, SE–221 00 Lund, Sweden*

[b] *Vehicular Systems, Department of Electrical Engineering, Linköping University, SE-581 83 Linköping, Sweden*

Abstract

We investigate optimal maneuvers for road-vehicles on different surfaces such as asphalt, snow, and ice. The study is motivated by the desire to find control strategies for improved future vehicle safety and driver assistance technologies. Based on earlier presented measurements for tire-force characteristics, we develop tire models corresponding to different road conditions, and determine the time-optimal maneuver in a hairpin turn for each of these. The obtained results are discussed and compared for the different road characteristics. Our main findings are that there are fundamental differences in the control strategies on the considered surfaces, and that these differences can be captured with the adopted modeling approach. Moreover, the path of the vehicle center-of-mass was found to be similar for the different cases. We believe that these findings imply that there are observed vehicle behaviors in the results, which can be utilized for developing the vehicle safety systems of tomorrow.

1 Introduction

Motivated by the desire to devise improved safety systems for vehicles and driver assistance technologies, development of mathematical models and model-based control strategies for optimal vehicle maneuvers in time-critical situations have emerged as powerful tools during the past years. Even though the solution to an optimal control problem depends on the particular choice of model and cost function, the fundamental behavior and control strategies found by optimization can be used as inspiration for, or be integrated in, future safety-systems.

One step towards this is to study the behavior of a vehicle in a time-critical maneuver under varying road conditions, *e.g.*, dry asphalt and snow. Therefore, we investigate a hairpin maneuver, see Figure 1. The objective is to perform the maneuver in minimum time, while fulfilling certain constraints on the control inputs and internal states of the vehicle. This means that the vehicle, and in particular the tires, are performing at their limits. We utilize established vehicle and tire modeling principles, and present a model-based optimal control problem with the solution thereof for different road conditions. In addition, we investigate how to scale the tire models for different surfaces. By this study, it is plausible that the understanding of vehicle dynamics in extreme situations under environmental uncertainties is increased.

Optimal control problems for vehicles in time-critical situations have been studied in the literature previously, see (Velenis and Tsiotras, 2005; Velenis, 2011) for different examples. In (Kelly and Sharp, 2010) the time-optimal race-

Figure 1: An example of a partly snow-covered hairpin turn.

car line was investigated, and in (Sharp and Peng, 2011) a survey on existing vehicle dynamics applications of optimal control theory was presented. Other examples are (Sundström et al., 2010; Funke et al., 2012). We presented a method for determining optimal maneuvers and a subsequent comparison using different methods for tire modeling in (Berntorp et al., 2013). Further, a comparison of optimal maneuvers with different chassis models was treated in (Lundahl et al., 2013). Scaling of nominal tire models for different surfaces was discussed and experimentally verified in (Braghin et al., 2006). Even though the vehicle and tire models utilized in this paper are similar to those presented in the mentioned references, previous research approaches focus on a particular vehicle model on a specific surface. Comparisons of optimal control maneuvers for different road conditions have been made, see (Chakraborty et al., 2011), but are limited to varying the friction coefficient, and we show that important tire-force characteristics might be neglected with that approach. To the best of our knowledge, no comprehensive approach to perform comparisons of optimal control maneuvers for different road conditions has been made, which motivates the study presented here.

2 Modeling

The vehicle dynamics is modeled with an extended single-track model together with a wheel model and a Magic Formula tire model.

2.1 Vehicle Modeling

The vehicle model considered is a single-track model (Kiencke and Nielsen, 2005; Isermann, 2006) with lumped right and left wheels. In addition, a rotational degree of freedom about the x-axis—*i.e.*, the roll—has been added. The coordinate system is located in the ground plane, at the xy-coordinates of the center of mass for zero roll angle, see Figure 2. The motivation for the single-track model is twofold; first, we are aiming for models possible to utilize together with

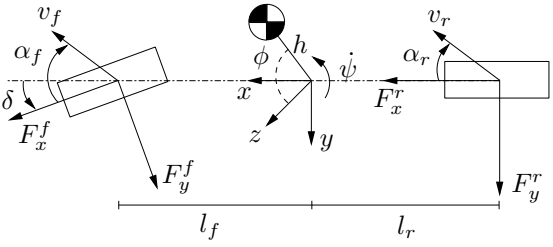

Figure 2: The single-track model including roll motion about the x-axis, resulting in a four degrees-of-freedom chassis model.

dynamic optimization algorithms. Second, we want to investigate what properties of a vehicle that can be captured with this comparably simple model. The roll dynamics is of importance, in order to verify that the vehicle is not overbalancing in the aggressive hairpin maneuver. The model does not incorporate load transfer, but the effect of this has previously been investigated in (Lundahl et al., 2013). The model equations are

$$m\dot{v}_x = F_X + mv_y\dot{\psi} - mhs_\phi\ddot{\psi} - 2mhc_\phi\dot{\phi}\dot{\psi}, \tag{1}$$

$$m\dot{v}_y = F_Y - mv_x\dot{\psi} - mhs_\phi\dot{\psi}^2 + mh\ddot{\phi}c_\phi - m\dot{\phi}^2hs_\phi, \tag{2}$$

$$\ddot{\psi} = \frac{M_Z - F_X hs_\phi}{I_{zz}c_\phi^2 + I_{yy}s_\phi^2}, \tag{3}$$

$$I_{xx}\ddot{\phi} = F_Y hc_\phi + mghs_\phi + \dot{\psi}^2\Delta I_{yz}s_\phi c_\phi - K_\phi\phi - D_\phi\dot{\phi}, \tag{4}$$

$$F_X = F_x^f c_\delta + F_x^r - F_y^f s_\delta, \tag{5}$$

$$F_Y = F_y^f c_\delta + F_y^r + F_x^f s_\delta, \tag{6}$$

$$M_Z = l_f F_y^f c_\delta - l_r F_y^r + l_f F_x^f s_\delta, \tag{7}$$

where c_ϕ, s_ϕ are short for $\cos(\phi)$ and $\sin(\phi)$, and similarly for c_δ, s_δ. Further, m is the vehicle mass, h is the height of the center of mass, I_{zz} is the vehicle inertia about the z-axis, $\Delta I_{yz} = I_{yy} - I_{zz}$, $\dot{\psi}$ is the yaw rate, ϕ is the roll angle, δ is the steering angle measured at the wheels, v_x, v_y are the longitudinal and lateral velocities, l_f, l_r are the distances from the center of mass to the front and rear wheel base, F_x, F_y are the longitudinal and lateral forces acting on the front and rear wheels, and F_X, F_Y and M_Z are the resulting tire forces and moment. The roll dynamics is derived by assuming that the suspension system can be modeled as a spring-damper system—*i.e.*, a dynamic system with stiffness K_ϕ and damping D_ϕ.

2.2 Wheel Modeling

The wheel dynamics is given by

$$T_i - I_w\dot{\omega}_i - F_x^i R_w = 0\ , \quad i = f, r. \tag{8}$$

Here, ω_i are the front and rear wheel angular velocities, T_i are the driving/braking torques, I_w is the wheel inertia, and R_w is the wheel radius. Slip angles α_f, α_r and slip ratios κ_f, κ_r are introduced following (Pacejka, 2006), and are described by

$$\alpha_f = \delta - \operatorname{atan}\left(\frac{v_y + l_f\dot{\psi}}{v_x}\right), \tag{9}$$

$$\alpha_r = -\operatorname{atan}\left(\frac{v_y - l_r\dot{\psi}}{v_x}\right), \tag{10}$$

$$\kappa_f = \frac{R_w\omega_f - v_{x,f}}{v_{x,f}}, \tag{11}$$

$$\kappa_r = \frac{R_w\omega_r - v_{x,r}}{v_{x,r}}, \tag{12}$$

$$v_{x,f} = v_x\cos(\delta) + (v_y + l_f\dot{\psi})\sin(\delta), \tag{13}$$

$$v_{x,r} = v_x. \tag{14}$$

The vehicle and wheel parameters used in this study are presented in Table 1.

The nominal tire forces—*i.e.*, the forces under pure slip conditions—are computed with a simplified Magic Formula model (Pacejka, 2006), given by

$$F^i_{x0} = \mu_x F^i_z \sin(C^i_x \text{atan}(B^i_x\kappa_i - E^i_x(B^i_x\kappa_i - \text{atan}B^i_x\kappa_i))), \tag{15}$$

$$F^i_{y0} = \mu_y F^i_z \sin(C^i_y \text{atan}(B^i_y\alpha_i - E^i_y(B^i_y\alpha_i - \text{atan}B^i_y\alpha_i))), \tag{16}$$

$$F^i_z = mg(l - l_i)/l,\ i = f, r,\ \text{where } l = l_f + l_r. \tag{17}$$

In (15)–(17), μ_x and μ_y are the friction coefficients and B, C, and E are model parameters. Combined slip is modeled using the weighting functions presented in (Pacejka, 2006):

$$B^i_{x\alpha} = B^i_{x1}\cos(\text{atan}(B^i_{x2}\kappa_i)), \tag{18}$$

$$G^i_{x\alpha} = \cos(C^i_{x\alpha}\text{atan}(B^i_{x\alpha}\alpha_i)), \tag{19}$$

$$F^i_x = F^i_{x0}G^i_{x\alpha}, \tag{20}$$

$$B^i_{y\kappa} = B^i_{y1}\cos(\text{atan}(B^i_{y2}\alpha_i)), \tag{21}$$

$$G^i_{y\kappa} = \cos(C^i_{y\kappa}\text{atan}(B^i_{y\kappa}\kappa_i)), \tag{22}$$

$$F^i_y = F^i_{y0}G^i_{y\kappa},\ i = f, r. \tag{23}$$

In contrast to (15)–(23), a more complete form is presented in (Pacejka, 2006). However, since a single-track vehicle model is utilized here, the tire models have been recomputed such that they are symmetric with respect to the slip angle α and the slip ratio κ.

2.3 Tire-Force Characteristics and Model Calibration

In an optimal maneuver the tires are performing at their limits, thus implying the need for accurate tire modeling. Given a set of tire parameters for a nominal surface, (Pacejka, 2006) proposes to use scaling factors, λ_j, in (15)–(23) to describe different road conditions. This method was used in (Braghin et al., 2006), where the scaling factors representing surfaces corresponding to dry asphalt, wet asphalt, snow, and smooth ice were estimated based on experimental data. Since that study included a set of different tire brands and models, the results presented could be seen as a general indication, or at least be used as

Table 1: Vehicle parameters used in (1)–(14).

Notation	Value	Unit
l_f	1.3	m
l_r	1.5	m
m	2 100	kg
I_{xx}	765	kgm^2
I_{yy}	3 477	kgm^2
I_{zz}	3 900	kgm^2
R_w	0.3	m
I_w	4.0	kgm^2
g	9.82	ms^{-2}
h	0.5	m
K_ϕ	178 000	Nm(rad)^{-1}
D_ϕ	16 000	Nms(rad)^{-1}

guidelines, on how the tire characteristics will vary. We use the scaling factors from (Braghin et al., 2006) as a basis for calibrating tire models approximately corresponding to the force characteristics on the different surfaces. However, since the nominal tire parameters used in that paper are not public domain, we use the parameters from (Pacejka, 2006) to represent dry asphalt. The relative scaling factors, with respect to dry asphalt, are introduced according to

$$\lambda_{\text{dry}} = 1, \quad \lambda_{\text{wet}} = \frac{\lambda^*_{\text{wet}}}{\lambda^*_{\text{dry}}}, \quad \lambda_{\text{snow}} = \frac{\lambda^*_{\text{snow}}}{\lambda^*_{\text{dry}}}, \quad \lambda_{\text{ice}} = \frac{\lambda^*_{\text{ice}}}{\lambda^*_{\text{dry}}}, \tag{24}$$

where λ is the scaling factor used in this paper and λ^* is the scaling factor presented in (Braghin et al., 2006). Since a different set of nominal parameters are used, and since uncertainties in the estimation of the original scaling factors exist—especially for larger slip values—some inconsistent characteristics appear for the snow and ice models. The original snow model will produce a longitudinal force F_x that changes sign for large slip ratios, which is avoided by adjusting the scaling factor for C_x. For the ice model, multiple sharp and narrow peaks in the resultant force occur. This is adjusted by recomputing the scaling factor affecting (21), as well as the parameters B_{x2} and B_{y2}. In addition, the lateral curvature factor E_y is adjusted to smoothen the sharp peak originating from the relations in (15)–(16), which contributes to the inconsistencies in the resultant force. The complete set of tire model parameters used are provided in Table 2. Several of these parameters are dependent on the normal force F_z on the wheel. Hence, the front and rear parameter values differ—*e.g.*, the friction coefficients $\mu_{x,f}$ and $\mu_{x,r}$.

Table 2: Tire model parameters used to represent dry asphalt, wet asphalt, snow, and smooth ice.

Parameter	Dry	Wet	Snow	Ice
$\mu_{x,f}$	1.20	1.06	0.407	0.172
$\mu_{x,r}$	1.20	1.07	0.409	0.173
$B_{x,f}$	11.7	12.0	10.2	31.1
$B_{x,r}$	11.1	11.5	9.71	29.5
$C_{x,f}, C_{x,r}$	1.69	1.80	1.96	1.77
$E_{x,f}$	0.377	0.313	0.651	0.710
$E_{x,r}$	0.362	0.300	0.624	0.681
$\mu_{y,f}$	0.935	0.885	0.383	0.162
$\mu_{y,r}$	0.961	0.911	0.394	0.167
$B_{y,f}$	8.86	10.7	19.1	28.4
$B_{y,r}$	9.30	11.3	20.0	30.0
$C_{y,f}, C_{y,r}$	1.19	1.07	0.550	1.48
$E_{y,f}$	-1.21	-2.14	-2.10	-1.18
$E_{y,r}$	-1.11	-1.97	-1.93	-1.08
$C_{x\alpha,f}, C_{x\alpha,r}$	1.09	1.09	1.09	1.02
$B_{x1,f}, B_{x1,r}$	12.4	13.0	15.4	75.4
$B_{x2,f}, B_{x2,r}$	-10.8	-10.8	-10.8	-43.1
$C_{y\kappa,f}, C_{y\kappa,r}$	1.08	1.08	1.08	0.984
$B_{y1,f}, B_{y1,r}$	6.46	6.78	4.19	33.8
$B_{y2,f}, B_{y2,r}$	4.20	4.20	4.20	42.0

3 Optimal Control Problem

The time-optimal hairpin maneuver problem is formulated as an optimization problem on the time-interval $t \in [0, t_f]$. The vehicle dynamics presented in the previous section is formulated as a differential-algebraic equation system (DAE) in the differential variables (states) x, algebraic variables y, and the inputs $u = (T, \delta)$, according to $\dot{x} = G(x, y, u)$, and similarly for the tire dynamics, $h(x, y, u) = 0$. Introducing the maximum and minimum limits on the driving/braking torques and the steering angle, the mathematical optimization problem can be stated as follows:

$$\begin{aligned}
\text{minimize} \quad & t_f && (25)\\
\text{subject to} \quad & T_{i,\min} \le T_i \le T_{i,\max}, \; i = f, r && (26)\\
& |\delta| \le \delta_{\max} \quad , \quad |\dot{\delta}| \le \dot{\delta}_{\max} && (27)\\
& \left(\frac{X_p}{R_1^i}\right)^6 + \left(\frac{Y_p}{R_2^i}\right)^6 \ge 1 && (28)\\
& \left(\frac{X_p}{R_1^o}\right)^6 + \left(\frac{Y_p}{R_2^o}\right)^6 \le 1 && (29)\\
& x(0) = x_0 \quad , \quad x(t_f) = x_{t_f} && (30)\\
& y(0) = y_0 \quad , \quad y(t_f) = y_{t_f} && (31)\\
& \dot{x} = G(x, y, u) \quad , \quad h(x, y, u) = 0, && (32)
\end{aligned}$$

where x_0, y_0 and x_{t_f}, y_{t_f} are the initial and final conditions, and (X_p, Y_p) is the position of the center-of-mass of the vehicle. The track constraint for the hairpin turn is formulated using two super-ellipses. In the implementation, the initial and final conditions are only applied to a subset of the variables.

The strategy for solving the optimal control problem is to use numerical methods for dynamic optimization. First, considering the setup of the hairpin turn, it can be concluded from a physical argument that existence of a solution is guaranteed. In this study, we utilize the open-source software JModelica.org (Åkesson et al., 2010), interfaced with the interior-point NLP-solver Ipopt (Wächter and Biegler, 2006), for solving the optimization problem. A direct collocation method (Biegler et al., 2002) is employed for discretization of the continuous-time optimal control problem. In order to achieve convergence in the NLP-solver, the hairpin turn problem is divided into smaller segments and thus solved in 4–8 steps sequentially, where the previous solution is used as an initial guess to the subsequent optimization problem. The final optimization solves the whole problem, thus not implying any suboptimality of the solution. From a numerical perspective, proper scaling of the optimization variables turned out to be essential for convergence. For details about the optimization methodology, the reader is referred to (Berntorp et al., 2013).

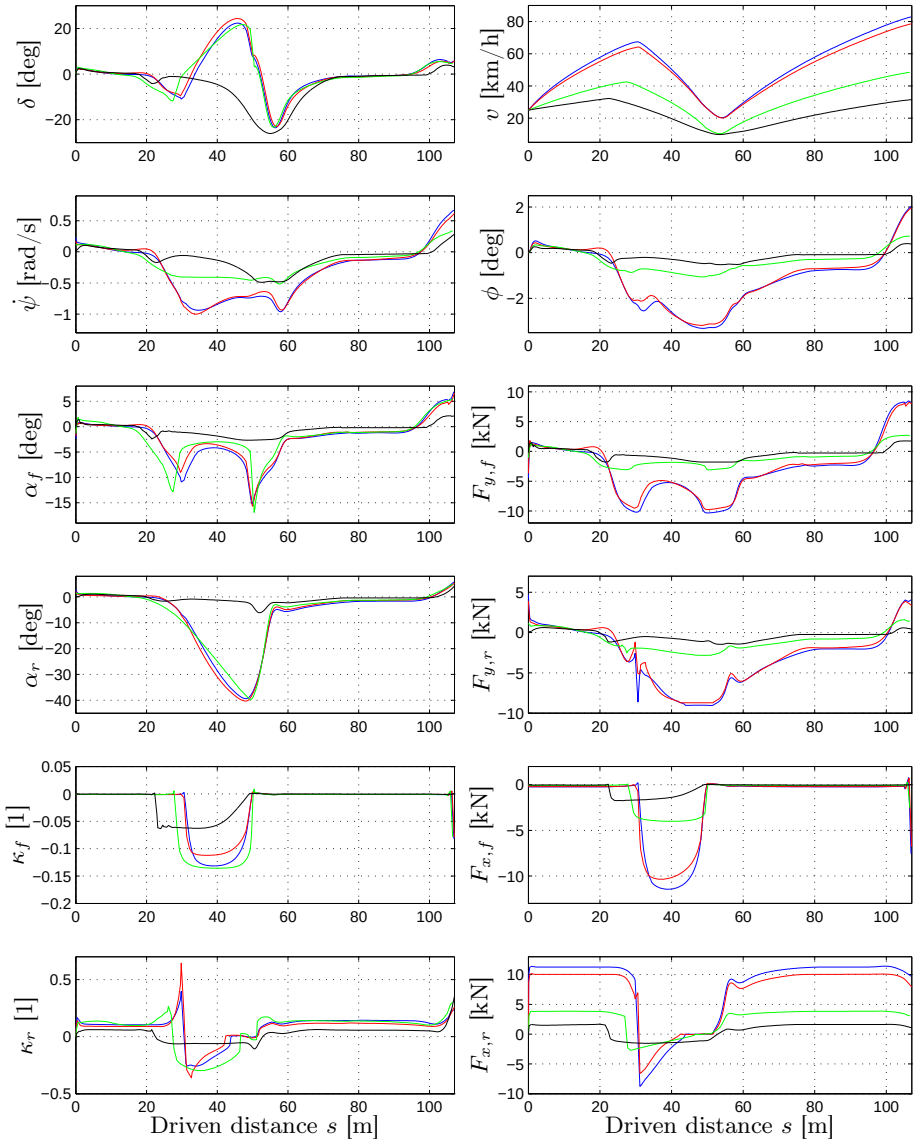

Figure 3: Variables of the vehicle model during the time-optimal hairpin maneuver on the different surfaces, plotted as function of the driven distance s. The color scheme is as follows: dry asphalt–blue, wet asphalt–red, snow–green, and smooth ice–black.

4 Results

The optimization problem (25)–(32) was solved for each of the surface models presented in Sec. 2. The road was 5 m wide. The bounds on the driving/braking torques and tire forces were chosen as follows:

$$T_{f,\min} = -\mu_{x,f} F_z^f R_w \ , \ T_{f,\max} = 0, \tag{33}$$

$$T_{r,\min} = -\mu_{x,r} F_z^r R_w \ , \ T_{r,\max} = \mu_{x,r} F_z^r R_w, \tag{34}$$

$$|F_x^i| \leq \mu_{x,i} F_z^i, \tag{35}$$

$$|F_y^i| \leq \mu_{y,i} F_z^i, \ i = f, r, \tag{36}$$

assuming that the vehicle is rear-wheel driven. Note that the bounds (35)–(36) on the forces were set for easier convergence, but are mathematically redundant. With the choice of the maximum driving/braking torques in (33)–(34), we introduce a dependency on the surface. This is motivated since the surface models adopted in this paper are only identified, and hence validated, for a certain region in the κ–α plane. Thus, allowing excess input torques might result in inconsistent behavior of the tire force model. Further, from a driver limitation argument the steering angle and steering rate were constrained according to

$$\delta_{\max} = 30 \text{ deg} \quad , \quad \dot{\delta}_{\max} = 60 \text{ deg/s}.$$

In addition, we constrained the wheel angular velocities ω_f, ω_r to be nonnegative—*i.e.*, the wheels were not allowed to roll backwards or back-spin.

With an initial velocity of 25 km/h, the results displayed in Figure 3 are obtained. For comparison of the different surfaces, the model variables are visualized as function of the driven distance s instead of time. Further, the geometric trajectories corresponding to these control strategies are presented in Figure 4. We also use the force–slip tire characteristic surfaces as a basis for analysis, as introduced in (Berntorp et al., 2013) and hereafter referred to as *Force-Slip (FS)-diagrams*. This 3D surface is defined as the resulting force

$$F_{i,\text{res}} = \sqrt{(F_x^i)^2 + (F_y^i)^2}, \ i = f, r,$$

as function of the longitudinal slip κ and slip angle α. Plotting the optimal trajectory in this surface for both front and rear wheel, respectively, gives an effective presentation of the tire utilization in two plots, see Figures 5–8. The time for execution of the maneuver is 8.48 s, 8.79 s, 13.83 s, and 19.18 s for dry asphalt, wet asphalt, snow, and smooth ice, respectively.

4.1 Discussion of Characteristics on Different Surfaces

The geometric trajectories of the vehicle center-of-mass, shown in Figure 4, are close to each other for the different surfaces. This result might be unexpected, given the different surface characteristics. However, if comparing the paths

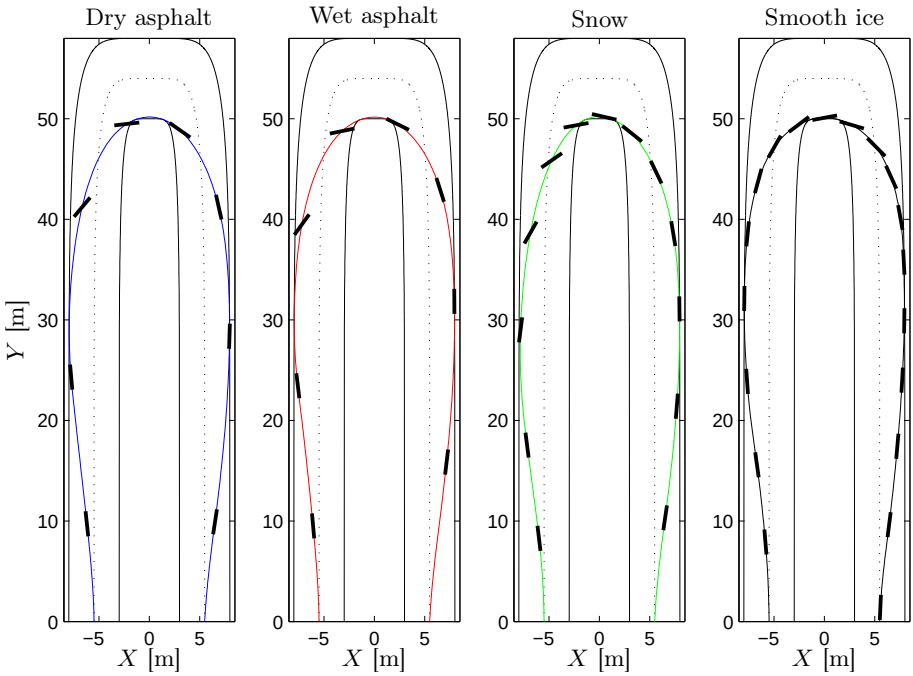

Figure 4: Trajectory in the XY-plane for the different road surfaces. The black rectangles indicate the position and direction of the vehicle each second.

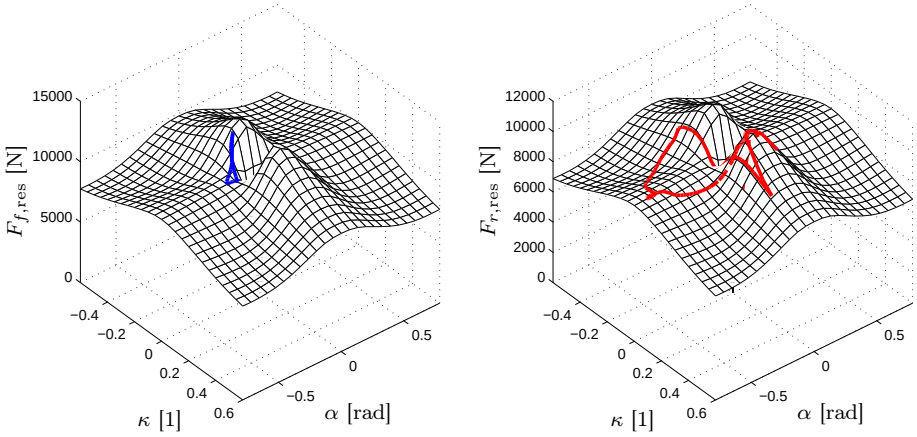

Figure 5: The resulting tire forces for the dry asphalt model. The front tire force is shown in blue and the rear tire force is shown in red. The rear tire force exhibits more variation, caused by the vehicle being rear-wheel driven.

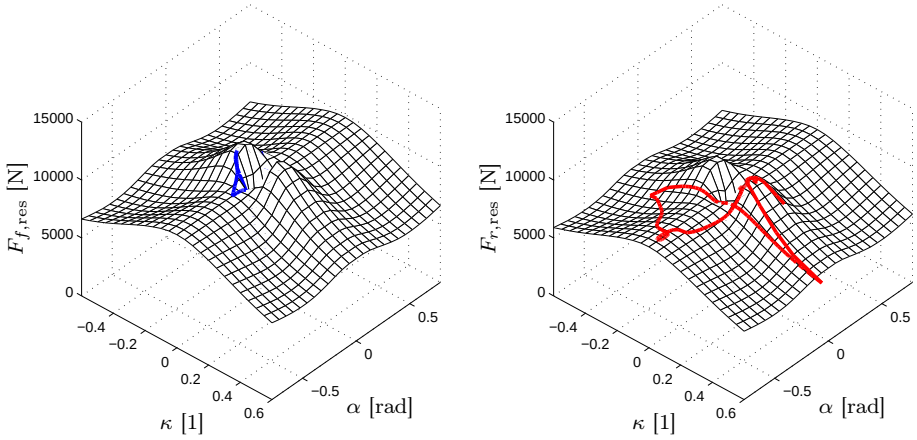

Figure 6: The resulting tire forces for the wet asphalt model.

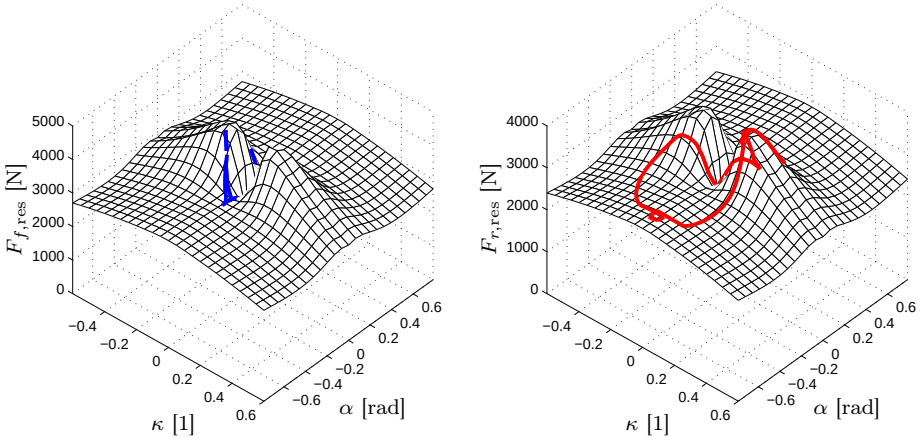

Figure 7: The resulting tire forces for the snow model.

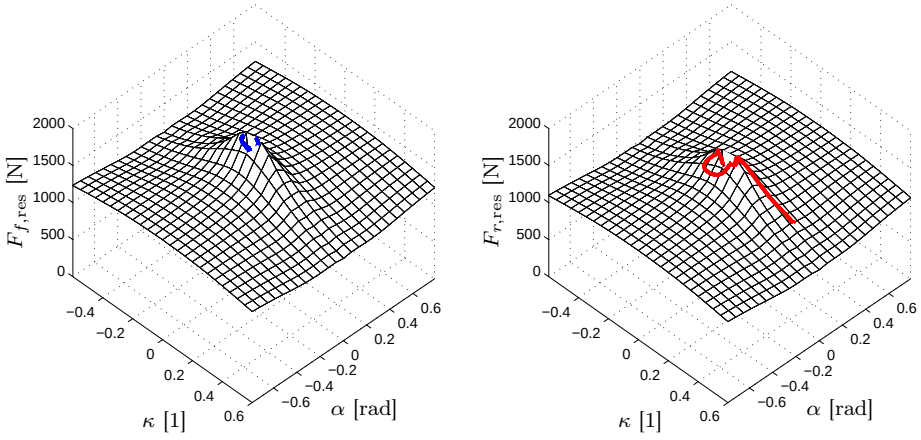

Figure 8: The resulting tire forces for the smooth ice model.

for other parts of the vehicle, such as the front or rear wheel, more pronounced differences are seen as a result of the different slip behavior. Obviously, the time for completing the maneuver is longer for the snow and ice surfaces than for asphalt. This is a result of the tire forces that can be realized on these surfaces. Further, the vehicle exhibits large slip in the critical part of the maneuver on all surfaces except smooth ice. The reason for this difference becomes evident when examining the force characteristics of the smooth ice model compared to, *e.g.*, the dry asphalt model. In Figures 9 and 10 the longitudinal and lateral tire forces are shown for these surfaces, *cf.* Figures 5 and 8. The tire forces for smooth ice exhibit a considerably sharper peak and thus decay faster, with respect to combined slip, than for dry asphalt. This means that combined slip yields a significantly smaller resultant force. Thus, to achieve the desired time-optimality on the ice surface, it is natural to choose a small-slip control strategy.

Comparison of Control Strategies

The internal variables of the vehicle model during the maneuver, see Figure 3, are similar for dry and wet asphalt. The similarity is expected, considering the tire force characteristics in the two cases. As anticipated, the major difference between the two surfaces is the time for execution of the maneuver, which is slightly longer for the wet asphalt surface. This is expected since the maximum tire forces are lower than for dry asphalt.

The differences between asphalt, snow, and ice when considering the control strategy are fundamental. First, it can be concluded that the optimal maneuver on snow and ice surfaces are more proactive in the sense that both the steering angle δ and braking forces are applied considerably earlier when approaching the hairpin. This is most certainly an effect of the significantly reduced tire forces that can be realized on these surfaces compared to asphalt. The steering angle also differs between ice and the other surfaces. The reason for this is that the vehicle employs counter-steering when it starts to slip on asphalt and snow as it approaches the hairpin. Further, we see that the roll angle is considerably smaller for the low-friction surfaces, which is caused by the torque about the roll axis (produced by the tire forces) being smaller. Moreover, even on dry asphalt the roll angle is kept below approximately 3.2 deg, verifying that no unstable modes are excited. The slip ratio κ differs in amplitude between the road-surfaces. The reason becomes clear when investigating the FS-diagrams and the corresponding tire utilization, Figures 5–8. The peak of the resultant force in the κ–α plane occurs at smaller slip values for ice, which implies a control solution with smaller slip angles for minimum-time.

Discussion on Tire Model Calibration

An integral part of the vehicle model is the tire characteristics. Consequently, different approaches to model calibration were investigated prior to the study.

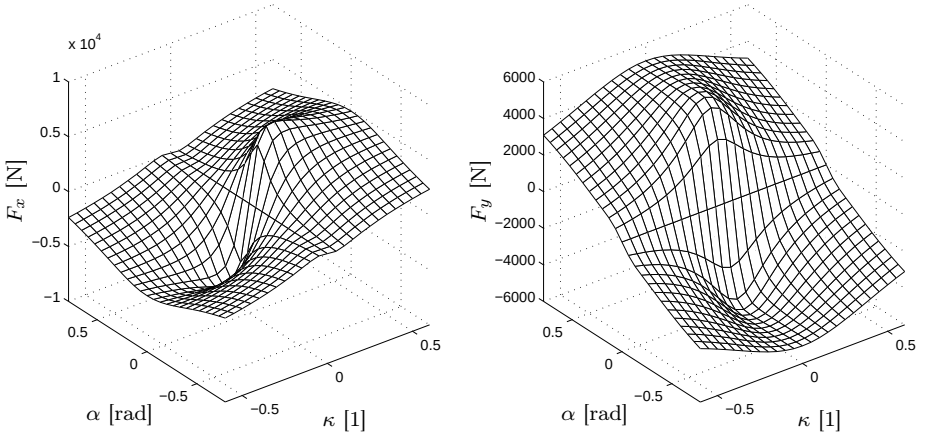

Figure 9: Front tire forces in the longitudinal and lateral wheel directions for dry asphalt, corresponding to Figure 5.

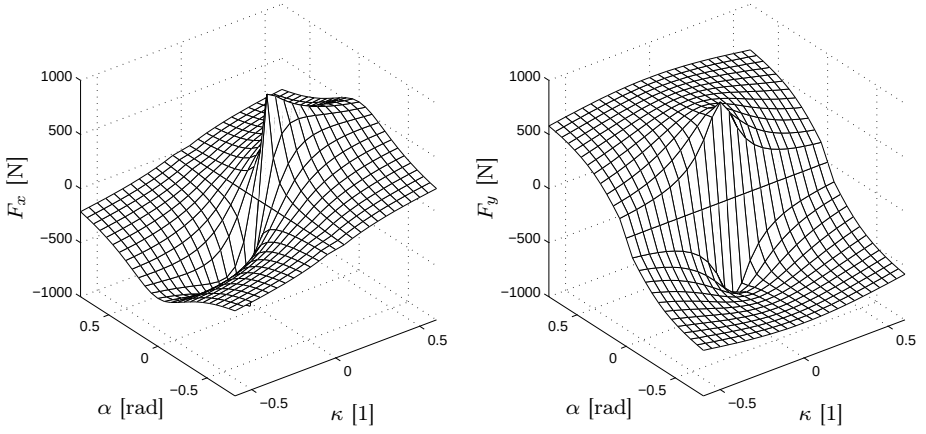

Figure 10: Front tire forces in the longitudinal and lateral wheel directions for ice, corresponding to Figure 8.

One approach would be to only scale the friction coefficients μ_x and μ_y, as done in (Chakraborty et al., 2011). However, the peaks in the tire-force surfaces occur at different lateral and longitudinal slip combinations, see Figures 5–8. Also, the sharpness and width of the maxima and minima change for the different models. Thus, only changing the friction coefficients will render different force characteristics—and thus different optimal solutions—compared to when changing the complete set of parameters. This is verified by constructing a tire force model where the dry asphalt parameters are used together with the friction coefficients corresponding to ice. Performing the optimization gives that the optimal solution has significant slip, on the contrary to the results obtained for the empirical smooth-ice model; see Figure 11 for the results obtained by scaling the friction coefficients only. Another approach to tire model calibration is to scale the slip stiffness (*i.e.*, the parameters B_x and B_y in (15)–(17)) in addition to the friction coefficients. This will change both the inclination and the slip value where the maximum tire force is attained. However, adjusting these parameters without considering the parameters corresponding to combined slip will, in this case, result in multiple sharp and narrow peaks in the resultant force, which might be unrealistic from a physical point-of-view.

5 Conclusions

Optimal vehicle maneuvers under varying road conditions give valuable insight into the dynamics when the vehicle performs at the limit. One observation was that tire-force modeling on different road surfaces using only a scaling of the friction coefficients is insufficient for the maneuver considered, at least when the tires perform at their limits. Rather, when combined longitudinal and lateral slip is present, more careful tire modeling may be required. The minimum-time hairpin maneuver, using tire models representing different road surfaces, gave as a first major observation that the path through the turn was almost the same independent of different road-surface characteristics, such as dry asphalt or ice. Of course, the total execution time is longer on ice than asphalt, but there are also other differences which lead to the second major conclusion: The optimal driving techniques—*i.e.*, the control actions—are fundamentally different depending on tire-road characteristics. This is an important finding since it implies that in order to enjoy the full benefits of improved sensor information, future safety systems will need to be more versatile than systems of today. Further, that the path of the vehicle center-of-mass is almost invariant gives inspiration to look for strategies based on path formulations when approaching the goal of developing new model-based vehicle safety systems more robust to road-surface uncertainties.

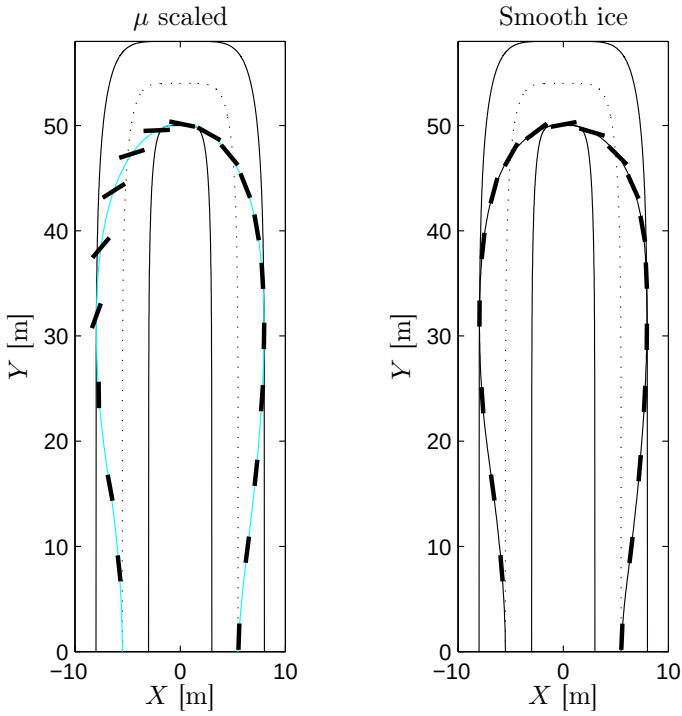

Figure 11: Optimal hairpin maneuver on ice for two tire model parametrizations: Scaling of friction coefficients (left) and empirical tire model (right). Scaling of μ only renders an optimal solution with large slip.

References

Johan Åkesson, Karl-Erik Årzén, Magnus Gäfvert, Tove Bergdahl, and Hubertus Tummescheit. Modeling and optimization with Optimica and JModelica.org—Languages and tools for solving large-scale dynamic optimization problems. *Computers and Chemical Engineering*, 34(11):1737–1749, November 2010.

Karl Berntorp, Björn Olofsson, Kristoffer Lundahl, Bo Bernhardsson, and Lars Nielsen. Models and methodology for optimal vehicle maneuvers applied to a hairpin turn. In *Am. Control Conf. (ACC)*, Washington, DC, 2013.

Lorenz T Biegler, Arturo M Cervantes, and Andreas Wächter. Advances in simultaneous strategies for dynamic process optimization. *Chemical Engineering Science*, 57:575–593, 2002.

F. Braghin, F. Cheli, and E Sabbioni. Environmental effects on Pacejka's scaling factors. *Vehicle System Dynamics: Intl. J. Vehicle Mechanics and Mobility*, 44(7):547–568, Jul. 2006.

Imon Chakraborty, Panagiotis Tsiotras, and Jianbo Lu. Vehicle posture control through aggressive maneuvering for mitigation of T-bone collisions. In *IEEE Conf. on Decision and Control (CDC)*, pages 3264–3269, Orlando, FL, 2011.

J. Funke, P. Theodosis, R. Hindiyeh, G. Stanek, K. Kritatakirana, C. Gerdes, D. Langer, M. Hernandez, B. Muller-Bessler, and B. Huhnke. Up to the limits: Autonomous Audi TTS. In *IEEE Intelligent Vehicles Symp.*, pages 541–547, Alcalá de Henares, Spain, June 2012.

Rolf Isermann. *Fahrdynamik-Regelung: Modellbildung, Fahrerassistenzsysteme, Mechatronik*. Vieweg-Verlag, Wiesbaden, Germany, 2006.

D. P. Kelly and R. S. Sharp. Time-optimal control of the race car: a numerical method to emulate the ideal driver. *Vehicle System Dynamics*, 48(12):1461–1474, 2010.

U. Kiencke and L. Nielsen. *Automotive Control Systems—For Engine, Driveline and Vehicle*. Springer-Verlag, Berlin Heidelberg, second edition, 2005.

Kristoffer Lundahl, Karl Berntorp, Björn Olofsson, Jan Åslund, and Lars Nielsen. Studying the influence of roll and pitch dynamics in optimal road-vehicle maneuvers. In *23rd Intl. Symp. on Dynamics of Vehicles on Roads and Tracks (IAVSD)*, Qingdao, China, 2013.

Hans B. Pacejka. *Tyre and Vehicle Dynamics*. Butterworth-Heinemann, Oxford, United Kingdom, second edition, 2006.

R. S. Sharp and Huei Peng. Vehicle dynamics applications of optimal control theory. *Vehicle System Dynamics*, 49(7):1073–1111, 2011.

Peter Sundström, Mats Jonasson, Johan Andreasson, Annika Stensson Trigell, and Bengt Jacobsson. Path and control optimisation for over-actuated vehicles in two safety-critical maneuvers. In *10th Intl. Symp. on Advanced Vehicle Control (AVEC)*, Loughborough, United Kingdom, 2010.

E. Velenis and P. Tsiotras. Minimum time vs. maximum exit velocity path optimization during cornering. In *IEEE Intl. Symp. on Industrial Electronics (ISIE)*, pages 355–360, Dubrovnik, Croatia, June 2005.

Efstathios Velenis. FWD vehicle drifting control: The handbrake-cornering technique. In *IEEE Conf. on Decision and Control (CDC)*, pages 3258–3263, Orlando, FL, 2011.

Andreas Wächter and Lorenz T Biegler. On the implementation of an interior-point filter line-search algorithm for large-scale nonlinear programming. *Mathematical Programming*, 106(1):25–57, 2006.